Characterisation of vadose zone processes in a tailings facility

IJ Baker
orcid.org 0000-0002-4379-1805

Dissertation submitted in fulfilment of the requirements for the degree *Masters of Science in Environmental Sciences* at the North-West University

Supervisor:	Mr J Koch
Co-supervisor:	Dr J van Tol
Co-supervisor:	Prof SA Lorentz

Graduation May 2019

24235687

PREFACE

A study of surface and near-surface water movement was recommended to acquire information regarding the movement of seepage water through a waste impoundment at a undisclosed mine in the Limpopo Province, South Africa. After various environmental impacts from mining activities specifically in the Olifants River, in-depth studies were proposed to remedy all impacts associated with the waste impoundments on the mine's property.

Various hydraulic and physical properties have been acquired from five different slopes on this tailings storage facility near the Olifants River. Additionally, Time Domain Reflectometry (TDR) sensors have been installed at various depths as well as run-off plots on the surface of these slopes. The latter mentioned datasets have been assessed to obtain additional information concerning the water balance within the cover and tailings material. These datasets have also been used (together with hydraulic and physical properties) to parametrise simulations from the HYDRUS-2D model.

This programme was used to simulate and characterise fluxes throughout the waste impoundment for each of the five slopes. This assessment represents all data, results, and discussions relevant to the quantification and assessment of various flow paths.

ACKNOWLEDGEMENTS

The writer of this dissertation would like to acknowledge the following individuals and entities for the role they played in the success of this study;

- Professor Johan van Tol, who invested a lot of time in assisting with theory, modelling and the general layout of this thesis. Without the help of Dr van Tol, a submission of this thesis would not have been possible. For his unselfish devotion, I'll forever be grateful;
- Mr. Piet van Deventer for liaising with SRK Consulting and Professor Simon Lorentz regarding the funding and logistics behind this project;
- Mr. Jaco Koch for his continues assistance regarding the dissertation itself;
- Mr. Johan McDonald (on site contact person) for taking the time in assisting with onsite logistics;
- My friends and family, for all their love and prayers leading up to the completion of this project;
- SRK Consulting for providing the funding for this project; and
- Professor Simon Lorentz for his assistance in the funding and on-site logistics.

DISCLAIMER

I, Ivan Baker, hereby claim the dissertation, “Characterisation of vadose zone processes in a tailings facility”, to be my own work and that I used the listed references completely without committing plagiarism.

Ivan Baker **Date: 2018/11/20**

ABSTRACT

The undisclosed mining company in Limpopo Province, where the study is undertaken, is one of the world's most accomplished copper mines. The waste dumps onsite (tailings storage facilities in particular) are known to provide ideal conditions for oxidation. An extensive investigation into the groundwater sulphate levels has indicated that only a small percentage of the sulphate load that reaches a nearby river, is contributed by groundwater. It was subsequently speculated that a significant sulphate load may result from sporadic rainfall-induced discharges, in the surface and near surface/vadose zone, potentially moving seepage water from the impoundments and the return water dams into the river. A study of surface and near-surface water and solute fluxes was proposed, for which this assessment will aid in quantifying water fluxes throughout the tailings storage facility on-site. This study aims at predicting, by means of a conceptual and a physically based model, the water fluxes that result in surface and near-surface sulphate loads. In order to develop reliable predictions, the waste materials need to be characterised. The material characterisation has included *in-situ* measurements of hydraulic characteristics as well as laboratory testing of the tailings storage facility material as well as the cover material overlaying the latter mentioned. *In-situ* observations include waste volumetric water content, runoff processes as well as meteorological observations. Before parameterising the *HYDRUS-2D* programme, a conceptual model was developed to define water flows and potential pathways through the tailings storage facility.

Key terms: Tailings storage facility, vadose zone, fluxes, physically based modelling, and hydraulic characteristics

LIST OF ACRONYMS AND ABBREVIATIONS

a	The Borehole Radius
a^2	The Macroscopic Capillary Length Parameter
AMD-	Acid mine drainage
BIC	Bushveld Igneous Complex
C1	The Soil Shape Factor
Cu	Copper
D	The Depth of the Cut-off Trench Below the Surface
DEAT	Department of Environmental Affairs and Tourism
DWAF	Department of Water Affairs and Forestry
ea	Actual Vapor Pressure
EC	Electrical conductivity
es	Saturation Vapor Pressure
ETo	Potential Evapotranspiration
FE	Finite Element
FeO	Iron Oxide
G	Soil Heat Flux
H1	The First Water Head Height
H	The Reservoir Head Above the Ground Surface
H_2O	Hydrogen Oxide
hCritA	The Absolute Value of the Minimum Allowed Pressure Head at the Soil Surface
Î	Slope of Vapor Pressure
Ka	The Apparent Dielectric Permittivity of the Growing Medium

Kcb	Basal Crop Coefficient
Ks	Saturated Hydraulic Conductivity
K_2O	Potassium Oxide
La	The apparent Length
L	The Actual Length
MgO	Magnesium Oxide
Offset	A Standard Offset Value of 0,085
PCC	Phalaborwa Carbonatite Complex
PPSD	Primary Particle Size Distribution
PSD	Particle Size Distribution
P(end)	The Probe at the End
P(start)	The Probe at the Start
RH	Relative Humidity
Rn	Net Radiation at Crop Surface
ROP	Run-off Plot
SC	Slope Component
SiO_2	Silicon Dioxide
SMP	Soil Matrix Potential
T	Mean Daily Temperature
TDR	Time Domain Reflectometry
TSF	Tailings Storage Facility
U2	Wind Speed at a Height of 2 m
WRD	Waste Rock Dump

VWC	Volumetric Water Content
Zr	Zirconium
W	The Bottom Width of the Cut-off Trench
θ	Volumetric Water Content
α	Adjusted Parameters
β	Adjusted Parameters

Table of contents

List of Tables

List of Figures

List of Equations

Chapter 1: Introduction

1.1 Preamble

The extensive mining operations of yesteryear have given rise to vast amounts of excess waste material, that often are associated with environmental impacts, specifically regarding the degradation of water resources. Waste material excavated from underground and opencast mines are treated to ensure that all valuable minerals are separated from waste material, which in turn is stored in waste impoundments. The latter mentioned impoundments (especially in the case of older impoundments that was constructed before the publication of best pollution control practise, (DWAF, 2007)) often are associated with seepage, which is the main source of contamination of nearby water resources. Contaminated plumes migrate through the waste material, continue to aid (in some cases) in the formation of acidic conditions and gather various contaminants in the process to ultimately end up in surface and underground water sources, which cause severe degradation of these sources, (McCarthy, 2011). Copper mining is often associated with various contaminants, including sulphides, which according to Campaner *et al.* (2013) is the main component needed for Acid Mine Drainage (AMD).

The copper mine in Limpopo Province, South Africa, at which this study is conducted, similarly experiences high concentrations of sulphates seeping through the waste impoundments into nearby water resources, complicating all intended closure plans. The study site is in close proximity of the Olifants River, which plays a substantial role in this study due to the concern of it being the receptor to major sources of contamination. The Olifants River has been branded as one of the rivers most affected by pollution in South Africa, (John *et al.,* 2012). A major concern is large mining operations up-stream and adjacent to the Olifants River (de Villiers & Mkwelo, 2009). John *et al.* (2012) mentions that, even though there are a variety of sources contributing to contaminants entering the Olifants River, mining activities seem to be the preeminent source. Unexplained crocodile and fish deaths in the Olifants River, including incidents in the Kruger National Park, began to raise some much-needed attention regarding the water quality of the river (Woodborne *et al.,* 2012). A study by De Villiers & Mkwelo (2009) proved that there is a significant concentration of sulphate in the Olifants River, specifically close to the mine in Limpopo Province. De Villiers & Mkwelo (2009) mentions that this specific site in the Olifants River reaches sulphate concentrations as high as 1200 mg/l. This value far exceeds the maximum allowed sulphate concentration of 250 mg/l for drinking water (Skipton *et al.,* 2010). Additionally, DWAF (1996) indicates that the average concentration of sulphates in surface water is 5 mg/l which could be exceeded by several 100 mg/l in cases of mine related pollution.

Seepage from waste impoundments which have a high concentrations of sulphate tends to pollute ground and surface water (Moukodi *et al*., 2009). In the case of the mine in Limpopo Province, similar discharges seem to occur within the Tailing Storage Facility (TSF). Certain seepage control measures are therefore vital to the mitigation of solutes migrating from waste impoundments to natural water systems (Klohn, 1979).

Hydropedology plays an integral role in predicting sub-surface flows and is associated with various hydrological characteristics, which in this case includes Volumetric Water Content (VWC), Particle Size Distribution (PSD), infiltration and hydraulic conductivity. These parameters play a considerable role in the understanding of water balances and are needed to parameterise the *HYDRUS-2D* tool. The mine in has continuously been challenged by seepage fluxes from waste impoundments to natural water bodies. Assumptions were made, pointing towards sporadic rainfall events being the key contributor to these discharges.

Even though monitoring and certain attempts to mitigate has been a part of the mine's history, contaminated plumes still manage to enter the river system, stressing the need for accurate sub-surface flow predictions. This objective will ultimately be achieved by ensuring a proper investigation into the migratory patterns of contaminated plumes from the sources (in this case the TSF) to the receptors (the Olifants River, which is fed by the Ga-Selati and other non-perennial streams). Therefore, it has been proposed that a study of surface and sub-surface water be initiated. Monitoring water balances from the impoundment's covers and the interaction between waste material, cover material, vegetation and meteorological data are vital to this study.

1.2 Problem Statement

The Olifants River has been characterised by deteriorating water quality over the past decade, originating from a wide range of sources. De Villiers & Mkwelo (2009) mentions that mining operations near the Olifants River are the main contributor to contaminants entering the river. An extensive investigation into the groundwater sulphate levels has indicated that only a small percentage of the sulphate load that reaches a nearby river, is contributed through the groundwater aquifers. It was subsequently speculated that a significant sulphate load may result from sporadic rainfall-induced discharges, in the surface and near surface/vadose zone, potentially moving seepage water from the impoundments and the return water dams into the river.

Sulphide bearing ores have been known to negatively influence the natural state and health of nearby water systems by means of AMD or similar to this case, by means of sulphate-contamination. The Waste Rock Dump (WRD), TSF as well as the return water dam on site are the main sources of contamination for the mine. Even though the seepage and discharge on site for the mine is alkaline of nature, large concentrations of sulphate tend to be the main subject of concern. High concentrations of sulphate can threaten an ecosystem as well as the health of humans consuming the contaminated water in various ways. Not only humans suffer from elevated sulphate levels, mass crocodile and fish deaths have also been recorded in the recent past within proximity to the mine. This disturbance has also been deemed to be the doing of sulphate contamination. Moukodi, Usher & Surmon (2009) mentions that the lack of rainfall (which is vital in oxidation and ultimately the formation of acidic conditions), as well as the abundance of carbonates within the project site of the mine, ensure that the conditions on site are alkaline of nature which eliminates AMD from the equation.

Sulphate contaminated plumes migrate through various pathways from the source (waste impoundments) to the natural river systems nearby. The focus, therefore, is to collect enough data regarding water balance to parameterise the software used for this study to ultimately ensure accurate predictions regarding potential flow paths. Similar studies to this study have been well documented in the past, including challenges regarding various models. Detailed descriptions of such studies are provided in Section 2.5-"Methods to Study Hydraulic Properties and Processes".

1.3 Aims and Objectives

The overall aim of this study is to characterise and quantify these pathways on the relevant TSF. The following objectives have been determined to ensure that the aim of the study is successfully attained;

I. Successful field monitoring: To measure and acquire data on key hydraulic properties and processes on the TSF;
II. The set-up of the conceptual model: To interpret observations, measurements and existing data to derive a model which conceptually characterise dominant flow paths on the TSF; and
III. Simulation of hydrological processes: The field monitoring data and conceptual model will be used to configure and parameterise a mechanistic model to quantify the dominant hydrological processes on the TSF.

1.4 Layout of Research

- Chapter one provides an introduction. This introduction covers the preamble, problem statement, aims and objectives and layout of research;
- Chapter two involves a literature study of the theory relevant to this study;
- Chapter three refers to the study area, including vegetation, climate and geology of the region as well as the methodology relevant to this study. More specifically, this chapter includes the methodology behind the field monitoring and the set-up of the physically based simulations;
- Chapter four includes results obtained from *In-situ* hydraulic characteristics and water balance data as well as meteorological data.
- Chapter five includes results simulated by the *HYDRUS-2D* tool, which will be illustrated graphically and discussed briefly.
- Chapter six includes conclusions from chapter 5.

- Chapter seven includes recommendations to improve the current state of contamination by means of surface and subsurface discharges.

Chapter 2: Literature Study

2.1 Laws and Legislations Regarding Waste Impoundments and Associated Pollution

The Department of Environmental Affairs and Tourism (DEAT) together with the Department of Water Affairs and Forestry (DWAF) (1997) emphasise the importance thereof to ensure that all South African citizens, as well as future generations, have the right to a clean and healthy environment. Section 24 of the constitution states that all South African citizens have the right to "an environment that is not harmful to their health or well-being", as well as "the right to "have the environment protected for the benefit of present and future generations, through reasonable legislative and other measures". These measures include the prevention of pollution and environmental degradation, the promotion of conservation and lastly to ensure sustainable development. One key aspect threatening this basic right for all citizens is ground- and surface water contamination, specifically from waste material. With an ever growing industrial and mining sector, densely populated areas across South Africa is ever more under the threat of intense pollution, creating unhealthy water conditions that might be life-threatening in some cases. DEAT & DWAF (1997) mentions that the focus should be on the successful and sustainable management of waste material. In addition to mass crocodile and fish deaths (as mentioned previously) that have been documented downstream of the mine in Limpopo Province, sulphate values measured on site far exceeds the average surface water sulphate concentration of 5 mg/l for South Africa (DWAF,1996). Together, DEAT and DWAF worked on a policy to set the framework consisting of functions, institutions and legislation. The goal of this policy is ultimately to control pollution and manage waste altogether. This is of much importance to the mine, seeing that the sulphate discharges to the nearby Ga-Selati River leads to unhealthy drinking water and coincidently the degradation of the natural environment.

Sustainable development is a key consideration regarding legislation involved in pollution control and waste management, (DEAT & DWAF, 1997). For sustainable development to be improved, the focus should be shifted towards a combination of aspects relevant to sustainable development in terms of pollution and waste management. These aspects include pollution prevention (focused on the main source), waste minimisation and lastly remediation, (DEAT & DWAF, 1997). It is of vital importance to focus on "pollution prevention" and not "pollution control", as has been focused on in the past. The reason for this statement is clear and basic; the importance lies in preventing pollution prior to any impact. DEAT & DWAF (1997) mentions that a key aspect regarding prevention lies within the design of mines, particularly in the design of waste impoundments. Seeing that contamination of water sources from the waste impoundments is already an issue in the case of the mine in Limpopo Province, control is understandably the focus for management and therefore of the study as well.

DEAT & DWAF (1997) mentions that a major impact on the health of natural water systems (ground- and surface water) includes salinisation. Salinisation is often caused by mining operation, e.g. AMD and the mobilisation of contaminants by means of surface run-off and infiltration, of which the latter is relevant to this specific study. The effects of salinisation are well documented (Podmore, 2009). Various negative effects of salinisation have been recorded in the past, including degradation of the environment and contaminating drinking water.

2.2 Nature and Properties of Tailings

The following sections refer to the generalised characteristics of waste material, the cover material used on the TSF and the vegetation used for phytostabilisation.

2.2.1 Waste Material

It is important to understand the physical properties of a traditional waste impoundment to accurately investigate the hydraulic properties of the site's waste material. Bhanbhro (2014) describes tailings as being granular material differing dramatically from natural soil. During mineral extraction, the natural state of the soil particles and rock mass is changed dramatically. Rocks are fragmented during this process, subsequently enlarging the surface area (McCarthy, 2011).

According to Rösner (1999), there are three general types of waste material used to create waste impoundments, depending on the waste material size. These structures include TSFs, WRDs and sand dumps, (of which the latter two is not relevant to this study). WRDs tend to consist of country rock and coarse-grained, low-grade rock. The material present in WRDs can't be mined through secondary processes like tailings material and is rather used for construction purposes.

TSFs can have a ratio of water to solids up to 1:1, which indicates a large amount of water that TSFs usually store (Rösner, 1999). Some tailing dams make use of evaporation ponds on top of the tailings dams, as in the case of the TSF referred to in this study.

The layers within a traditional TSF consist of coarse and fine material, divided by a transition zone between them. The grading is an important factor for geotechnical properties which is vital in determining the material's shear strength, particle shape, density and permeability. Construction methods and their placement plays a predominant role in the gradation and ultimately the established characteristics and properties of tailings material. These properties differ largely from those of natural soils due to the shape of traditional tailings particles being more angular than natural soil, (Bhanbro, 2014).

2.2.2 Vermiculite as Cover Material

Vermiculite is the only cover material applied by the mine to ensure sustainable management. Vermiculite is a type of mica and has the composition of 22 MgO. 5 Al_2O_3. FeO. 22 SiO_2. 40 H_2O. (Schoeman, 1989). Vermiculite has a wide range of properties which are hugely beneficial to the rehabilitation of TSFs. These properties include fire resistance, soil aeration, low density and, most importantly, the water holding capacity thereof (Potter, 2002).

Studies on the effects of vermiculite have shown a positive effect on revegetation and reducing cracks, compaction as well as crusting, (Potter, 2002). The application of vermiculite as cover material will thus counteract the negative effects of salts and decrease infiltration due to its water holding capacity. The less water that infiltrates, the fewer contaminants are seeped out. This statement is backed by (Dippenaar, 2014) in a statement emphasising the effect of infiltration on groundwater contamination. According to Dippenaar (2014), ions are mobilised and dissolved, where after precipitation or deposition of these ions take place deeper down into a waste impoundment and is often associated with the contamination of ground water sources. The presence of vermiculite will, therefore, regulate any form of water in such a way that run-off and infiltration are properly balanced.

Raw vermiculite is expensive, which challenges the rehabilitation of large areas. The first vermiculite mining operations in South Africa started at the mine in Limpopo Province, where this study was done. Vermiculite mining was started by Doctor Hans Merensky in 1946 and continues to this day. Therefore, the mine has a rather large supply of weathered vermiculite for everyday use. Vermiculite isn't only used for rehabilitation of waste dumps. The vermiculite blasted at the mine in Limpopo, was transported all over the country and exported overseas, (Schoeman, 1989).

The orebody stretches for a radius of 2 km^2 and reaches a maximum depth of 50 m. The vermiculite orebody was mined by means of open-cast mining with benches not exceeding a height of 5 m. The reserves of the orebody at the mine was estimated to be approximately 56 million tonnes with an average of 21% to 22% of vermiculite, (Schoeman, 1989).

2.2.3 The Formation of Vermiculite

The formation of vermiculite starts with the addition of water and the loss of alkali, and ultimately the hydration of phlogopite. Evidence indicates that the previously mentioned hydration process can be described by the continues percolation of water through the vermiculite mineral. Another factor in the formation of vermiculite is the intense leaching of alkalis (K_2O) within phlogopite while the amount of water drastically increases (Schoeman, 1989).

2.2.4 Vegetation

There are a wide variety of plant species used in South Africa for rehabilitating waste impoundments. One of the main reasons for revegetation is to ensure stability of tailings material through means of mechanical binding of the roots (Edraki *et al.*, 2014). Improving the mechanical properties of tailing material will ensure the productive regulation of passing pollutants and metals by means of absorption (Edraki *et al.,* 2014). Some plant species assist in the uptake of certain metals and pollutants by absorbing groundwater (Neuman & Ford, 2006). As in the case of many other successful rehabilitation plans, the relevant mine has also made use of revegetation on the TSF on which specific tests have been done to ensure the success thereof, (Surmon, 2010). Continuous monitoring from the environmental department at the mine ensures that vegetation on the waste impoundments stays healthy. This is done by ensuring that there are no bare spots, especially regarding basal cover, (Surmon, 2010). Reseeding is the first priority once an area is identified as not fulfilling the requirements in terms of the vegetation status.

According to Surmon (2010), the plant and tree species used to revegetate the waste impoundments all over the mine include *Eragrostis tef*, *Chloris gayana*, *Anthephora pubescens*, *Digitaria eriantha*, *Cynodon dactylon* and *Cenchrus ciliaris*. The tree species used for similar purposes include *Vachelia spp.*, *Bolusanthus speciosus*, *Combretum* and wild sand olives. One key challenge in terms of maintaining these plant species is the continuous issue of animals grazing on the above-mentioned species, (Surmon, 2010). The presence of animals can be explained by the proximity to the Kruger National Park. Animals enter the mine through the river bed, which is not fenced properly, giving the mine a great deal of biodiversity. Even though the wildlife is a challenge, it can also be seen as an advantage. According to Ashmole & Motlaung (2008), the presence of wildlife ensures biodiversity on the mine. Trees like *Vachelia spp.* attract a variety of animals. Baboons, for instance, brings in an abundance of different seeds, which will, in turn, grow and improve revegetation and biodiversity even further. Furthermore, it is important to notice that each of the above-mentioned plant species contribute to rehabilitation in different ways.

2.2.4.1 Eragrostis Tef

Eragrostis tef, also known as “Williams Love Grass”, is perfectly suited for rehabilitation of waste dumps mainly due to the ability of the species to grow in poor quality soil. This species is also known for its ability to adapt in conditions where climate and soil conditions tend to vary significantly. *Eragrostis tef* even flourishes in sandy soils with a low pH and has trouble growing in wet, waterlogged soils, (Truter *et al.*, 2014). This statement emphasises the effectiveness of *Eragrostis tef* to flourish in TSF’s. Not only is this species well suited for low-quality soils, it also tends to improve the quality by some degree. The vigorous root system that this species have is one of the factors contributing to the decrease of erosion in sandy soils due to mechanical binding of particles. *Eragrostis tef* has also been proven to increase the amount of organic matter, (Truter *et al.,* 2014).

2.2.4.2 Vachelia spp.

The *Vachelia* species are becoming ever more popular in rehabilitation due to its ability to grow with great ease in infertile, saline and acidic soils. *Vachelia* is known to improve soil structure and fertility and are therefore commonly used in mining for rehabilitation purposes (Brockwell *et al.,* 2005).

2.2.4.3 Chloris gayana

Chloris Gayana, also known as “Rhodes grass”, is suited for rehabilitation purposes in a sense that it is tolerant of saline conditions, (Morgenthal, 2003). *Chloris Gayana* has also been proven to be generally widely adaptable with a high seed production, (Nel *et al.,* 2015).

2.2.4.4 Anthephora pubescens

Anthephora pubescens, also known as “Wool grass”, is proven to be highly palatable for grazing animals, therefore attracting animals and ultimately increasing biodiversity in the area. *Anthephora pubescens* grows easily in soils with low nutritional value with a high resistance to drought, (Westcott, 2011)

2.2.4.5 Digitaria eriantha

Truter *et al.,* (2014) mentions that *Digitaria eriantha*, also known as “Smuts finger” is a plant species adapted to a variety of climatic conditions. *Digitaria eriantha* is also known to grow in almost any soil, regardless of the quality.

2.2.4.6 Cynodon dactylon

Cynodon dactylon has a high tolerance level for high levels of copper and spreads extremely fast after planted and acts as an incredibly good form of cover, (O’Connor & Granger, 2014). O’Connor & Granger (2014) further mentions that *Cynodon dactylon* is tolerant to a large variety of factors, including fire, drought, physical damage, heavy metals and heat. *Cynodon dactylon* is extremely drought resistant due to its ability to grow root systems up to 2 m long, (Reza, 2016).

2.2.4.7 Cenchrus ciliaris

Cenchrus ciliaris, also known as “Buffel grass”, is extremely drought and grazing tolerant, (Jackson, 2004). These strengths are present as a result of the species stem bud development that is slightly below ground level. Another clue lies behind a deep penetrating root system, (Jackson, 2004). *Cenchrus ciliaris* has been known to absorb a high concentration of carbohydrates due to a swollen stem. This ability ensures that the plant greens up much easier, ensuring fire and drought tolerance, (Jackson, 2004).

Cenchrus ciliaris is adaptable in a wide variety of soils, requiring little nutrition with an easy establishment, (Jackson, 2004). This species does also have a slight tolerance for salts, which might be an issue on certain waste impoundments, (Jackson, 2004).

2.3 Hydraulic Properties and Processes of Tailings

Hydraulic characteristics play an integral part in predicting fluxes and flow paths. These characteristics are unique for tailings material given the degradation of particles during the processing phase. The following hydraulic characteristics are applicable to this particular study.

A study completed by Kim & Mohanty (2016) emphasises on the importance of various hydraulic properties in the successful predictions of lateral subsurface flows.

2.3.1 Infiltration

Infiltration is defined as the entry of water in soil due to gravitational movement (Mazaheri & Mahmoodabadi, 2012). To predict infiltration rates in different soil profiles, one key characteristic is required, namely particle size distribution (PSD), (Mazaheri & Mahmoodabadi, 2012). The infiltration rates are also reliant on the nature of hydraulic conductivity as well as soil texture classes present.

Mazaheri & Mahmoodabadi (2012) use double ring infiltrometers to determine infiltration rates. The reason for using this method is quite simply due to its simplicity and convenience. Additionally, extracted soil samples from each site are used to determine the PSD from the specific soil/tailing material. PSD is divided into two main categories: primary particle size distribution (PPSD) and secondary particle size distribution (SPSD). PPSD involves soil textural classes, which is used as diagnostic characteristics in most classification schemes. These textural classes include sand, silt and clay. SPSD characterises PSD in terms of aggregates, and specifically aggregate sizes. The larger aggregates in a specific soil profile are, the larger the macropores between these aggregates will be and thus the higher infiltration rates involved would be (Mazaheri & Mahmoodabadi, 2012). Mazaheri & Mahmoodabadi (2012) mentions that hydraulic properties, including PSD, is vital to understanding and ultimately controlling infiltration, runoff rate as well as the migration of contaminated plumes.

A study presented by Rumynin (2015) focusses on infiltration during a study on surface run-off as well as sub-surface flows to determine the transfer of boundary conditions. The rate at which the water enters the soil is known as the infiltration rate. The infiltration rate in a soil that has a rather large degree of cracks, macropores etc. would be far higher than that of a densely packed soil profile, (Rumynin, 2015). The nature and properties of infiltration in each soil profile is therefore vital in understanding the nature of run-off and sub-surface flows.

According to Casanova (1998), various limits exist in measuring infiltration *in-situ*, of which topography (the gradient of the slope), the presence of large abnormal macropores, sealing conditions (crusting and/or compaction) and aspect. Casanova (1998) continues to emphasise on the possibility of sealing conditions as a result of droplet impact.

2.3.2 Water Retention Capacity

Water retention characteristics are traditionally determined in a laboratory for repacked samples of the tailings and cover material. The soil water potential of one bar is measured with the use of a controlled outflow cell apparatus. As per personal communication with Professor Simon Lorentz, the vermiculite on-site (the material covering the TSF) has a higher water retention capacity than the tailing material with a value between the tailing material and a Hutton soil form. Water retention capacity is proportionate to the amount of clay present in the relevant material. This phenomenon is due to the presence of menisci and micropores which generates capillary forces, (Reichert *et al.,* 2009).

Furthermore, clay increases the soil matrix's specific surface area, ultimately increasing the adsorption ability of aggregates. The two factors, capillary and adsorption forces directly influence the water retention capacity, (Reichert *et al.,* 2009). Soils that favour adsorption and capillary conditions, will have a rather high water retention capacity.

2.3.3 Volumetric Water Content

According to Kim & Mohanty (2016), volumetric water content (VWC) plays a significant role in the estimation of lateral sub-surface flows. VWC is defined as being water held within pores, both in the vapour phase and liquid phase (Mweso, 2003). VWC is related to various hydraulic characteristics and is directly proportionate to hydraulic conductivity, (Mweso, 2003).

In this study, VWC is determined through VWC sensors installed at all slope components at depths of 100 mm, 500 mm and 1 000 mm below the surface. These sensors, known as TDR sensors, are joined to a Campbell Scientific TDR 100 wave generator/response analyser. This device delivers a VWC and bulk Electrical Conductivity (EC) measurement to a CR800 logger at pre-set intervals via co-axial cables.

2.3.4 Hydraulic Conductivity

According to Kim & Mohanty (2016), similarly to VWC, hydraulic conductivity is key in understanding lateral sub-surface flows, of which the success thereof has been well documented. Mweso (2003) defines hydraulic conductivity as the rate at which water moves through soil, which acts as a porous medium. According to Bevan & German (1982), hydraulic conductivity would be substantially higher in a soil profile characterised by large macropores, cracks, bio pores etc., seeing that the percolation of water in such a profile would far exceed that of a densely packed soil profile. Hydraulic conductivity is a key factor in understanding a variety of environmental challenges, i.e. ecological challenges, issues with soil, environmental pollution etc., which are similar to those challenges experienced by the mine in Limpopo Province. Hydraulic conductivity is directly influenced by certain characteristics, namely structural characteristics, organic matter as well as texture. Hydraulic conductivity of soil or tailing material is directly proportionate to the degree of water content available in the material, (Mweso, 2003).

Prior to this study, Guelph permeameters, tension infiltrometers and double ring infiltrometers have been used to determine the hydraulic conductivity of the material present at all slope component sites. Guelph permeameter and double ring infiltrometers were used to determine the saturated hydraulic conductivity (*Ks*), whereas tension infiltrometers were used to determine the material's unsaturated hydraulic conductivity. Kim & Mohanty (2016) furthermore mentions that hydraulic conductivity for a study of this nature should normally be derived according to soil texture by means of various equations including the relevant van Genuchten equation, of which the latter is also made use of for this study. Only *Ks* was used for this study given its importance in parameterising the *HYDRUS-2D* tool and predicting sub-surface flow paths.

2.3.5 Percolation

The internal drainage in soil or tailing material is termed percolation (Smiley & Martin 2016). Of the total amount of precipitation falling on a soil or tailings surface, only a fraction thereof is infiltrated. The rest either runs off via overland flow or is evaporated prior to accumulation. Of the total amount infiltrated, a sizable percentage is taken up by vegetation, and the remainder is percolated vertically through the porous medium, (Hunt *et al.,* 2017).

2.4 Effectiveness of Hydropedology in Assessing the Nature of Sub-Surface Flows

Water, in the form of irrigation or precipitation, infiltrates waste covers and percolates through the porous medium, absorbing organic and inorganic matter in the process (Vale *et al.,* 2017). Preferential flow is defined by Bruggeman (1997) to be the internal flow of water in a structured soil via small-scale pathways within a soil matrix due to different gradients, gravitation and most importantly macropores within. A structured soil is characterised by the nature of flow and is dependent on the size, continuity and geometry of macropores present (Bruggeman, 1997). This phenomenon is a healthy way of distributing organic matter and nutrients throughout the soil, although sometimes, as in the case of waste impoundments, contaminants might be dissolved and transported, (Vale *et al.,* 2017). This process stresses the negative impact of leaching contaminants into underground water sources by means of percolation, stressing the need for accurate predictions regarding this aspect. Therefore, the importance of hydraulic properties in parameterisation models like the *HYDRUS-2D* tool lies in the nature hydropedology itself.

2.5 Methods to Study Hydraulic Properties and Processes

Various methods exist to determine hydraulic properties, of which all have their advantages and limitations. Depending on the desired outcome and unique soil conditions, some techniques are more relevant than others.

2.5.1 Physically Based Modelling

A study on the contamination of healthy water systems nearby a TSF, as the source of contamination, was carried out by (Puhalovich *et al.,* 2012). This study shows similar intentions than those for the current study by using different programmes and modelling software. Instead of using the physically based *HYDRUS-2D* model that was used during this particular study, one- and three-dimensional modelling have been chosen for the Puhalovich *et al.,* (2012) study. Similarly, the intended goal was to quantify and assess seepage flux rates, solute migration, general seepage mechanisms and the possible implications thereof. Puhalovich's study was proposed due to management recognizing that groundwater sources are being heavily influenced by seepage processes from the TSF on site. Assumptions have been made that point toward increased levels of seepage and overall solute transport in the wet season. Additional to seepage flux rates and solute migration, tailing consolidation, as well as pore pressure changes, have been determined.

Solute transport is a key aspect of this study, to ensure successful predictions are made regarding the transport of contaminated plumes. Glaesner & Gerke (2013) completed a study on solute migration through different soil mediums with infiltrating water containing traces of manure. The ultimate goal was to predict the leaching of plant nutrients that potentially might cause eutrophication, which in this case is represented by similar methane traces to those that would be found in manure. The authors made use of similar modelling than those described to investigate solute mass exchange and solute transport between the surface and pore water regions. By implementing the *HYDRUS-1D* numerical code, single and double porosity models where implemented within this numerical code. Bromium and titanium were used in this case as tracers with the option of a fixed bottom seepage face value. Even though all of the modelling for the mine in Limpopo Province's case was done by means of the *HYDRUS-2D* programme, the *HYDRUS-1D* model being described by (Glaesner & Gerke, 2013) could also be used for solute migration with great success.

Predictions of preferential flow are extremely difficult due to the heterogeneity of soil layers, necessitating the need for hydrological models to successfully predict the movement of water through soil matrix (Vale *et al.,* 2017). Vale *et al.* (2017) recently made use of a 1-D dual permeability model. This model illustrates seepage fluxes through macro pores which are useful in determining the nature of flow through either soil or tailing material. As in the cases of the above-mentioned models used for prediction, this 1-D permeability model requires parameters to ensure successful simulation. These parameters are characterised by various hydraulic properties. Water retention, soil diffusivity functions and parameters regarding macropore flow are all properties used to calibrate this model. This data is somewhat expensive and time-consuming to collect, potentially bringing inverse modelling into action to provide assistance. This model can be used to improve simulations in the HYDRUS-1D, 2D (as is used in this study) and 3D models, (Vale *et al.,* 2017).

The *HYDRUS-3D* package uses dual porosity models to define water flow by restricting the water flow to macropores and assuming that the water in the matrix is stagnant, (Šimůnek *et al.,* 2008). Similarly to the *HYDRUS-2D* model, the formulation of the dual porosity model regarding water flow is defined by the Richards equation. The dual permeability model, on the other hand, is defined by those equations suggested by van Genuchten which ultimately helps define solute transport, (Šimůnek *et al.,* 2008). This model, owing to the similarities between the latter and the *HYDRUS-2D*, would be just as efficient.

Similarly to the *HYDRUS-2D* model used for this study, by assuming various tailing hydraulic conductivities as well as a “free drainage” layer, predictions were made regarding the potential amount of vertical seepage flux rates, (Puhalovich *et al.,* 2012). A transport and numerical flow model were developed in this study using the computer programme called FEFLOW (version 6), which was developed by the Wasy Institute. FEFLOW is used to simulate 3-D solute movement and groundwater flow by means of a finite element modelling code. Elevated hydraulic conductivities in regions characterised by faults are assumed to contribute to the success of this simulation. Seepage rate, specific yield and storage were used for the calibration processes. Ultimately, applied seepage rates appropriate to groundwater levels were compared to measured data to ensure that the most likely scenario representing seepage and migration of contaminated plumes are identified, (Puhalovich *et al.,* 2012). The end results of this study and the one undertaken in Limpopo are very similar. One key difference lies in the inclusion of remedial options. As in the case of the current study, various remedial measures are included in the simulation after different flow paths are identified. These flow paths will be individually simulated and illustrated by 2-D longitudinal transects.

A finite, physically-based element model, called MICMAC, was used with great success by Bruggeman (1997) to predict the solute transport and flow through the soil matrix and macropores in general. The convection-dispersion and Richards equation was used by Bruggeman (1997) to describe solute transport and flow. Flow through macropores, on the other hand, was determined by the Hagen-Poiseuille equation. Flow and solute transport from the macropores present in a soil medium to the all surrounding soil matrix was simulated by means of an axisymmetric coordinate system, (Bruggeman, 1997).

1-D consolidation modelling has been done by using the PLAXIS-2D software package, (Puhalovich *et al.,* 2012). This programme simulates anisotropic, non-linear and time-dependent soil or tailing material behaviours. This simulation is done after measuring water levels in the covers, (Puhalovich *et al.,* 2012). The characteristics of the tailing material are based on laboratory and *in-situ* data. Additionally, tailings were modelled using a model called "the hardening soil model," (Puhalovich *et al.,* 2012). This model is used to account for an increase in tailing material stiffness because of compression. The relationships between effective stress versus tailing porosity make up part of the simulation. Ultimately, the seepage flux is calculated with changing hydraulic conductivity, which is related to effective stress resulted due to consolidation processes, (Puhalovich *et al.,* 2012).

Even though, as discussed, various tool exists in the prediction of various flow paths, the *HYDRUS-2D* tool was used in this study.

The combined effects of water input and soil temperature on water redistribution and water flows have been documented by Nakhaei & Šimůnek (2013). Regardless of the software used, they followed a similar approach to that of this particular study. The van Genuchten hydraulic characteristics were one of the main areas of focus (Nakhaei & Šimůnek, 2013). Additionally, heat transport parameters have also been a key aspect in their study, from which temperature probes have been measured. Similarly to the data accumulation prior to this study, double ring infiltrometers have been used in the (Nakhaei & Šimůnek, 2013) study to determine relevant hydraulic characteristics. To ensure the successful simulations of fluxes through the vadose zone, soil hydraulic properties of the material/soil need to be determined to ensure successful parameterisation of these models, (Vrugt *et al.,* 2008). These properties, i.e. hydraulic conductivity and water retention is traditionally determined in a laboratory environment after sampling and *in-situ* measurements. This method of sampling and measurement, however, is incredibly time-consuming, stressing the need for an alternative approach, (Vrugt *et al.,* 2008).

Weiler (2017), on the other hand, emphasises key aspects, which is well documented by the likes of Bevan and German (1982) with the intent of criticising physically based models relying on the Richards equation to define capillary movement. According to Weiler (2017), physics suggests that the Richards equation is not an accurate representation of hydrological flow processes through a soil matrix that is heterogenic of nature. Weiler also continues to make statements including; models following the same approach fails to accurately and consistently predict infiltration rates successfully and that models tend to give inaccurate results during high rainfall events due to the importance of preferential pathways through cracks, fractures and macropores.

The relevance thereof lies in the fact that a similar physically-based model (*HYDRUS-2D*) is used for this study to quantify and assess lateral sub-surface flows by means of the Richards equation, which according to (Weiler, 2017) is not scientifically correct. The previous statement by (Weiler, 2017) is also troubling in the sense that high rainfall events is one of the most important aspects involved in this study and is one of the aspects most criticised by (Bevan and German, 1982). Bevan and German (1982) were one of the first to recognise the importance of preferential flows and macropores. According to Weiler (2017), Keith Bevan also recognised the importance of preferential flow paths for run-off purposes, which is a major part of the assessments done on the mine in Limpopo Province. The *HYDRUS-2D* software gives a fairly accurate representation of flow paths with the reliance on accurate hydraulic properties used to back results and to successfully parameterise the model. Additionally, Weiler (2017) admits that the models relying on the Richards equation is quite successful when it comes to root uptake, slow water redistribution and soil evaporation which is all important aspects in this.

2.5.2 Evapotranspiration

Evapotranspiration is essential in ensuring an accurate representation of climatic conditions relevant to the atmospheric boundary set-up in the *HYDRUS-2D* tool. According to Dippenaar (2014), in addition to percolation, lateral movement of water and overland flow, evapotranspiration plays a significant role as one of the major flow paths within a soil profile, which emphasises the need for accurate measurements in regard to evapotranspiration.

According to Sing *et al.* (2008), four main types of evapotranspiration exist and can be used to define evapotranspiration conditions:

(1) Free water evaporation defines the process of which water is evaporated from open water sources (i.e. lakes, oceans etc.) and is returned directly to the atmosphere.

(2) Actual evapotranspiration described those processes involved in returning water within the surface or near-surface to the atmosphere. This process is applicable to natural conditions only.

(3) Reference evapotranspiration is defined as "the rate of evapotranspiration from a hypothetical reference crop with an assumed height of 0.12 m and a fixed surface resistance of 70 sec m^{-1} and an albedo of 0.23, closely resembling the evapotranspiration from an extensive surface of green grass of uniform height, actively growing, well-watered, and completely shading the ground".

(4) Potential evapotranspiration is defined as "the amount of water transpired in a given time by a short green crop, completely shading the ground, of uniform height and with adequate water status in the soil profile".

Various methods exist in determining potential evapotranspiration, of which most rely on monthly or daily temperatures, which according to (Rijtema, 1965) is not accurate enough to successfully determine evapotranspiration processes. Makkink (1955) incorporated air temperature and radiation to determine evapotranspiration, Turc (1957) used temperature, rainfall and radiation to determine evapotranspiration whereas Haude (1952) makes use of empirical formulas. These formulas are based on the saturation deficit at 14:00. Lastly, the Penman-Monteith equation was set-up to determine evaporation from soil and transpiration from vegetation by incorporating aerodynamics and energy balance, (Zotarelli *et al.,* 2010).

Evapotranspiration then needs to be split into evaporation and transpiration given these two component's roles in parameterising the *HYDRUS-2D* tool. The potential evapotranspiration calculated is divided into potential evaporation and potential transpiration by means of the dual crop coefficient (Allen *et al.,* 2006).

2.5.3 Volumetric Water Content

According to a set of instructions set up by Campbell for Decagon Devices, Inc., various methods exist in determining the VWC of a soil profile, namely (1) direct water content measurements, (2) the neutron thermalization probe, (3) dual needle heat pulse and (4) the Time Domain Reflectometry (TDR) instrumentation.

2.5.3.1 Direct Water Content Measurement

Direct water content measurement is a common method and entail sampling, weighing the sampled soil, drying the sample at 105°C and weighing the sample after drying to determine the difference (which will be the calculated VWC). According to (Campbell, 2010) the advantages of this methodology is that it is inexpensive, measurements are direct and that the methodology is simple. Disadvantages include time restraints and the fact that an oven is required to dry the soil samples.

2.5.3.2 Dual Needle Heat Pulse Technique

The dual needle heat pulse technique is based on the principle that changes in heat within a soil profile is strongly dependent on the VWC of a soil profile. A dual needle probe includes a heater on the one needle and a temperature measuring device on the other. Maximum temperature rise is then used to calculate the heat capacity, which in turn can be converted to VWC, (Campbell, 2010). The advantages of this technique include the fact that this technique can measure VWC around a growing seed and that a small volume is enough to successfully calculate VWC. Disadvantages include the fact that a data logger is required, which requires precise temperature analysis and measurements. This technique can be susceptible to temperature gradients within a soil profile dependent on both depth and time, is fragile and integrates small soil volumes.

2.5.3.3 Neutron Thermalisation Probes

Neutron thermalisation probes make use of a radioactive source, a low energy detector and releases neutrons into the soil to interact with hydrogen atoms in the soil. Hydrogen subsequently slows these neutrons down after which this data is used to determine the VWC, (Campbell, 2010). A hole is quite simply augered after which a tube is installed and lowered to specific depths for measurements to be taken. Advantages include the measurement of large volumes, the insensitivity of this methodology to salinity and temperature and the fact that a single instrument can measure multiple sites. Disadvantages include the expensiveness of the instrument, the weight of the instrument, the fact that the instrumentation requires a radiation certificate to operate and that no continues record is obtained, (Campbell, 2010).

2.5.3.4 TDR Instrumentation

TDR instrumentation was used for this study due to its ability to give an accurate and immediate reading of the available VWC (Panuska *et al.,* 2015). Campbell (2010) mentions that other advantages include the insensitivity of calibration to textural differences, the fact that this instrument is accurate, is insensitive to changes in salinity (unless EC is high) and the fact that output waves provide information about the electrical conductivity. Disadvantages include the expensiveness of this instrumentation, the fact that a waveform analysis is required, the ineffectiveness of this instrument under high EC conditions and the sensitivity to gaps in soil. According to Campbell (2010), this instrumentation measures apparent length (La) of a probe from an electromagnetic wave which is spread along metallic rods. The measured apparent length is then related to epsilon (ε) and indirectly to VWC (Figure 1 and Figure 2) By calibrating the electrical and magnetic dissipation and storage, the available soil moisture within the soil is calculated, (Panuska *et al.,* 2015)**.** Firstly, an electromagnetic pulse is injected into the soil profile, (International Agency of Atomic Energy, 2008). The time that the pulse takes to travel along this cable is determined by the bulk electrical conductivity of the soil. A waveform is captured to determine the highest frequency of the pulse.

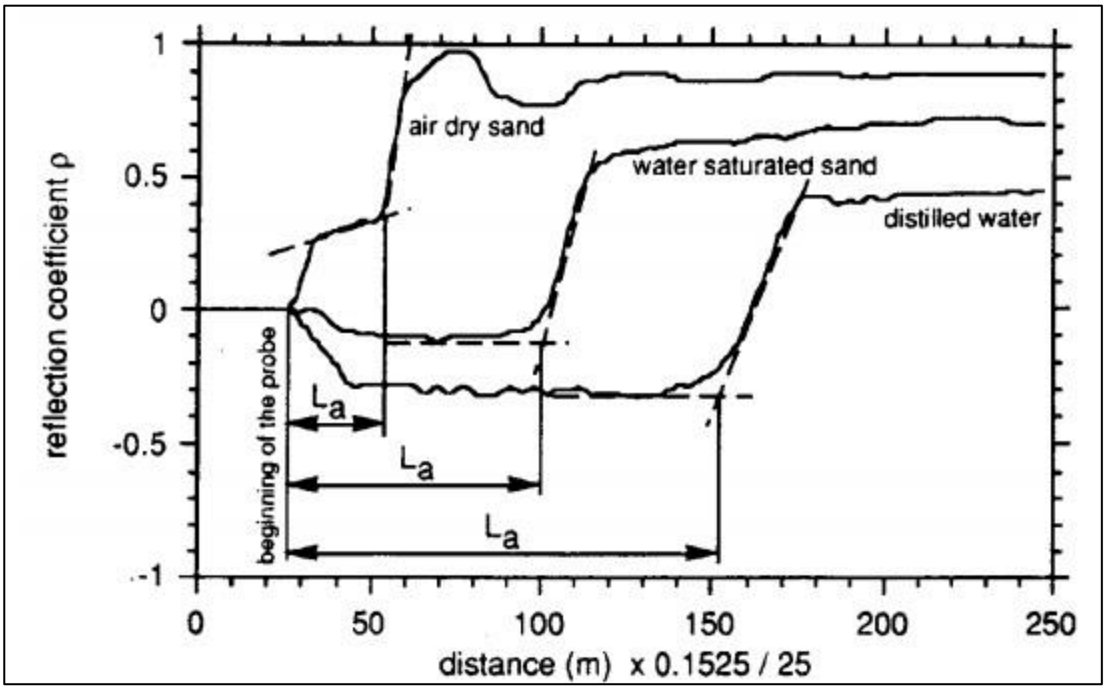

Figure 1: Graph relevant to measurements by the TDR instrumentation, (Campbell, 2010).

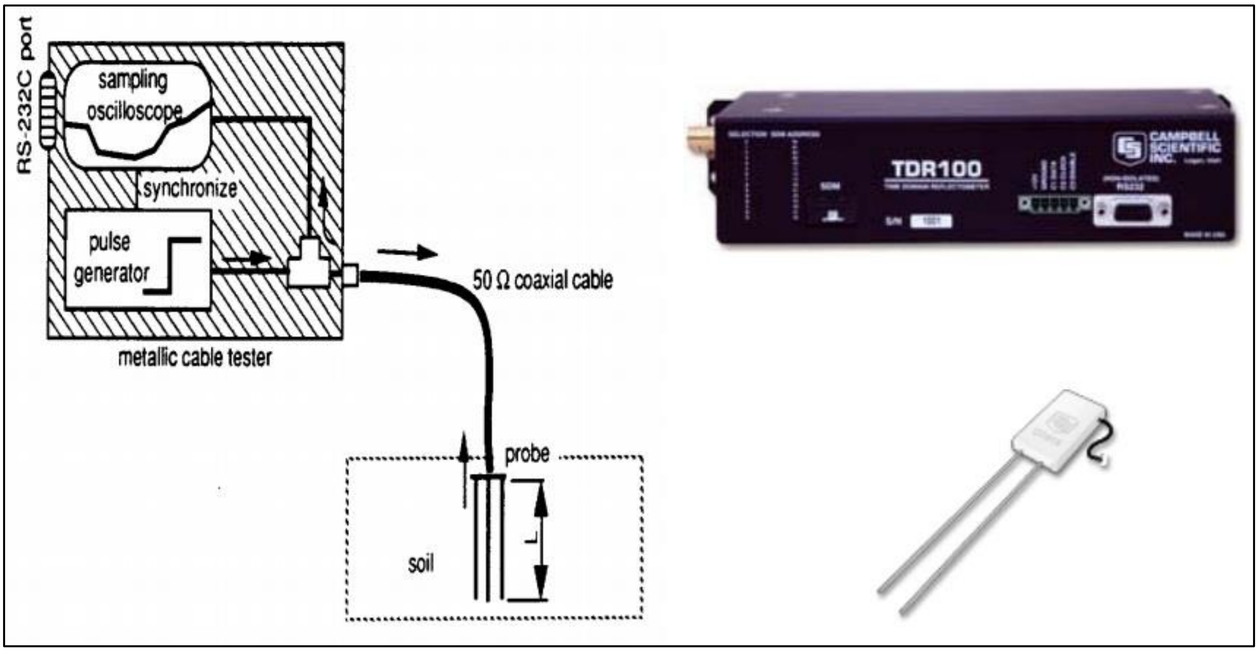

Figure 2: TDR instrumentation layout, (Campbell, 2010).

2.5.4 Overland Flow

Overland flow is defined as the movement of water over a surface as a result of the precipitation rate exceeding the infiltration rate of a soil (Liu *et al.,* 2004). A set-up of a run-off plot is illustrated in Figure 3. Rainwater falling within the galvanic sheets flows downwards to a trough, constructed with the same galvanic steel. Once the water is gathered in the trough, it is redirected towards the tipping bucket, which has a mechanism attached which records every tip from this tipper bucket. ROPs are ultimately used to measure the flow rate and volume of overland flow. The splitter box and accumulation are used for another phase of this study and is irrelevant to the findings of this study.

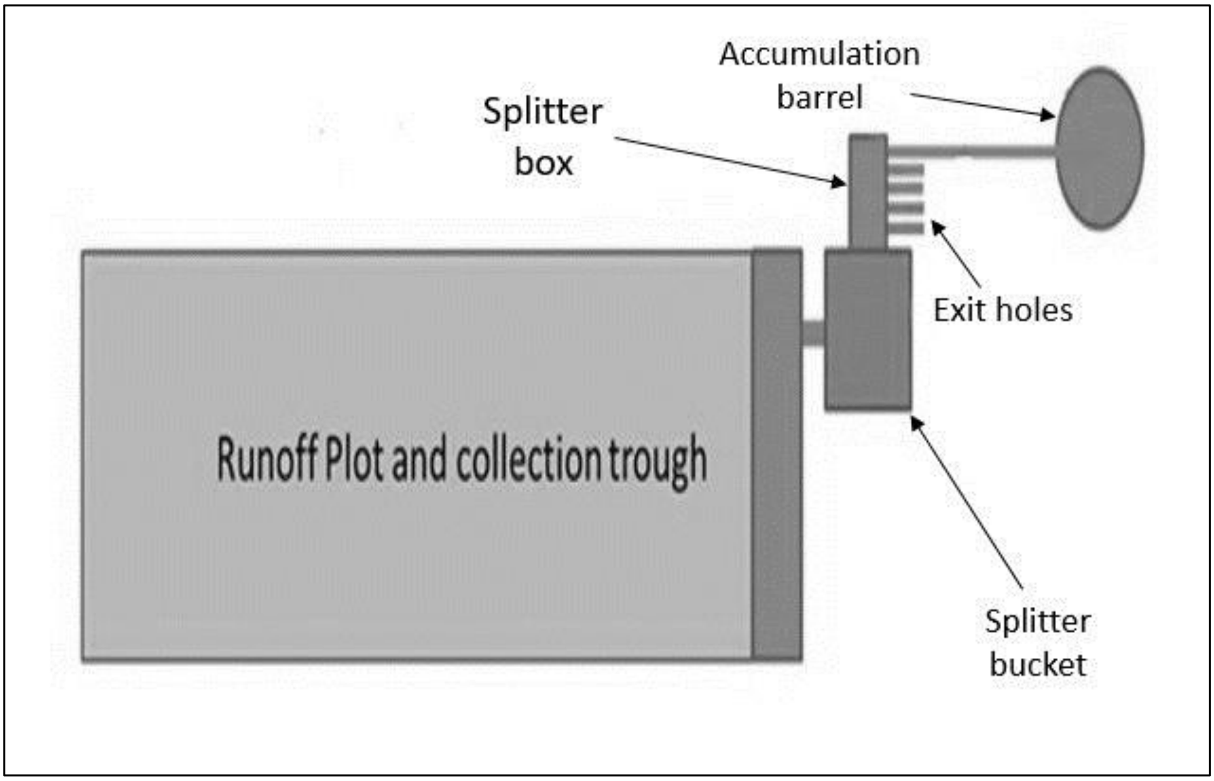

Figure 3: A theoretical example of the methodology behind a run-off plot

2.6 Seepage Control Measures

According to Omofunmi *et al.* (2017), there are various seepage control measures used by engineers to reduce seepage, ultimately avoiding the contamination of nearby water sources and ensuring the stability of waste impoundments. These include grout curtains, cut-off trenches, toe drains and relief boreholes.

2.6.1 Grout curtains

According to Bruce *et al.* (2008), grout curtains are unique seepage control measures that are extremely sensitive with regard to proper construction and planning. The party responsible for the construction of this control measure must be experienced in grout curtain installation due to the fact that a lack of knowledge will result in environmental degradation and financial loss.

Grout curtains are implemented by drilling holes in strategically placed locations to fill up geological features characterised by cracks which channels discharge water from structures to natural water sources (Engemoen, 2012). This seepage control measure might be valuable for studies assessing discharge by assessing geological features and using 3D modelling to detect specific problem areas pertaining to geological features. Therefore, this control measure will be excluded from this assessment.

2.6.2 Cut Off-Trenches

Cut-off trenches are constructed by excavating at a specific location to cut-off seepage at the pathway. In cases referring to vast amounts of seepage from large impoundments, Engemoen (2012) recommends thin foundation cut-offs like a diaphragm wall due to the cost effectiveness thereof. According to Engemoen (2012), such a trench must be at least 6 m deep with the width of such a trench calculatable with eq. 1.

Equation 1: Width of the trench [1]

$$W = H - D$$

Where:

W= the bottom width of the cut-off trench;

H= the reservoir head above the ground surface; and

D= the depth of the cut-off trench bellow surface.

According to Rezagholilou (2006), there are three main types of cut-off trenches, including slurry trenches, compacted backfill trenches and concrete wall trenches. These trenches should be constructed at the base of the waste impoundment and excavated through the impermeable layer to accumulate vertical seepage.

2.6.3 Trench Drain

According to Rezagholilou (2006), trench drains consist of a perforated collector pipe within an excavated area, which is backfilled with a certain filter material. This control measure is applicable to situations where the top alluvium is thin, and the underlaying impermeable layer is shallow, subsequently allowing the penetration of the aquifer. Not penetrating the aquifer will leave this specific seepage control technique ineffective, (Rezagholilou, 2006).

2.6.4 Relief Boreholes

Relief wells are most efficient in cases where the foundation consist of an impermeable geological layer. This control measure increases the seepage quantity by 20 to 40% and concentrates it to a specific area to control and treat these fluxes, (Rezagholilou, 2006).

2.6.5 Downstream Seepage Berms

According to Rezagholilou (2006), downstream seepage berms are installed downstream of a waste impoundment to reduce uplift pressure from the pervious foundation underneath the waste impoundment. This technique is incorporated with that of relief boreholes and toe trench drains and is used to control under seepage efficiently. This measure is useful in situations where the top stratum downstream is relatively thin and uniform or where no top stratum is present, (Rezagholilou, 2006).

2.6.6 Shallow Boreholes

These systems are applicable only to shallow systems and can be constructed in two different ways, namely per hand and via heavy machinery (Collins, 2000). Those systems dug by hand have various risks associated therewith and will not be applicable to the mine under investigation due to the rocky nature of the soils. The latter mentioned has large diameters which will threaten the livelihood of animals due to the ease of which these systems collapse. According to Collins (2000) construction via heavy machinery, a drill rig can allow for a small diameter without only the exception of large felsic geological features and dolomite troubling the drilling system.

Chapter 3: Study Area and Methodology

3.1 Study Area

The study area is situated in Limpopo Province, alongside the Ga-Selati River and the Olifants River confluence. The Olifants River flows directly into the Kruger National Park, emphasising the need to minimize any source of water contamination due to strict regulations regarding pollutants entering the park. The Olifants River suffers from a variety of pollution sources contributing to the unacceptable level of water quality (De Villiers & Mkwelo, 2009). The layout of the mine and the adjacent river systems has not been presented to ensure that the identity of the mine stays undisclosed.

3.1.1 Vegetation

According to Mucina & Rutherford (2006), the project area is located within the Lowveld Rugged Mopaneveld (SVmp6) vegetation type. The Lowveld Rugged Mopaneveld is distributed throughout Mpumalanga and Limpopo and includes broken veld south of Giyani. The Lowveld Rugged Mopaneveld stretches further from Giyani to the west and east. The western parts include Shimuwini and the eastern area includes Boulders Camps. The southern parts of Phalaborwa which include the Olifants River is characterised by this vegetation type, which is the main focus of this study. The altitude for the Lowveld Rugged Mopaneveld is 250 meters above sea level to 550 meters above sea level.

The area characterised by the Lowveld Rugged Mopaneveld has slightly to extremely irregular plains with the addition of several large hills and steep slopes. The areas surrounding the Olifants River has steeper ridges and slopes with barely any ground cover and limited trees. The vegetation in the northern parts tends to be more open with the inclusion of parts of the Kruger National Park. Areas isolated from veld fires by means of rocky outcrops tend to have dense growing tree patches, as in the case of some areas surrounding the Olifants River (Mucina & Rutherford, 2006).

The conservation status of the Lowveld Rugged Mopaneveld is of least concern with 34% of the vegetation type being protected within the boundaries of the Kruger National Park. Other smaller, private reserves contribute to another 5% of the Lowveld Rugged Mopaneveld is protected, including Klaserie, Letaba Ranch and Selati Game Reserve. Most of the remainder of the area is transformed into agriculture and urbanised areas. It is worth noting that the parts of the Kruger National Park enclosing the Lowveld Rugged Mopaneveld includes rather rare species of vegetation that is not found in other areas of the park, such as *Kirkia wilmsii* and *Hexalobus monopetalus* (Mucina & Rutherford, 2006).

As in the case of any rehabilitation plan, the mine focuses on phytostabilisation as key rehab method. Species used to revegetate the impoundments on the study site includes *Eragrostis tef, Chloris gayana, Anthephora pubescens, Digitaria eriantha, Cynodon dactylon* and *Cenchrus ciliaris*. The tree species used for similar purposes include *Vachellia spp., Bolusanthus speciosus, Combretum* and wild sand olives (Surmon, 2010). One key challenge in terms of maintaining these plant species is the continuous issue of animals grazing on grass species and destroying tree species, both saplings, and mature trees, (Surmon, 2010).

The presence of animals can be explained by the close proximity to the Kruger National Park. Animals enter the mine through the river bed, which is not fenced properly, giving the mine a great deal of biodiversity. Even though the wildlife can be seen as a challenge, it can be extremely beneficial to the rehabilitation of the mine. According to Ashmole & Motlaung (2008), the presence of wildlife ensures biodiversity at the mine. Trees like the *Vachellia* attract a variety of animals. Baboons, for instance, bring in an abundance of different seeds, which will, in turn, grow and improve revegetation and biodiversity even further (Ashmole & Motlaung, 2008).

3.1.2 Climate

The area's climate is characterised by warm temperatures, ranging between 23˚C and 35˚C, (John *et al.,* 2012) and reaching temperatures up to 45˚C, (Hitsinani, 1999). The average minimum temperature during the colder months ranges between 10˚C and 12˚C. The area receives a summer rainfall (between October and March) of approximately 570 mm per year and an average evaporation of 2 130 mm per year, (Munnik *et al.*, 1996). The evaporation potential therefor exceeds the annual rainfall in this dry subtropical climate, (Munnik, Verster & van Rooyen, 1996).

3.1.3 Geology

Phalaborwa's geological history is characterised by the Phalaborwa Carbonatite Complex (PCC). This complex is located in the western boundary of the Kaapvaal Craton with close proximity to the Bushveld Igneous Complex (BIC) (Figure 4). The Kaapvaal Craton is responsible for the rise of two mineral-rich complexes formed millions of years ago called the BIC and the PCC, (Burger, 2013). The Archean Basement Gneisses was intruded by the PCC at approximately 0.5 Ma. This intrusion took place in several alkaline cycles, which emplaced a suite of rocks in successive stages, ranging from peralkaline to ultramafic, (Letts, 2007).

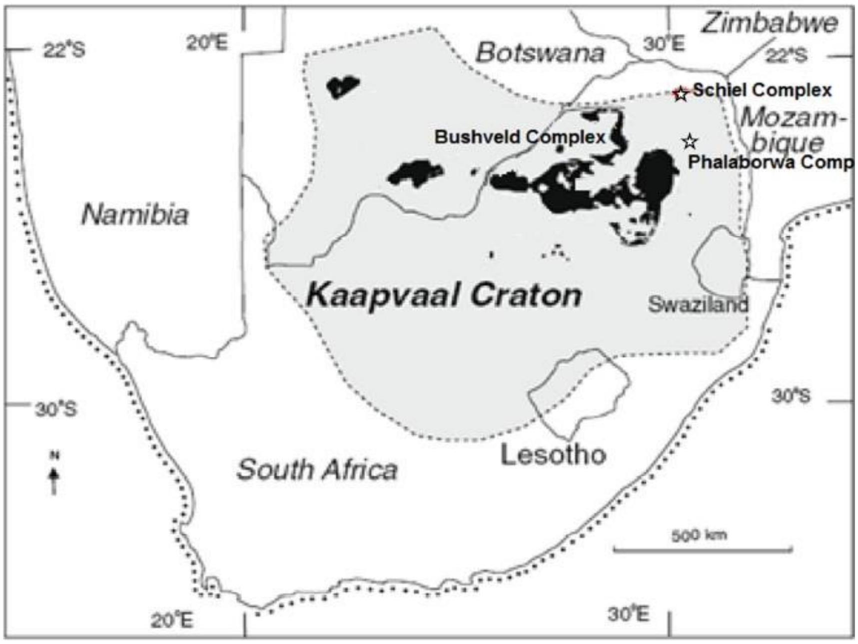

Figure 4: Location map of Kaapvaal craton, BIC and the Phalaborwa Complex (Burger, 2013).

The pyroxenite pipe-like body intrusion was the first of these phases. The phase that followed this intrusion was alkaline, in which the surrounding syenite bodies were emplaced. Foskorite and banded carbonatite was emplaced at a much later stage, followed by an intrusion of transgressive carbonatites (Letts, 2007).

The PCC consists predominantly of pyroxenite, foskorite, carbonatite and is associated with syenite and granites with mineralisation being characterised by Copper (Cu) and Zirconium (Zr) (Burger, 2013). A more recent study regarding paleomagnetic research of the PCC, describes the PCC being elongated-kidney shaped (Letts, 2007). The above-mentioned pyroxenite body is in the form of a vertical pipe, whereas the foskorite body is more oval shaped (Letts 2007). The PCC consists of a copper-bearing carbonatite intrusion in the centre of the complex, called the Loolekop carbonatite pipe (Burger, 2013).

Phalaborwa has a rich mining history, predominantly because of the high amount of economically valuable minerals the PCC entails. This vast range of minerals includes copper, phosphates, vermiculite, magnetite zirconium, uranium, nickel and gold. These days, the mine at which this specific study takes place focusses on vermiculite as well as secondary products of magnetite and nickel. The mining company involved in this study has been mining copper from carbonatite since the closure of the open pit mine in 2002 (Burger, 2013).

3.2 Methodology

Detailed descriptions of methodological processes and instruments involved have been described in Section 2.5-“Methods to Study Hydraulic Properties and Processes”. The following aspects therefore only cover the practical fundamentals involved in each aspect;

3.2.1 Field Monitoring

Field monitoring was carried out on each of the slope components given the location of ROP and TDR instrumentation on each of the slope components (Figure 5).

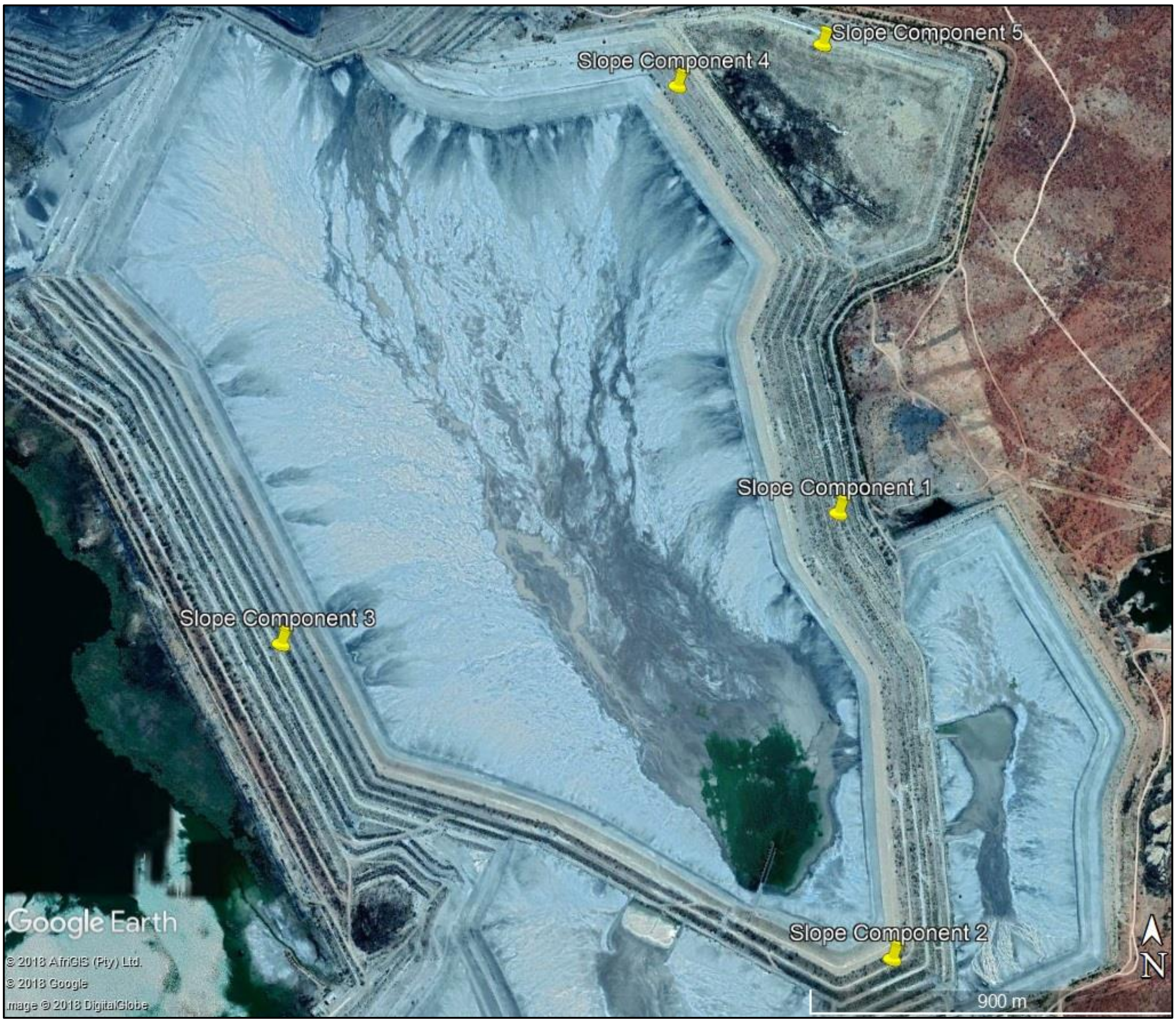

Figure 5: Location of the relevant slope components

3.2.1.1 Overland Flow

Loggernet data loggers were fitted to the ROPs on each slope component to automatically calculate the number of tips from the tipping buckets, as explained in Section 2.5.4- “Overland Flow”. A handheld device was used to extract data from the fitted Loggernet device on the same intervals as the extraction of VWC data from the TDR instrumentation.

The handheld logger is then plugged into a computer to extract the data into the *Loggernet Datalogger Support Network (v.4.1)* software from *Campbell Scientific*. Results were then exported to an excel sheet, after which data processing commenced.

3.2.1.2 Water Moisture Content

TDR instrumentation have been installed on the TSF to ensure proper monitoring of the water balance in the covers.

A hand-held device was used to upload current readings from the TDR in regard to each of the cables. Readings were done as often as possible (as conditions allowed) and were carried out on each of the five slope components to ensure an overall complete set of data.

The water content sensors used are TDR sensors which are connected to a Campbell Scientific TDR 100 wave generator/response analyser. This instrumentation delivers a VWC and a bulk electrical conductivity measurement to a Campbell CR800 logger at pre-set intervals via co-axial cables. Soil water probes have been installed at three depths (100 mm, 500 mm and a 1 000 mm) adjacent to the ROPs to measure the VWC content at each slope component (Figure 5). These measurements serve to improve accuracy when predicting potential flow paths and water balance within the cover material. VWC readings were taken as often as possible from the TDR instrumentation.

The apparent length is measured which in turn is used to calculate the VWC at respective depths. Using slope component 1's measurements on the 22nd of February 2016 as an example, a raw dataset is acquired from the uploaded datasets (Figure 6). The "Probe Start" and "Probe End" data in the two last columns at the bottom table is extracted from the dataset and used in a set of equations to determine the VWC. To ensure successful VWC readings, two equations were used to determine VWC after which the average between the two values was used as the finalised VWC, namely the polynomial equation of Topp (Equation 2) and the linear equation of Ledieu (Equation 3) (de Almeida *et al.,* 2017).

Equation 2: polynomial equation of Topp, (de Almeida et al., *2017).*

$$\theta = \alpha 0 + a1ka + a2Ka^2 + a3ka^2$$

Where;

θ = Volumetric Water Content;

α = adjustment parameters; and

ka = The apparent dielectric permittivity of the growing medium.

Equation 3: The linear equation of Ledieu

$$\theta = \beta 0 + \beta 1\sqrt{Ka}$$

Where;

θ = Volumetric Water Content;

β = adjustment parameters; and

ka = The apparent dielectric permittivity of the growing medium.

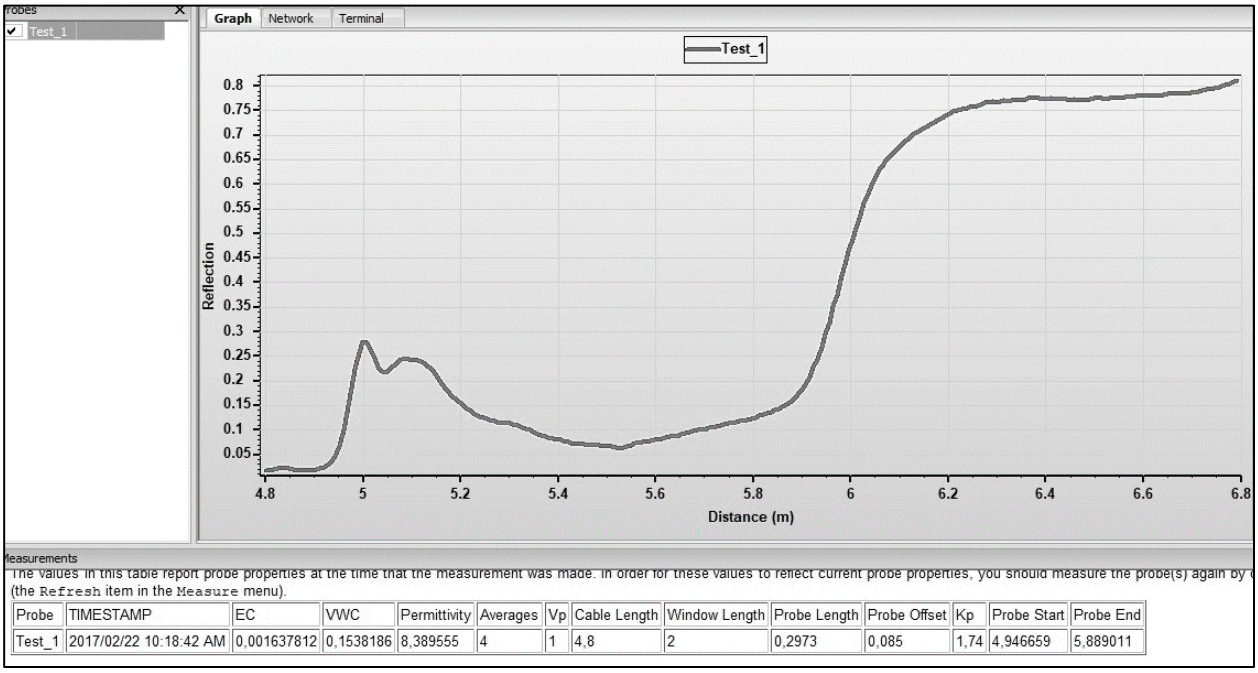

Figure 6: Example of raw dataset acquired from uploads from the TDR instrumentation

Ka is calculated by means of the following equations (Equation 4);

Equation 4: Calculations relative to the apparent dielectric permittivity of the growing medium

$$Ka = (\frac{La}{L})^2$$

Where;

Ka = The apparent dielectric permittivity of the growing medium;

La = The apparent length; and

L = The actual length.

The apparent length inturn is calculated by means of the following equation (Equation 5);

Equation 5: Calculation for the apparent length

$$La = (Pend - Pstart) - offset$$

Where;

La = The apparent length;

P(end) = The probe at the end;

P(start) = The probe at the start; and

Offset = a standard offset value of 0.085.

3.2.1.3 Saturated Hydraulic Conductivity

For this study, saturated and unsaturated hydraulic conductivity was tested, of which only *Ks* was used given its importance in the *HYDRUS-2D* tool. For *Ks*, two popular methods in determining conductivity are by means of double ring infiltrometers and Guelph-permeameters.

The *in-situ* methodology used to determine the *Ks* is that of a Guelph permeameter test and double ring infiltrometer tests. *Ks* was measured on laboratory reworked material by means of the constant head permeameter test. The unsaturated hydraulic conductivity was measured *in-situ* by means of tension infiltrometers. It is worth noting that only the saturated hydraulic conductivity was used for this particular study due to inaccuracies from the laboratory tests.

A Guelph permeameter is a constant head permeameter which is associated with the principles of a Mariotte bottle, (Eijelkamp Agrisearch Equipment, 2012). The Guelph permeameter is placed in an augered hole, after which water from the permeameter constantly flows into the hole and penetrates the soil (Figure 7). After a saturation bulb is formed, water outflow from the storage cylinder will reach a constant value which then is measured. The level of water in the hole, the diameter of the hole and the measured constant value is then used to calculate *Ks*.

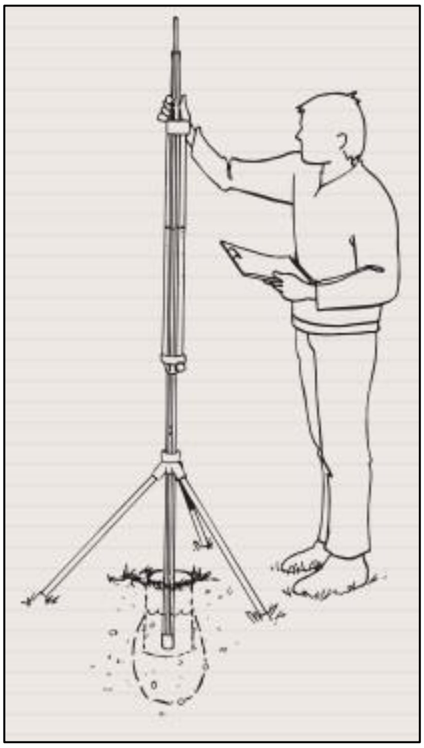

Figure 7: Illustration regarding the operation of a Guelph permeameter (Eijelkamp Agrisearch Equipment, 2012).

Double ring infiltrometers can be used to determine *Ks* by means of the ponding depth constant to the constant positive pressure, (Kohne *et al.,* 2011). A double ring infiltrometer consists of an inner ring, a pipe in the centre and a bevel at the bottom of the ring which aids infiltration into the underlaying soil. The entire ring system has another additional ring surrounding the system and sealed to avoid lea *Ks* (Figure 8).

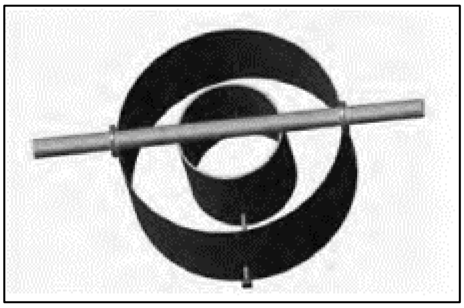

Figure 8: Illustrationn of a double ring infiltrometer (Arriaga, 2010).

According to Fatehnia *et al.,* (2014) a common method in determining *Ks in-situ* is by means of Tension Disc Infiltrometers (TDIs). The disk's size mechanical limitations result in very shallow tests and a small area. This method is three dimensional (Figure 9) and is well documented to successfully determine the unsaturated hydraulic conductivity in surfaces.

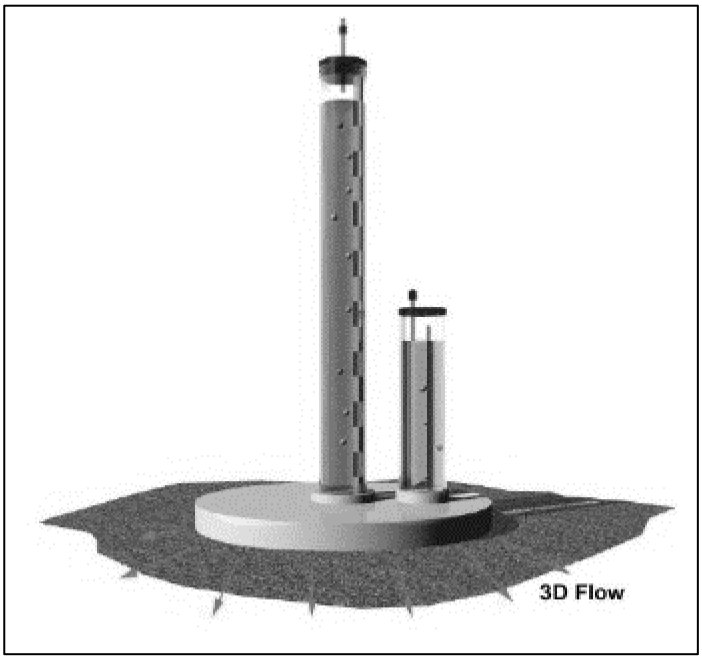

Figure 9: Illustration of a TDI in-situ test, (Bund, 2014).

Tension infiltrometers are used to determine the unsaturated hydraulic conductivity from infiltration results performed at negative or zero pressures (Kohne *et al.,* 2011). A tension infiltrometer is an apparatus used for *in-situ* measurements of infiltration (Reynolds & Zebchuk, 1993). Infiltration is measured through a porous disk on which a “bubble tower” is used to apply a constant pressure (Figure 10).

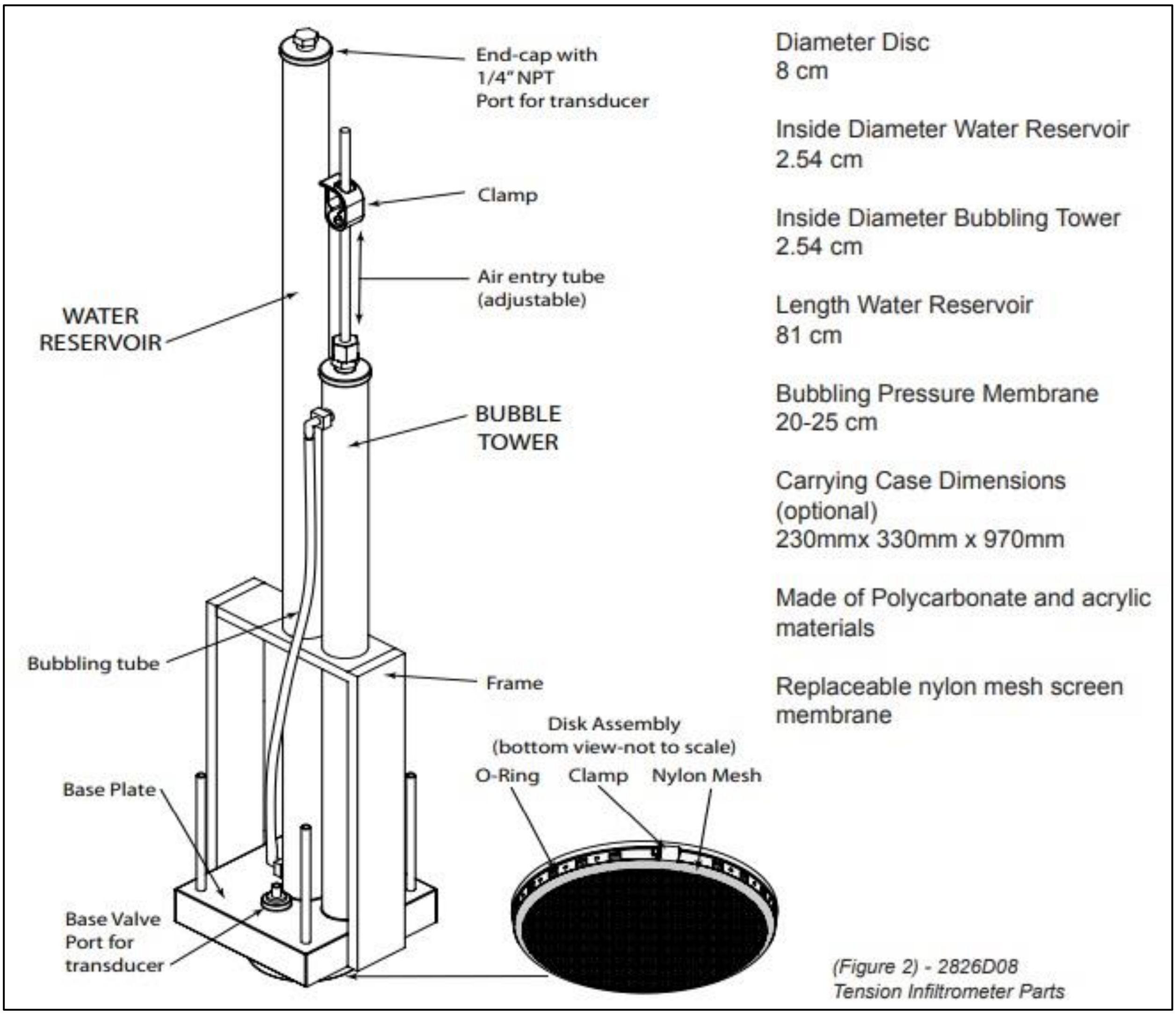

Figure 10: Ilustration of a tension infiltrometer (Soilmoisture Equipment Corp, 2010).

The saturated hydraulic conductivity (*Ks*) for this study was determined by means of the Guelph permeameter methodology at various depths with two repetitions at most depths to increase accuracy. Double ring infiltrometers were used to determine the *Ks* on the surface of each of the slope components. The average *Ks* value between two repetitions was then calculated and used as the *Ks* for the specific site at the respective depth.

The *Ks* was calculated by means of the one head, combined reservoir method equation (see Equation 6).

Equation 6: One head, combined reservoir method equation

$$Ks = \frac{C1 \times \theta 1}{2\pi H1^2 + \pi a^2 C1 + 2\pi(\frac{H1}{a})}$$

Where;

Ks = Saturated hydraulic conductivity;

C1 =The soil shape factor;

Θ = Ambient soil water content;

H1 = The first water head height

a^2 = The macroscopic capillary length parameter; and

a = The borehole radius.

3.2.2 Particle Size Distribution

PSD results have only been obtained from slope component 5. Various samples of the surface at slope component 5 have been taken and sent away for laboratory analysis. Particle Size Distribution (PSD) was then determined by means of sieves and hydrometers or pipettes. A transect was done from north to south from the northern boundary of the TSF at slope component 5 to the middle of the arrow-shaped TSF on which slope component 5 is located (Figure 5). Seven areas have been sampled in the latter mentioned transect at various depths, which totals to 22 samples. The PSD results from these tests were then analysed to determine the textural class.

3.2.3 Meteorological Measurements

Rainfall, humidity, temperature and wind speeds were measured by means of a Davis weather station on-site. Rainfall was recorded with a 0.2 mm tipping bucket. The results from this weather station were exported into an excel sheet for data analysis and conversion to relevant time scales.

3.2.3.1 Potential Evapotranspiration

As mentioned earlier, the potential evapotranspiration was calculated by means of the Penman-Monteith equation (Equation 7) which incorporates wind velocity, humidity (maximum and minimum) as well as temperature (maximum, minimum and average).

Equation 7: Penman-Monteith Equation, (Zotarelli et al., 2010)

$$\mathrm{ET0} = \frac{0.408\Delta(\mathrm{Rn} - \mathrm{G}) + \gamma\frac{900}{T + 273}\,\mu2(\mathrm{es} - \mathrm{ea})}{\Delta + \gamma\,(1 + 0.34\,\mu2)}$$

Where:

ET0 = the potential evapotranspiration;

Rn = the net radiation at the crop surface;

G = soil heat flux;

T = mean daily temperature;

U2 = wind speed at a 2 m height;

es = saturation vapour pressure;

ea = actual vapor pressure; and

î = slope of vapor pressure.

After calculating ET0, the potential transpiration was calculated by means of the dual crop coefficient and calculated by means of Equation 8.

Equation 8: Potential transpiration, (Allen et al., 2006).

$$Potential\,Transpiration = Kcb \times Eto$$

Kcb represents the basal crop coefficient, which is a standard value between zero and one, depending on the growth stage of the crop and the type of crop, (Allen *et al.,* 2006). A *Kcb* constant value for Turf grass was used to represent the Kcb value of the vegetation on the TSF on-site. Between Kcb initial stage, Kcb middle stage and Kcb end stage, Kcb middle was chosen for the potential transpiration calculations given the fact that the cover vegetation has not recently been established and is not expected to be nearing the end of its growth stage. It is, however, worth noting that according to Allen *et al.* (2006), a Kcb mid or a Kcb end value equal or higher than 0.45 in conditions characterised by less than 45% minimum relative humidity or an average wind speed of less than 2 $m.s^{-2}$ needs to be adjusted by means of Equation 9.

Equation 9: Adjustments for relevant Kcb values (mid and end), (Allen et al., 2006)

$$Kcb = Kcb(Tab) + (0.04(U2 - 2) - 0.004(RHmin - 45))(\frac{h}{3})^{0.3}$$

Where;

Kcb (Tab) = the standard value for either Kcb mid or Kcb end;

U2 = the mean daily average wind speed at a height of 2 m above the crop;

RHmin = the mean minimum relative humidity;

h = the standard value according to Allen *et al.,* (2006) for the relevant crop's height.

Potential evaporation is then determined by calculating the difference between potential evapotranspiration and the calculated potential transpiration.

3.2.4 Predictions

The *HYDRUS-2D* programme was used as a tool to predict fluxes throughout each of the relevant slope components to determine the volume of overland flow, lateral sub-surface flows, and vertical seepage during each one of the significant rainfall events. The *HYDRUS*-2D software was selected for this study given the fact that it represents the exact physics of porous media flow in saturated media, the software model includes meteorological data as a parameter and the *HYDRUS*-2D tool can model irregular shapes and material distributions similar to that of a TSF. The model configuration and parameterisation are discussed in the following sections.

3.2.4.1 Domain Type and Units

A general type of geometry was selected for the relevant simulations with a 2D vertical XZ plane. The units chosen to represent the geometry of simulations is in millimetres with a standard epsilon of 0.0766 mm. The maximum size of the x-axis was set on 30 000 mm (30 m) with the z-axis set at a maximum of 10 000 mm (10 m). Simulations were done in hours (equalling 2 424 hours for the study period, 1 January 2017 to 11 April 2017) to ensure finely detailed simulations.

3.2.4.2 Main Process and Add-on Modules

Water flow was selected as the main desired component to be measured. Inverse solution was selected to improve the accuracy of the model, which will be described in more detail in Section 3.2.4.10- “Data for Inverse Solution”.

3.2.4.3 Inverse Solution

Soil hydraulic parameters are the main focus for inverse modelling, of which the inversion data was weighted by “no internal weighting”. The data points in the objective function indicate the amount of VWC readings from the TDR instrumentation for the given slope component, see Section 3.2.4.10- “Data for Inverse Solution”.

3.2.4.4 Time Information

The time units selected for all six simulations is set in hours with the initial time (hour) set at zero. The final time (hour) was set at 2424 with the initial time step being 0.0024. The maximum and minimum time step (hour) was set at 10 and 0.00024. Lastly, the number of time-variable conditions was set at 2424 to represent a time variable condition for every hour.

3.2.4.5 Output Information

For the 2424-time variable conditions, 202 counts have been selected which has resulted in every count representing 12-time variable conditions. T-level information and screen output have been selected.

3.2.4.6 Iteration Criteria

A maximum number of iterations was set at 10, with a water content tolerance of 0.001 and a pressure head tolerance of 10. Lower and upper optimal iteration ranges have been set at three and seven respectively with the lower- and upper-time step multiplication factor set at 1.3 and 0.7. The lower and upper limit of tension interval was set at 0.001 mm and 100 000 mm with initial conditions selected as water content.

3.2.4.7 Soil Hydraulic Model

The "van Genuchten – Mualem" single porosity model was selected for the simulations with no hysteresis selected.

3.2.4.8 Water Flow Parameters

The water flow parameters include various parameters unique to each of the slope components of which all except for *Ks* is derived via the neural network predictor pertaining to the PSD of both materials. The *Ks* values have been measured *in-situ* for each of the slope components and will be used accordingly instead of using the neural network predictor to determine the *Ks*. The simulated results will be compared to the observed results for VWC and overland flow to determine whether or not the *in-situ* results is an accurate representation of the saturated hydraulic properties for the relevant profile. In cases where the Ks has been deemed to be to high or to low, the *Ks* value will be decreased/increased up to 0,1 m/s per simulation until the closest match between observed and simulated results are achieved.

If the simulated overland flow is significantly higher than the observed overland flow and the simulated VWC is lower than the observed VWC, it would be evident that the *in-situ* measured *Ks* is to low. In such a case, the *Ks* will be increased gradually for each simulation until a near-perfect match is achieved between observed and simulated results.

3.2.4.9 Time Variable Conditions

The data illustrated in Table 1 is a theoretical example of the first 10-time variable conditions of 2 424 for the entire study period. Zero rainfall was recorded during this period with a potential transpiration of 0.1432703 mm/hour and a potential evaporation of 0.271977. Potential transpiration and potential evaporation were calculated daily and then divided by 13 to represent the hours of daylight for each day. hCritA was set at a constant 100 000 mm throughout the study period with no "Var.Fl1" or "Var.H-1" for the study period. hCritA is defined as the absolute value of the minimum allowed pressure head at the soil surface. "Var.Fl1" represents the drainage flux across the bottom boundary, of which no data exist in this case whereas that of "Var.H-1" represents the groundwater level (of which no data exist for these simulations). The surface length associated with transpiration was set at 14 000 mm (14 m).

Table 1: Theoretical example of time variable boundary conditions

Time Variable Condition	Time (Hours)	Precipitation	Potential Evaporation (mm/hour)	Potential Transpiration (mm/hour)	hcritA (mm)	Var.Fl1 (mm/hour)	Var.H-1 (mm)
1	1	0	0	0	100 00	0	0
2	2	0	0	0	100 00	0	0
3	3	0	0	0	100 00	0	0
4	4	0	0	0	100 00	0	0
5	5	0	0	0	100 00	0	0
6	6	0	0	0	100 00	0	0
7	7	0	0,27	0,14	100 00	0	0
8	8	0	0,27	0,14	100 00	0	0
9	9	0	0,27	0,14	100 00	0	0
10	10	0	0,27	0,14	100 00	0	0

3.2.4.10 Data for Inverse Solution

The data illustrated in Table 2 represents the data relevant to the entire study period for slope component 1 (as per example). Observation nodes have been placed in the same depths as the TDR cables (which measures VWC) to parameterise the inverse component with. The X column represents the time variable condition relevant to measurements. The Y column illustrates the VWC measured for the specific time variable condition with "Type" referring to the type of data, which in this case is water moisture content (2) according to *HYDRUS-2D* specifications. The position refers to the position of the observation node. The TDR sensors required for the TDR instrumentation was installed at depths of 100 mm, 500 mm and 1 000 mm below the surface. The observation nodes, therefore, represent these TDR sensors with position number 1 referring to the probe at a depth of 100 mm below the surface, the 2nd for the one at 500 mm and the 3rd at 1 000 mm below the surface. The weight accounts for the weight of each of the datasets, which in this case is one for all the sets.

As can be seen in Table 2, an example is illustrated of the first five readings for observation node 1 (100 mm below the surface) for slope component 1.

Table 2: Example of data for inverse solution

	X	Y	Type	Position	Weight
1	108	0,19	2	1	1
2	396	0,093	2	1	1
3	588	0,1	2	1	1
4	636	0,123	2	1	1
5	708	0,125	2	1	1

3.2.4.11 Geometry

The geometry of all five slope components consists of two materials, the first being a 200 mm thick vermiculite cover material (material number one) and the copper tailings material for the rest of the tailings material (material two). The geometry was carried out by means of a polyline, where after surfaces were applied to each of the relevant materials. The red surface in Figure 11 represents the cover material (200 mm thick) and the blue material represents the copper tailings. Each of the slope component's geometry is unique in regard to length and slope angle to ensure accurate predictions.

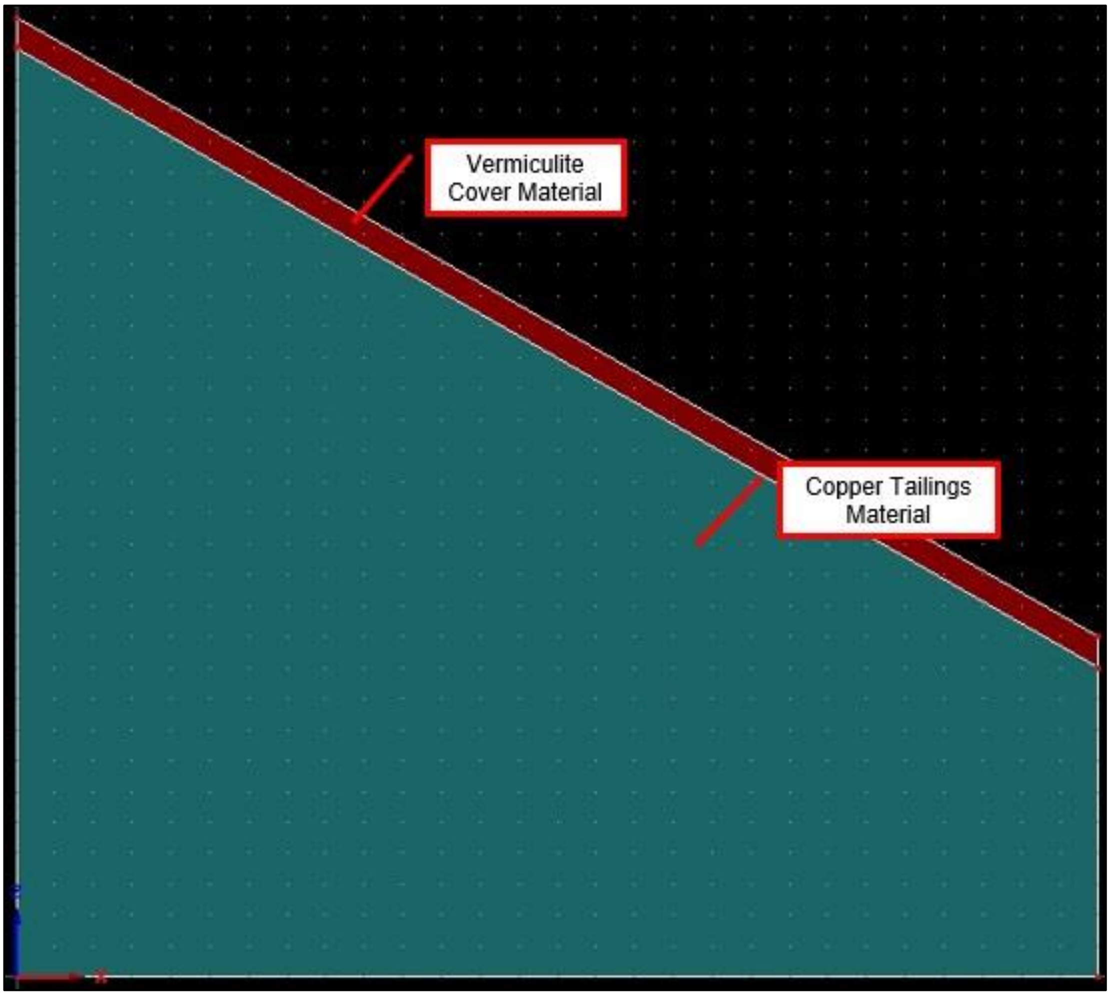

Figure 11: Example of the geometry of all five slope components

3.2.4.12 FE-Mesh

The Finite Element (FE)-Mesh characteristics for the 1st surface have been set at a size of 100 mm, which is small in comparison to the second surface. The size of this surface's mesh can be described to the sensitivity of the upper 200 mm to mesh refinements. The second mesh refinements have a size of 300 mm due to the larger scale of the surface. After the insertion of these refinements, the FE-Mesh was calculated for the entire profile, of which the end results are presented in Figure 12.

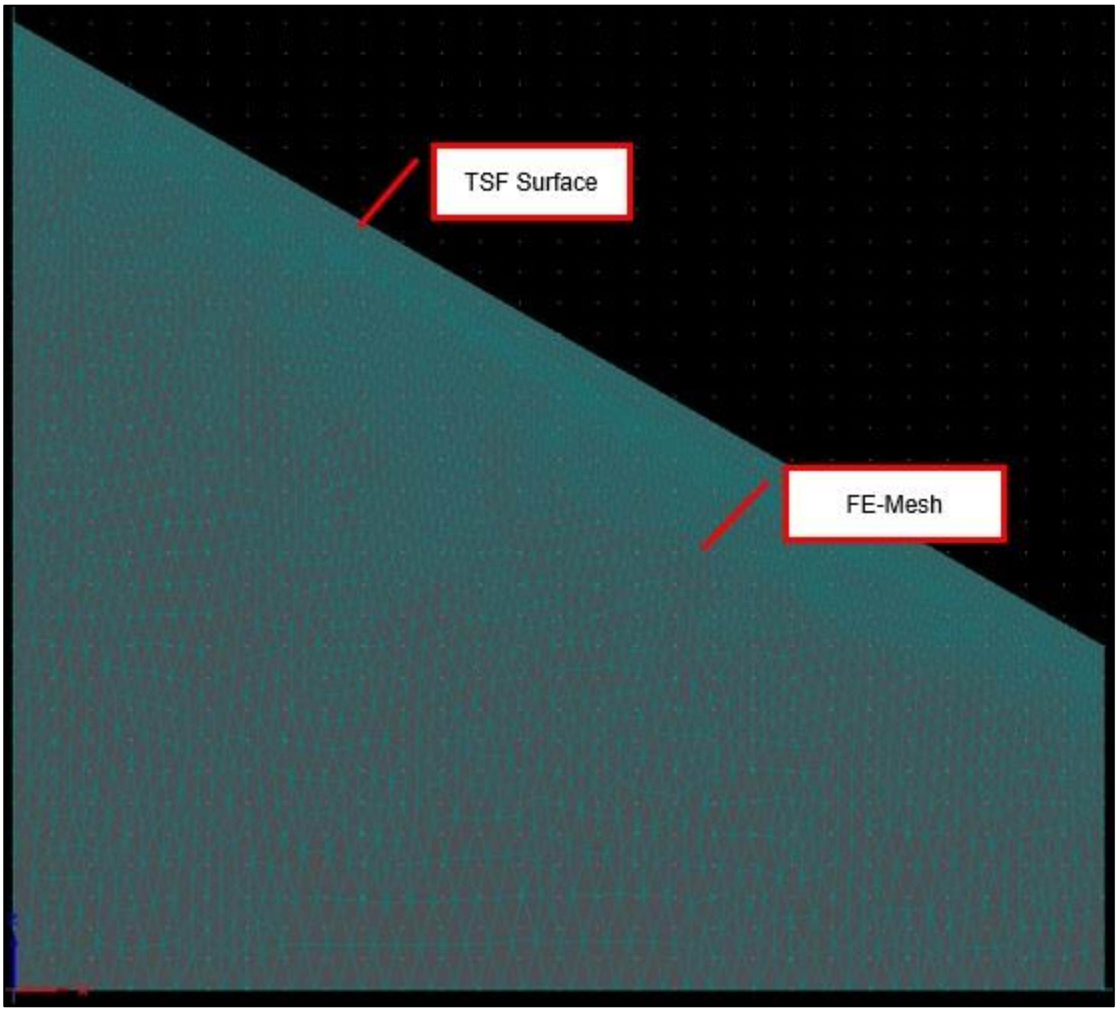

Figure 12: Example of all five slope component's mesh refinements

3.2.4.13 Domain Properties

The only domain properties relevant to these simulations are observation nodes, which only is applicable to the first simulation (hour 1 to hour 394) due to the importance thereof for inverse modelling. These observation nodes represent the three TDR sensors (at 100 mm, 500 mm and 1 000 mm below the surface). VWC measurements from field observations have been imported into these observation nodes to improve the accuracy of simulations. Additionally, inverse solution was used to fix the

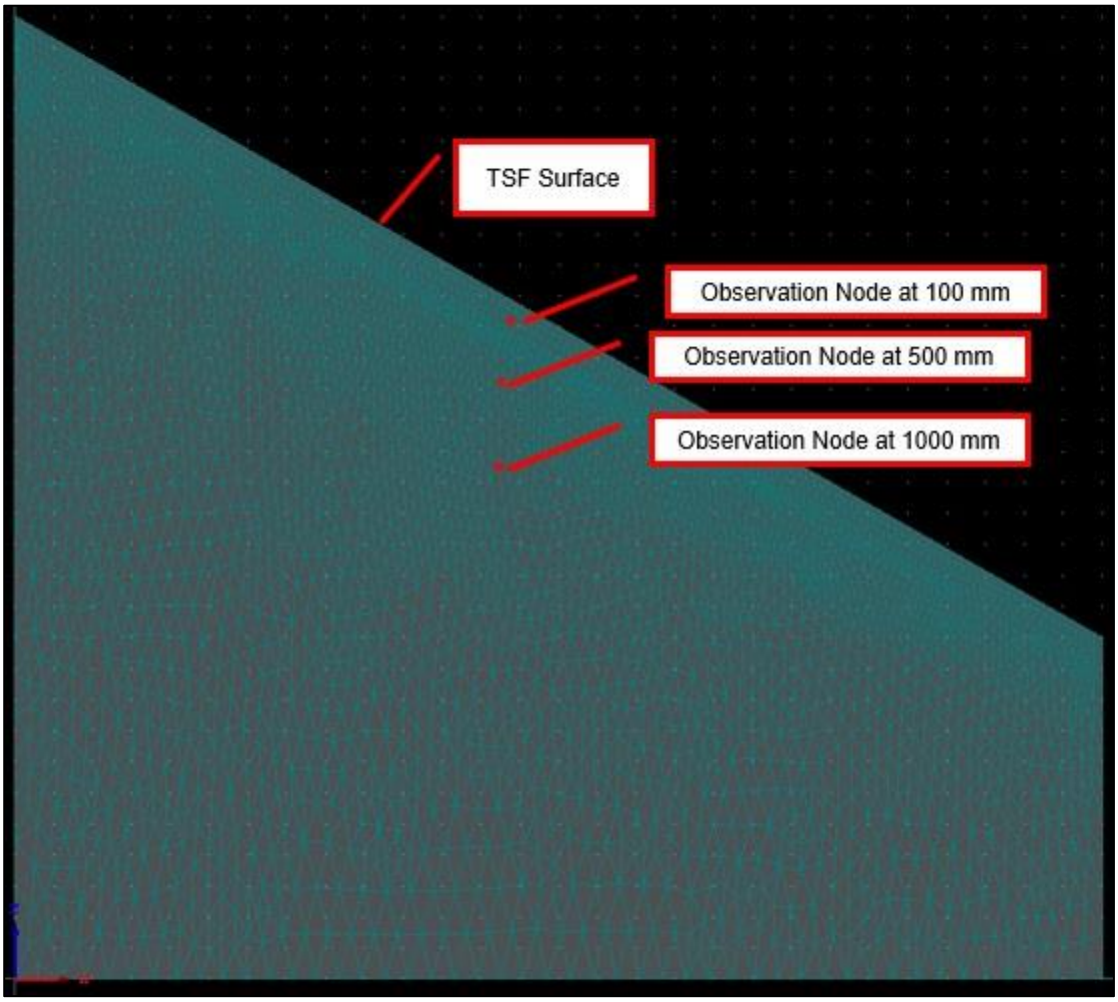

Figure 13: Example of the domain properties for all five slope components. depths.

3.2.4.14 Initial Conditions

The initial conditions were imported from the end results of the same simulation without rain for 500 hours, in order for the simulation to settle. The initial conditions, therefore, represent settled conditions similar to that of the start of the wet season. The final VWC from the settled version is then imported as the initial conditions for the final version to ensure accurate initial conditions.

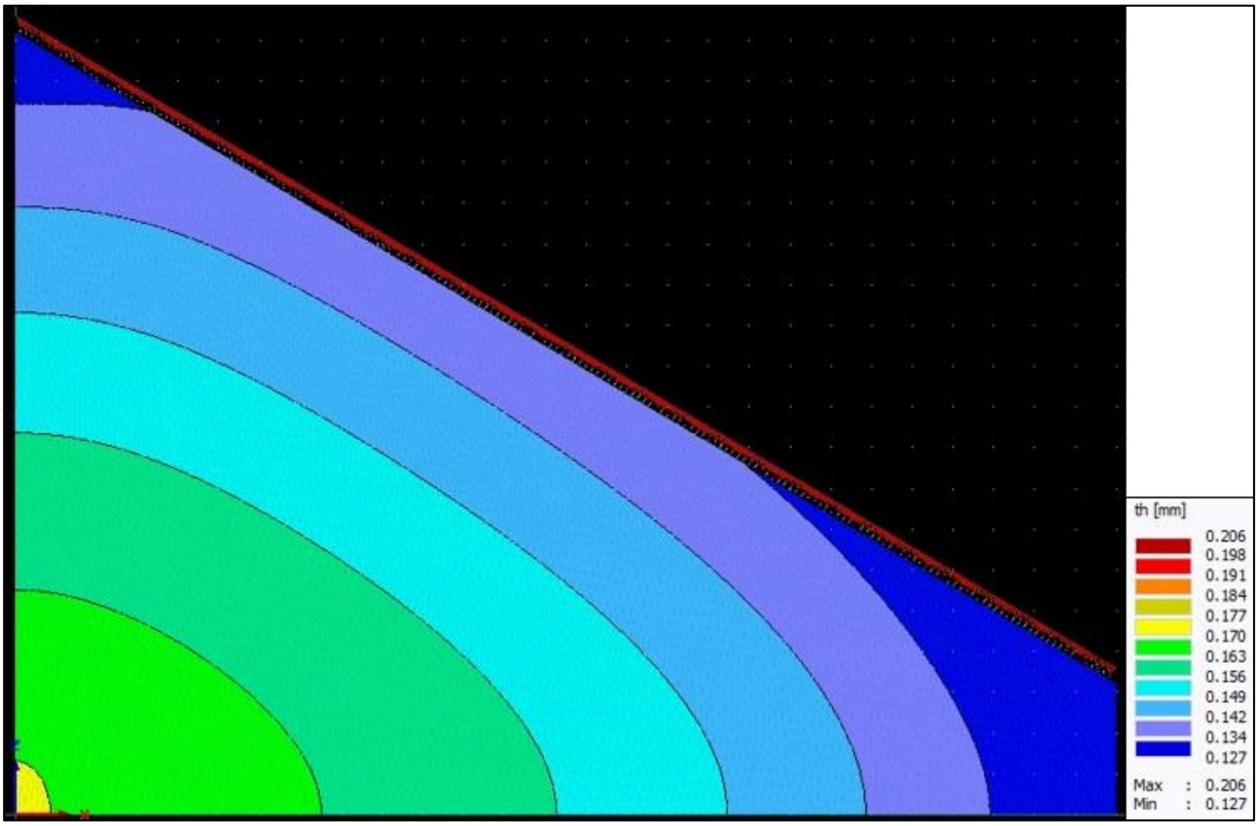

Figure 14: Initial conditions for all five slope components

3.2.4.15 Boundary Conditions

Four different boundary conditions were created for all five of the slope component's, namely an atmospheric boundary, a "no flux" boundary, a seepage face boundary, and a free drainage boundary. The atmospheric boundary responds to all the climatic conditions recorded during the study period, i.e. precipitation, potential evaporation, and potential transpiration. The "no flux" boundary ensures that a certain boundary does not allow any fluxes through the relevant boundary. The seepage face boundary allows lateral seepage through the boundary whereas deep drainage is characterised by deep vertical seepage, see Figure 15. These boundaries will be used to calculate results after calculations, i.e. the total volume of seepage through the seepage face.

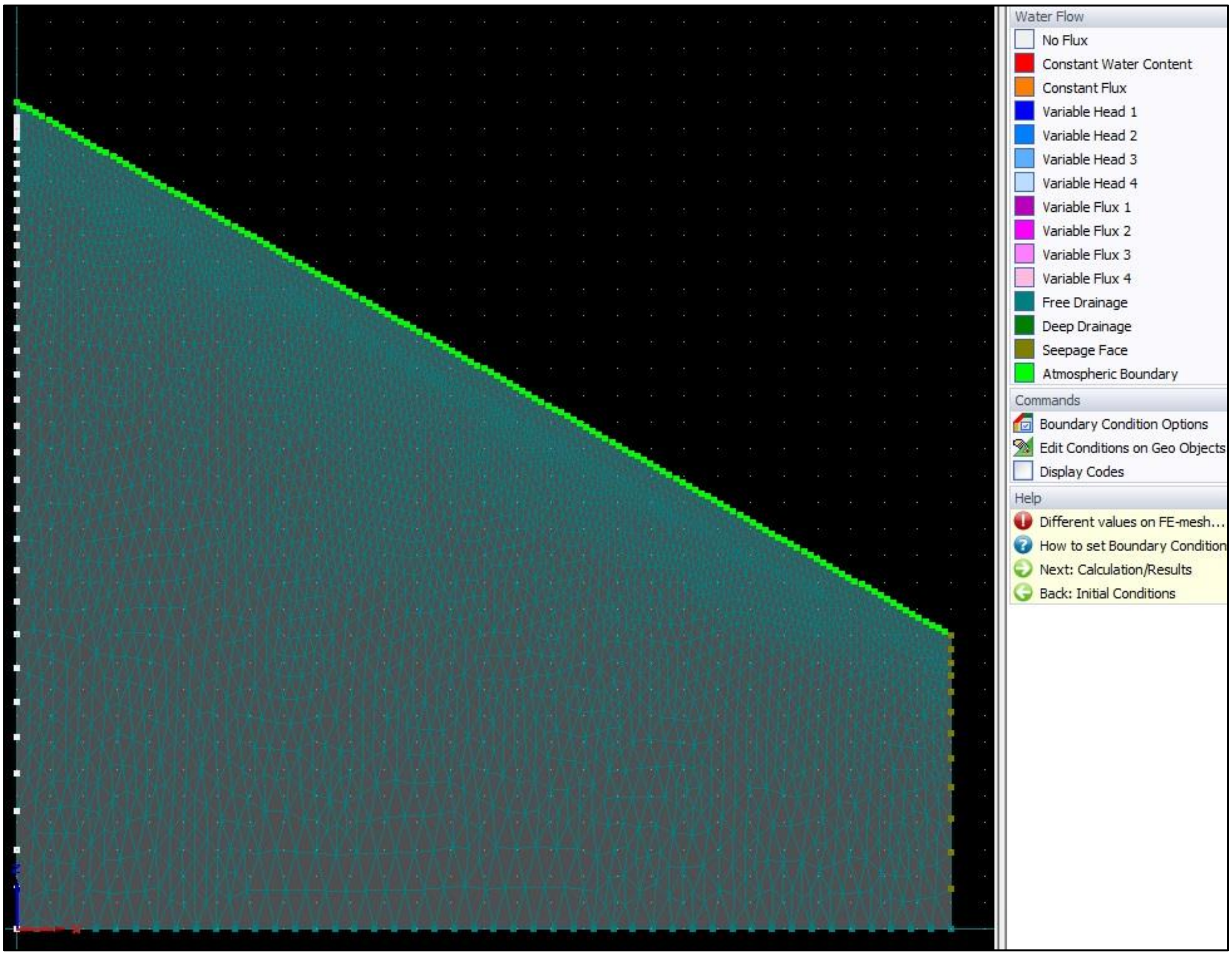

Figure 15: Boundary conditions for all five slope components

3.2.4.16 Auxiliary Objects

The only auxiliary object inserted into simulations is that of “cross-sections”. A cross-section auxiliary object was inserted vertically and horizontally within the tailings profile to measure results over a certain timeframe across the cross-section, see Figure 17. The vertical cross-section was inserted to obtain simulated VWC results through the profile at various depths and at various lengths for the horizontal cross-section.

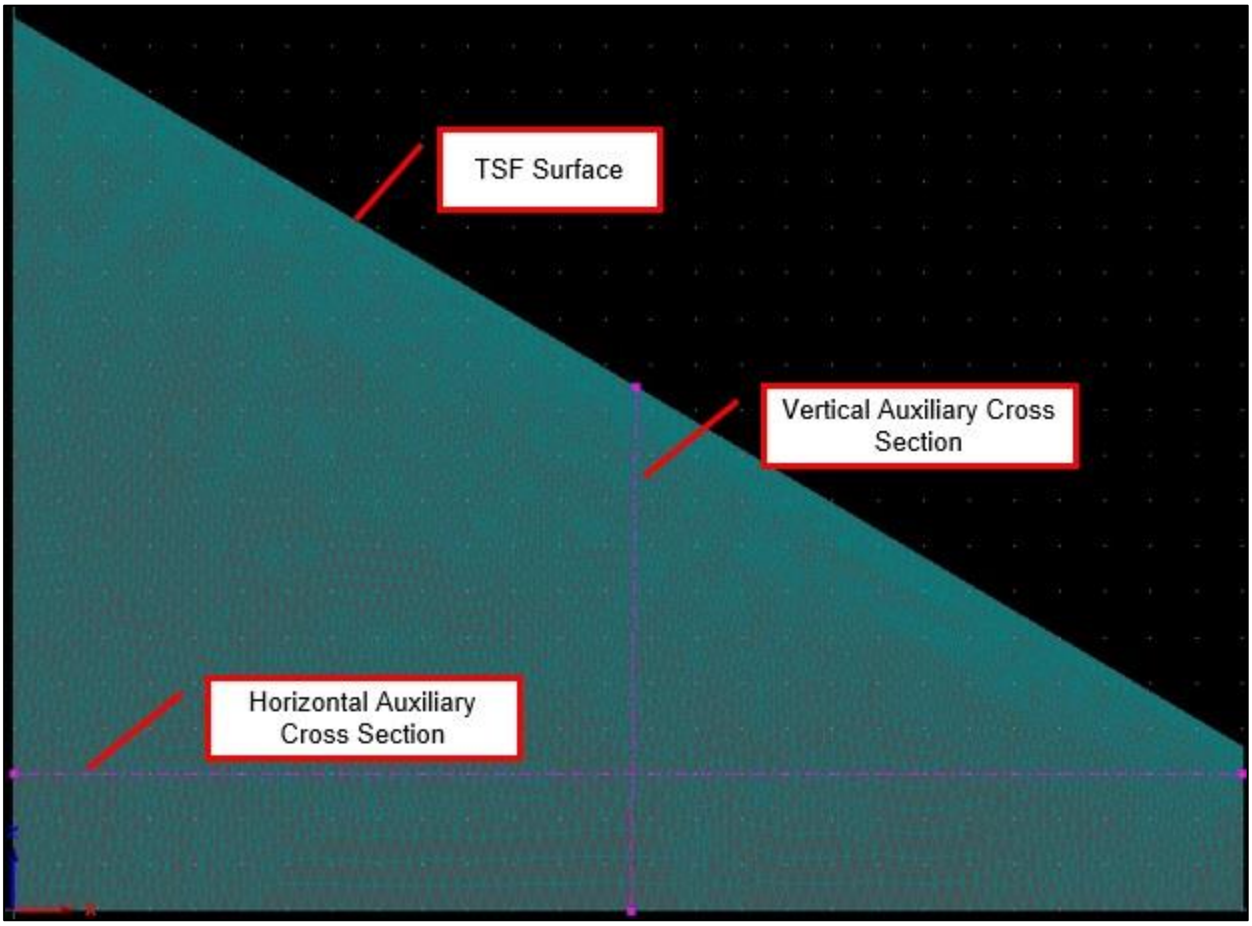

Figure 16: Cross section auxiliary objects inserted into simulations.

Chapter 4: Results

4.1 Conceptual Model

As has been illustrated in Figure 17, several potential flow paths occur in a TSF, namely overland flow, lateral drainage and vertical drainage. The ultimate goal is to quantify and assess all relevant flow paths by parameterising the *HYDRUS* programme with.

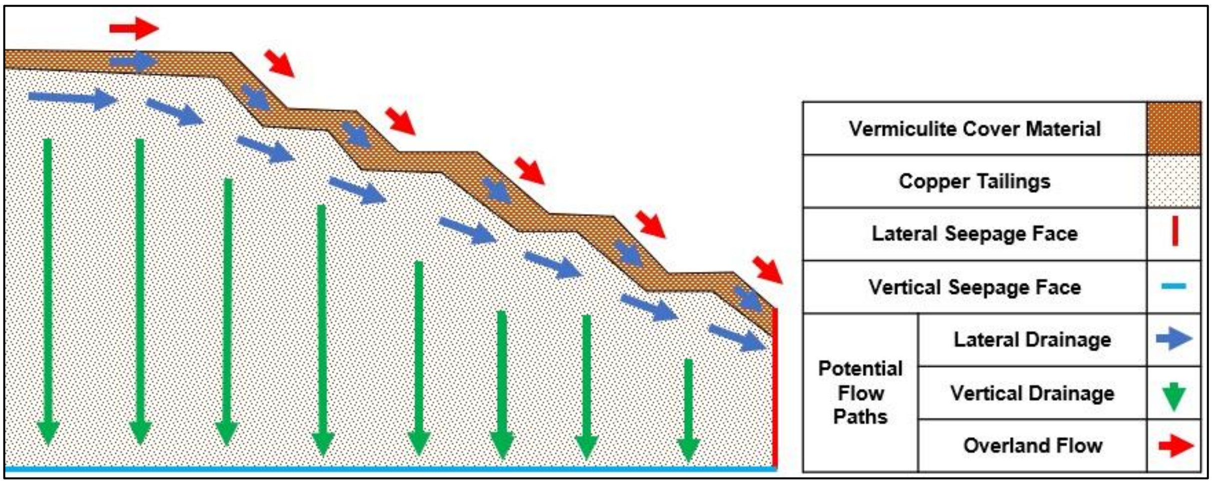

Figure 17: Potential flow paths within TSF

4.2 Meteorological Data

The following sections include the final results from all meteorological parameters, including relative humidity, wind speed, temperature, precipitation, and potential evaporation- and transpiration.

4.2.1 Relative Humidity

The maximum daily Relative Humidity (RH) and minimum RH for the study period is illustrated in Figure 18. The maximum RH ranges from 69% to 100% and the minimum RH ranges from 24% to 91%. These datasets have been directly determined by means of a Davis weather station on-site and exported for data analysis.

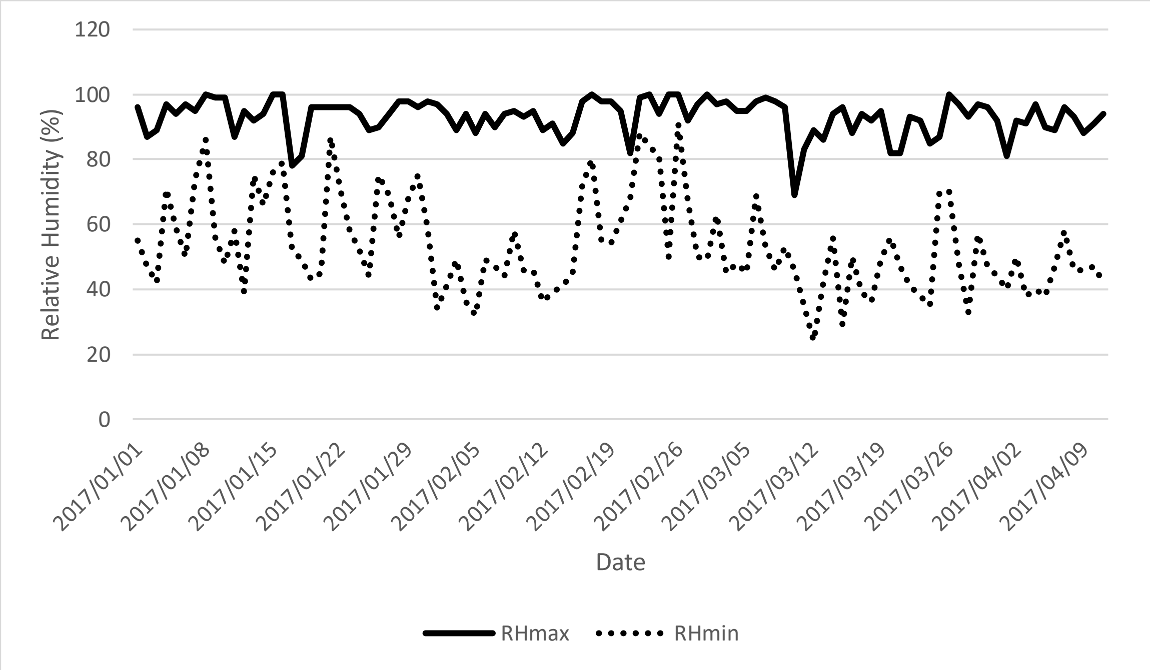

Figure 18: Daily maximum and minimum humidity for the study period

4.2.2 Wind Speed

The average daily wind speed during the study period is illustrated in Figure 19. The average daily wind speed ranges from 0.14 $m.s^{-1}$ to 2.54 $m.s^{-1}$ and plays an integral part in calculating and understanding the potential evapotranspiration relevant to the study period. This dataset was directly determined by means of a Davis weather station on-site and exported for data analysis.

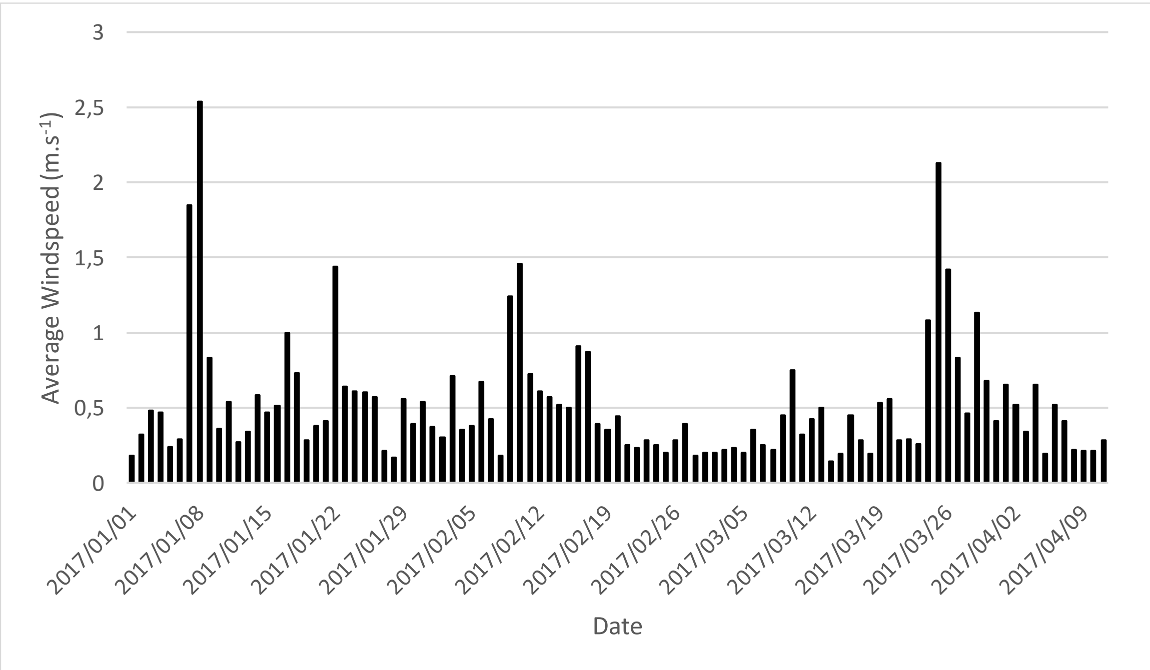

Figure 19: Average daily windspeed during the study period

4.2.3 Average, Maximum and Minimum Daily Temperature

The average, maximum and minimum daily temperatures are illustrated in Figure 20. The maximum daily temperature ranges from 22.4 ˚C to 39.4 ˚C, the minimum daily temperatures ranges from 16.2 ˚C to 25.3 ˚C with the average daily temperatures ranging from 17.5 ˚C to 31.23 ˚C. These datasets have been directly determined by means of a Davis weather station on-site and exported for data analysis.

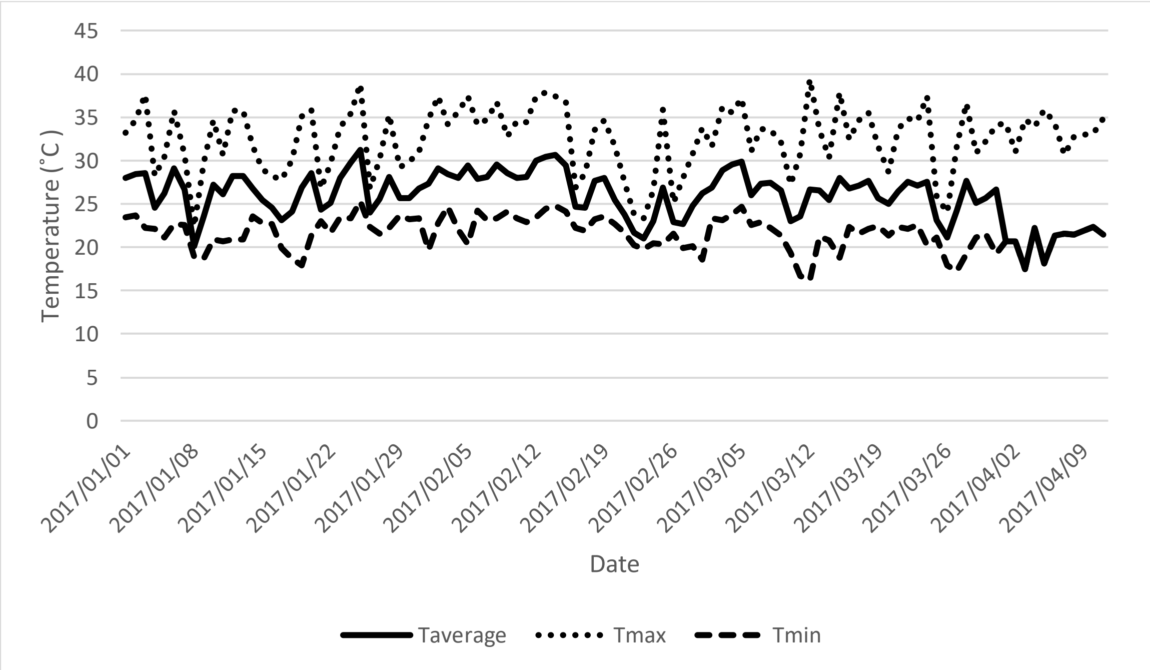

Figure 20: Daily average, maximum and minimum temperatures recorded for the study period

4.2.4 Precipitation

Figure 21 illustrates the rainfall recorded during the research period. Two high-intensity rainfall events have been recorded during the study period, which include;

- The 3rd to the 5th of January or hour 49 to hour 120 (1st high-intensity rainfall event); and
- The 12th to the 17th of January or hour 265 to hour 408 (2nd high-intensity rainfall event).

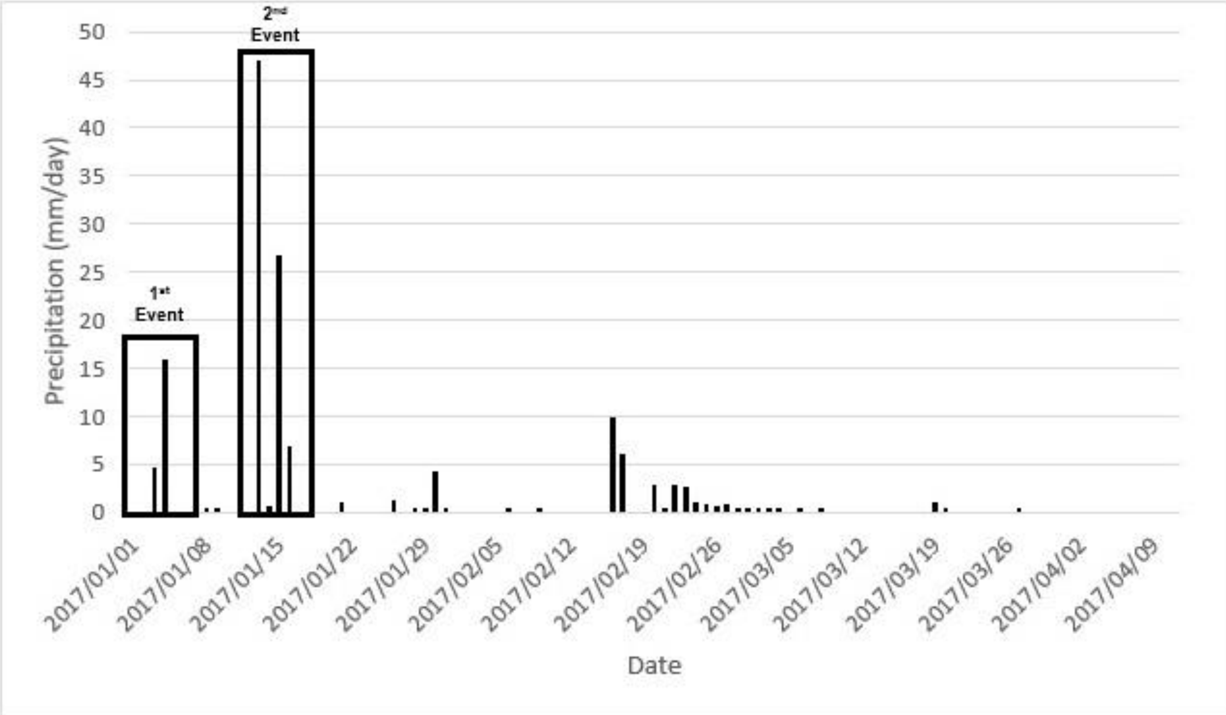

Figure 21: Precipitation during the research period

The hourly precipitation for these dates (including 24 hours before and after the rainfall event) is illustrated in Figure 22. Hour 1 illustrates the first hour of the 3rd of January (01:00) and hour 71 illustrates the 71st hour in the three-day period (23:00 the 5th of January). Figure 22 indicates a high-intensity rainfall event between the 12th and 13th hour (12:00-13:00) with a gentle rainfall event from the 36th hour to the 38th hour (12:00-14:00, 4th of January).

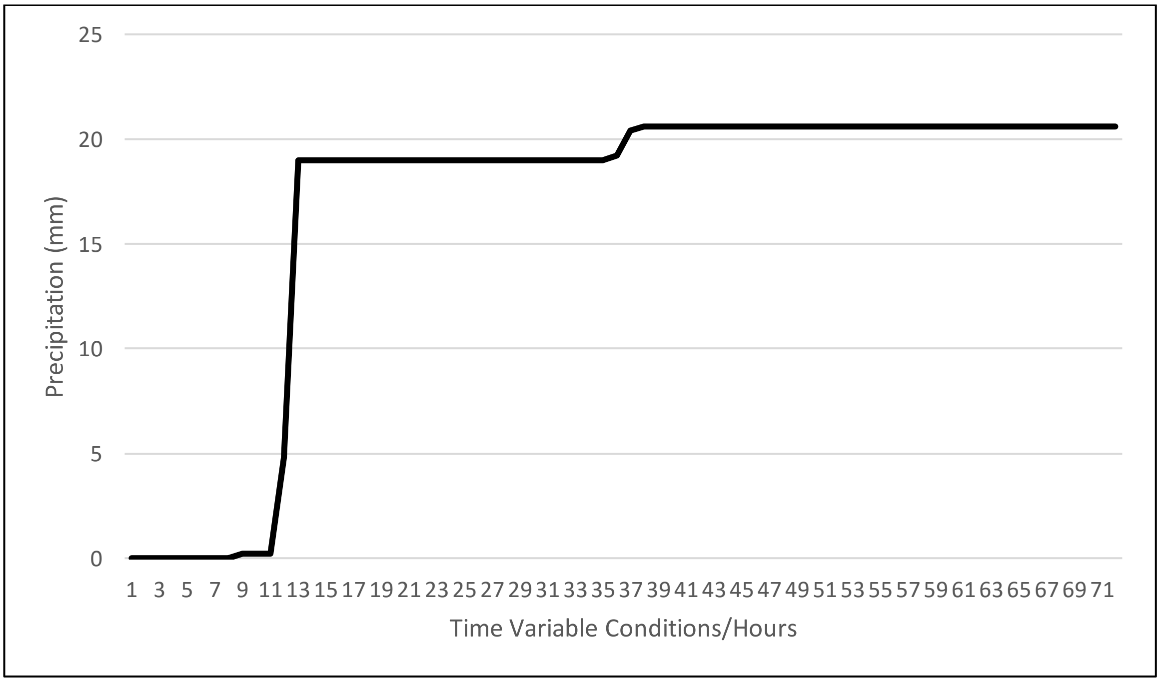

Figure 22: Cumulative hourly precipitation recorded from the 3rd to the 5th of January (1st high-intensity rainfall event)

The hourly precipitation for these dates (including 24 hours before and after the rainfall events) are illustrated in Figure 23. Hour 1 illustrates the first hour of the 12th of January (01:00) and hour 141 illustrates the 141st hour in the six-day period (23:00 the 17th of January). Figure 23 indicates a high-intensity rainfall event between the 12th and 13th hour (12:00-13:00) with a gentle rainfall event from the 36th hour to the 38th hour (12:00-14:00, 4th of January). A high-intensity rainfall event of 47 mm in five hours was recorded between hour 36 and hour 40 (12:00-16:00, 13th of January) and another high-intensity rainfall (gentler than the previous) was recorded between the 94th hour and the 98th hour (22:00-02:00, 15th and 16th of January).

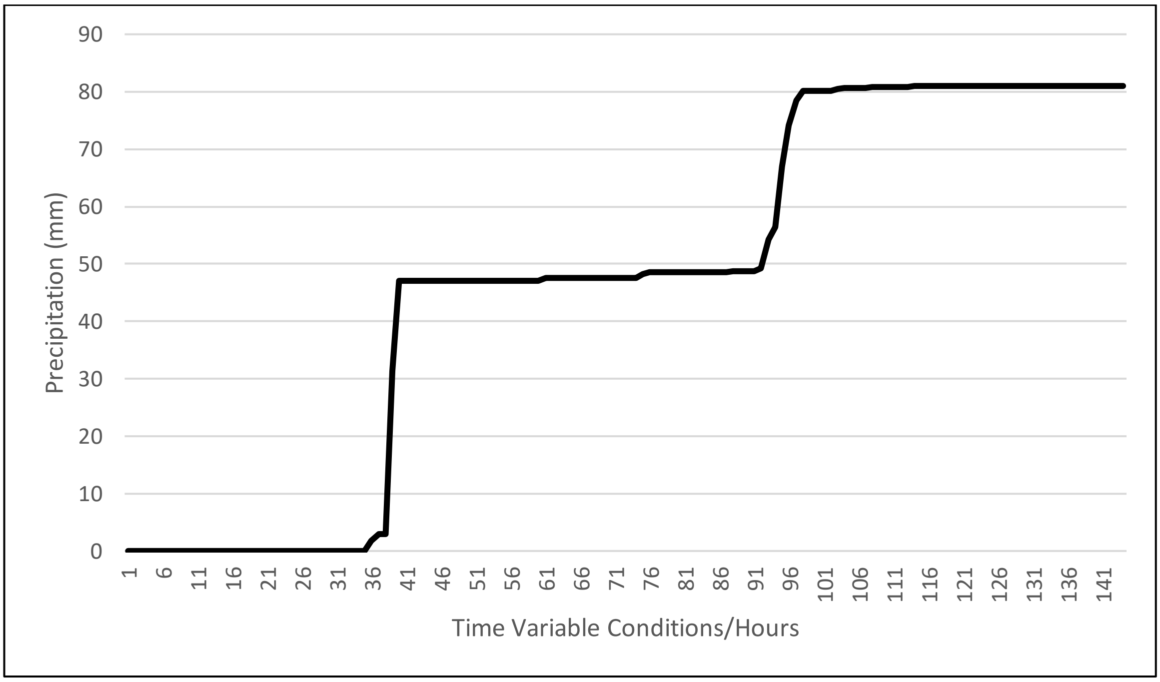

Figure 23: Cumulative hourly precipitation recorded from the 12th to the 17th of January (2nd high-intensity rainfall event)

4.2.5 Potential Transpiration and Potential Evaporation

Potential evaporation and transpiration were calculated according to the Penman-Monteith equation and the dual crop coefficient, (Figure 24).

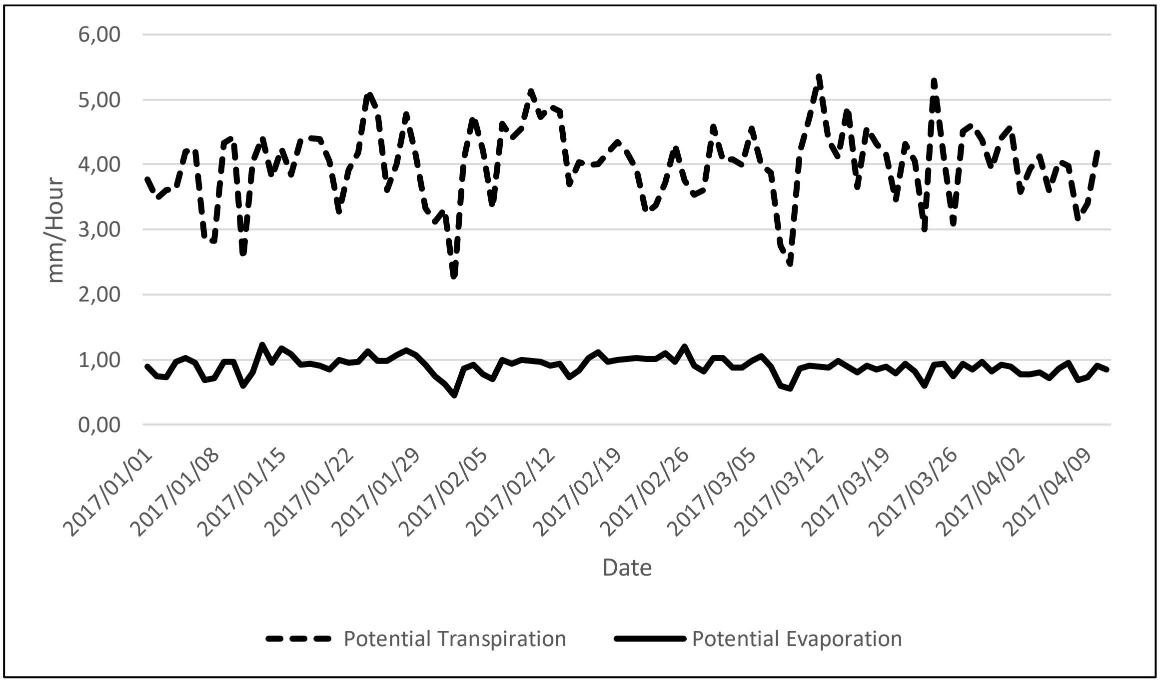

Figure 24: Potential transpiration and potential evaporation calculated for the study period

4.3 Physical Properties of Cover- and Tailings Material

PSD results have only been obtained from slope component 5. The average results for the cover material (at a depth of 200 mm below the surface) and the copper tailings material (deeper than 200 mm below the surface) was calculated and are presented in Table 3. These results are applicable to all of the other slope components given the similarities between all slope component's tailings material and cover material.

Table 3: The average PSD for the cover and tailings material

Material	Sand (%)	Silt (%)	Clay (%)
Cover material (Vermiculite)	84	9	7
Copper Tailings Material	68	26	6

4.4 Saturated Hydraulic Conductivity

Figure 25 illustrates the *Ks* results for each of the slope components at various depths. The nature of each slope component in regard to *Ks*, especially the results from the *Ks* values will be discussed after the latter mentioned figure. It is clear from Figure 25 that slope component 5 has a low *Ks* close to the surface which increases significantly deeper into the profile. Even though the *Ks* of the relevant slope components differ, the PSD has been assumed to be similar throughout the TSF given the fact that the same material has been used to construct the TSF. Various potential reasons exist for the difference in *Ks* which due to practical reasons has not been taken into consideration for this study.

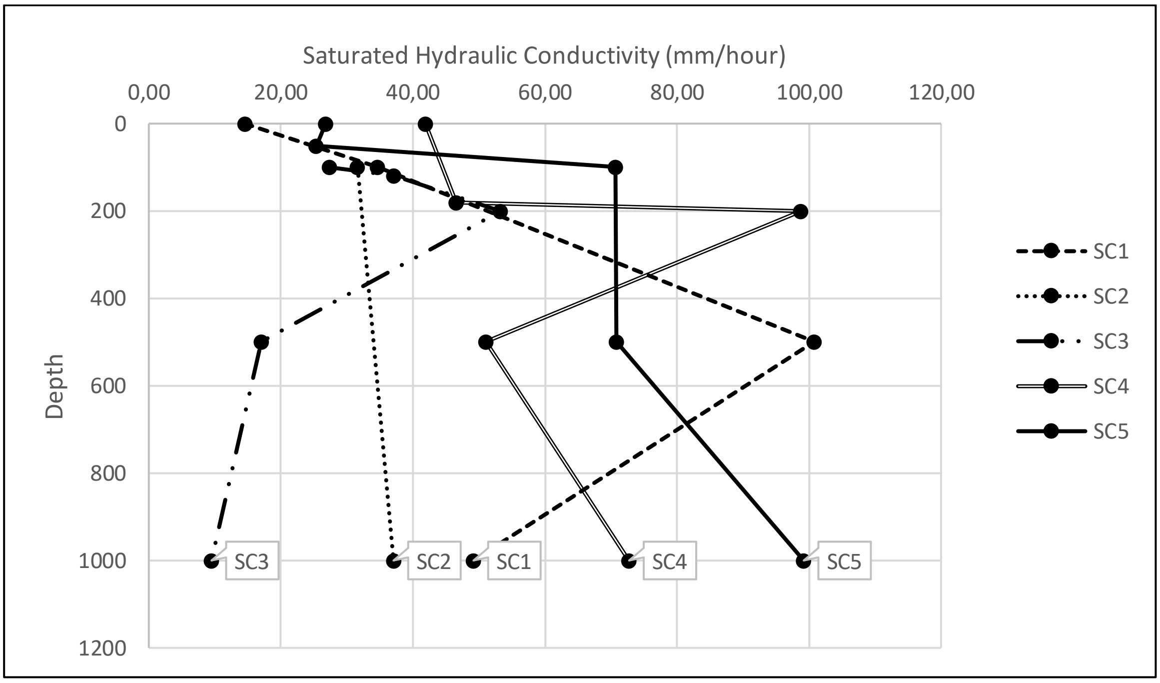

Figure 25: Saturated hydraulic conductivity at various depths for all five slope components

Figure 26 illustrates the saturated hydraulic conductivity (*Ks*) for slope component 1. *Ks* was measured at the surface and at depths of 100 mm, 500 mm and 1 000 mm below surface. The results indicate low *Ks* at the surface, which gradually increases up to a depth of 500 mm, after which a slight decrease in *Ks* can be noticed from 500 mm below surface to 1 000 mm below surface.

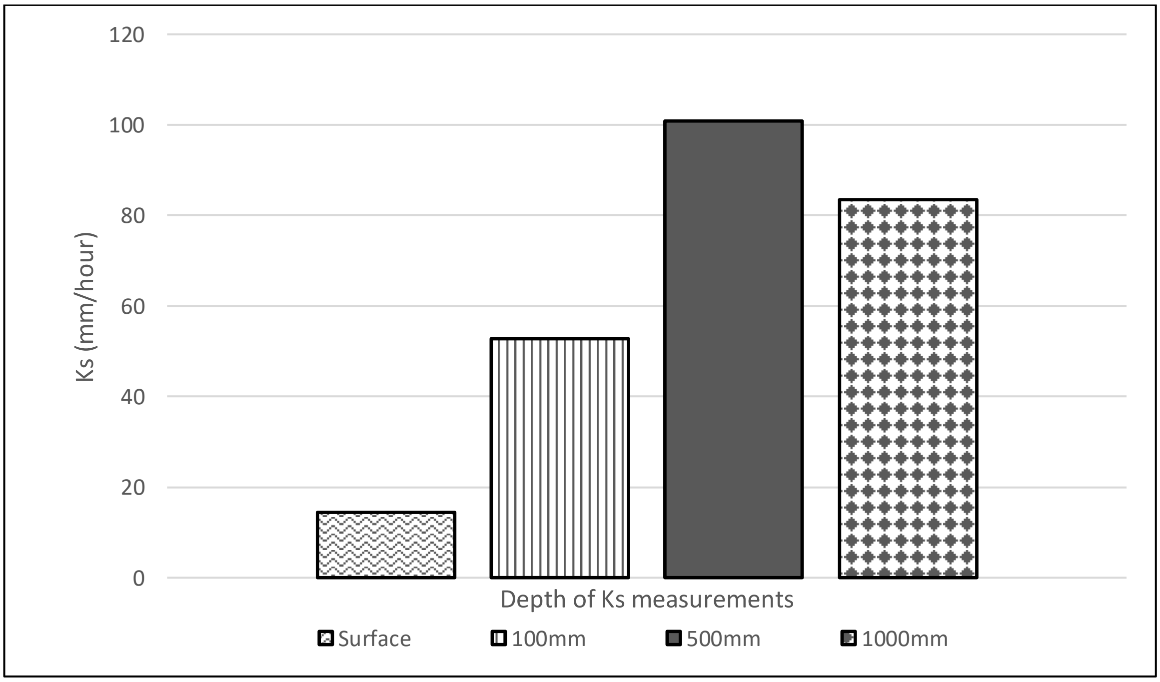

Figure 26: Saturated hydraulic conductivity at various depths for slope component 1

Figure 27 indicates the results for the *Ks* measured at depths of 100 mm and 1 000 mm below surface for slope component 2. As in the case of slope component 1, these results indicate a gradual increase in *Ks* from the surface to the 1 000 mm below surface mark.

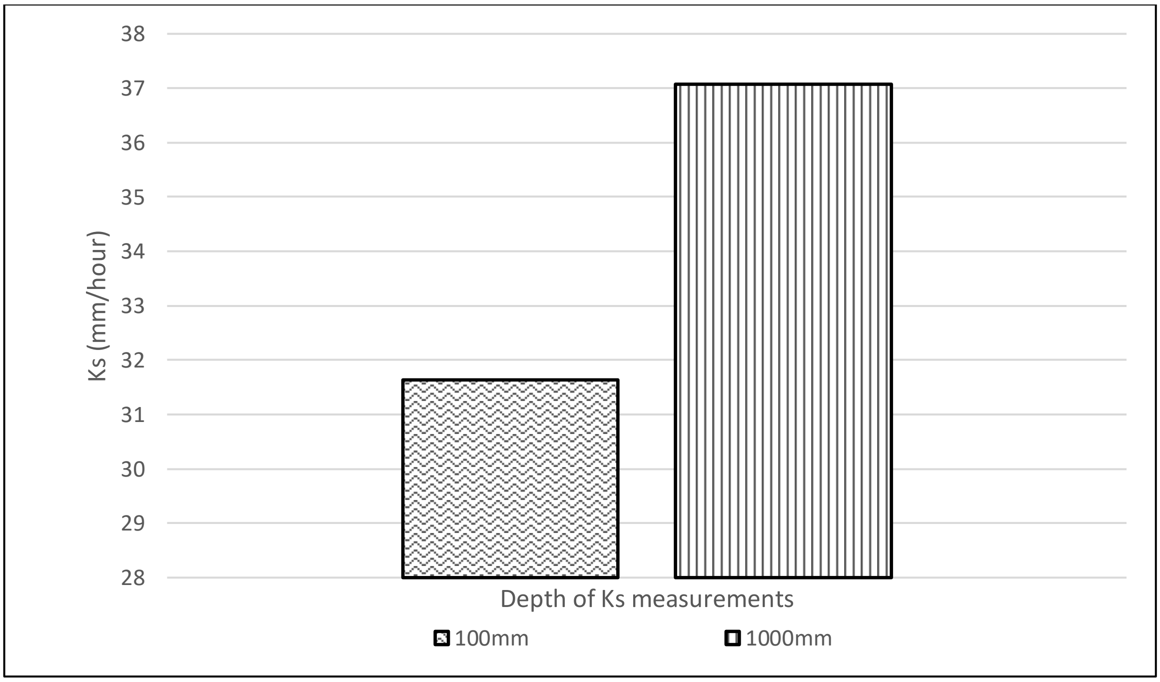

Figure 27: Saturated hydraulic conductivity at various depths for slope component 2

Figure 28 illustrates the results from the *Ks* measured for slope component 3 at a depth of 100 mm, 120 mm, 200 mm, 500 mm and a 1 000 mm. As was the case for the first two slope components, a gradual increase in *Ks* is noticed from the surface to a depth of 200 mm, where after a sudden decrease in *Ks* can be noticed. The *Ks* values then decrease further from 500 mm below surface to 1 000 mm below surface.

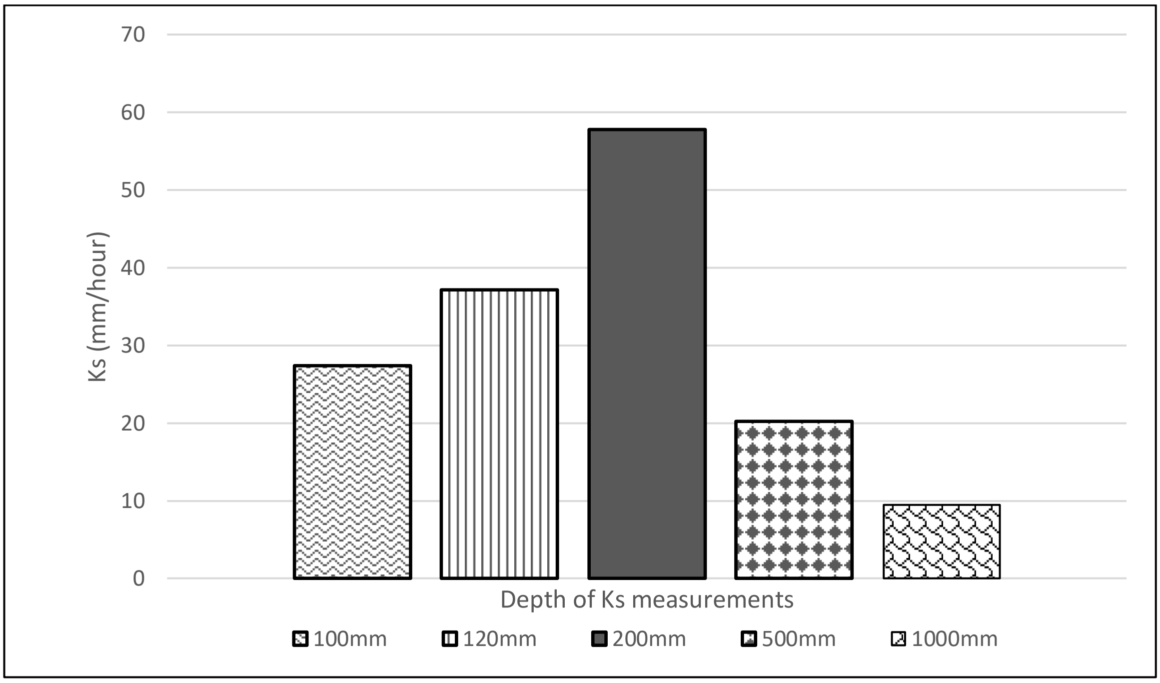

Figure 28: Saturated hydraulic conductivity at various depths for slope component 3

Figure 29 illustrates the *Ks* results for slope component 4 at the surface and depths of 180 mm and 1 000 mm below the surface. For this dataset, the *Ks* for the surface is abnormally high in comparison to that of the slope component 1. The *Ks* decreases between the surface and 180 mm below surface which emphasises the cover material's ineffectiveness in water holding capacity. The cover material has likely been washed away and resulting in larger fragments as the residual material with high concentrations of preferential flow paths, which ultimately has a very high *Ks*.

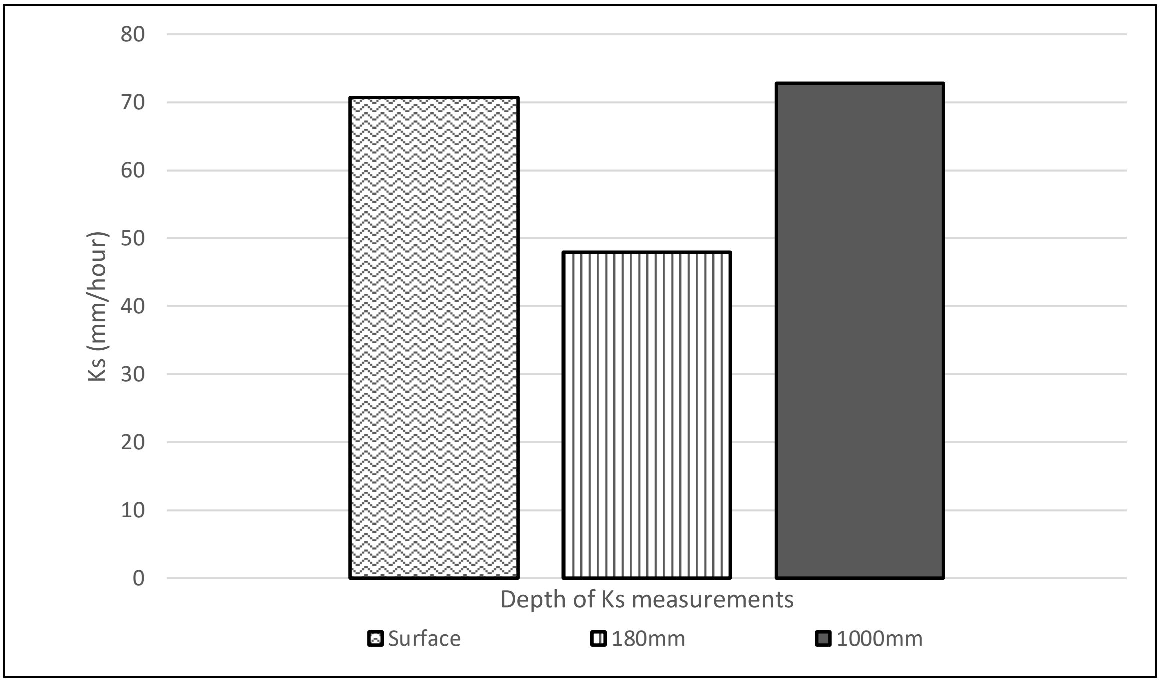

Figure 29: Saturated hydraulic conductivity at various depths for slope component 4

Figure 30 illustrates the *Ks* recorded for slope component 5 at the surface and at depths of 500 mm and 1 000 mm. The *Ks* increases roughly by three times from the surface to a depth of 500 mm below surface. The *Ks* then remains constant from 500 mm below surface to 1 000 mm below surface.

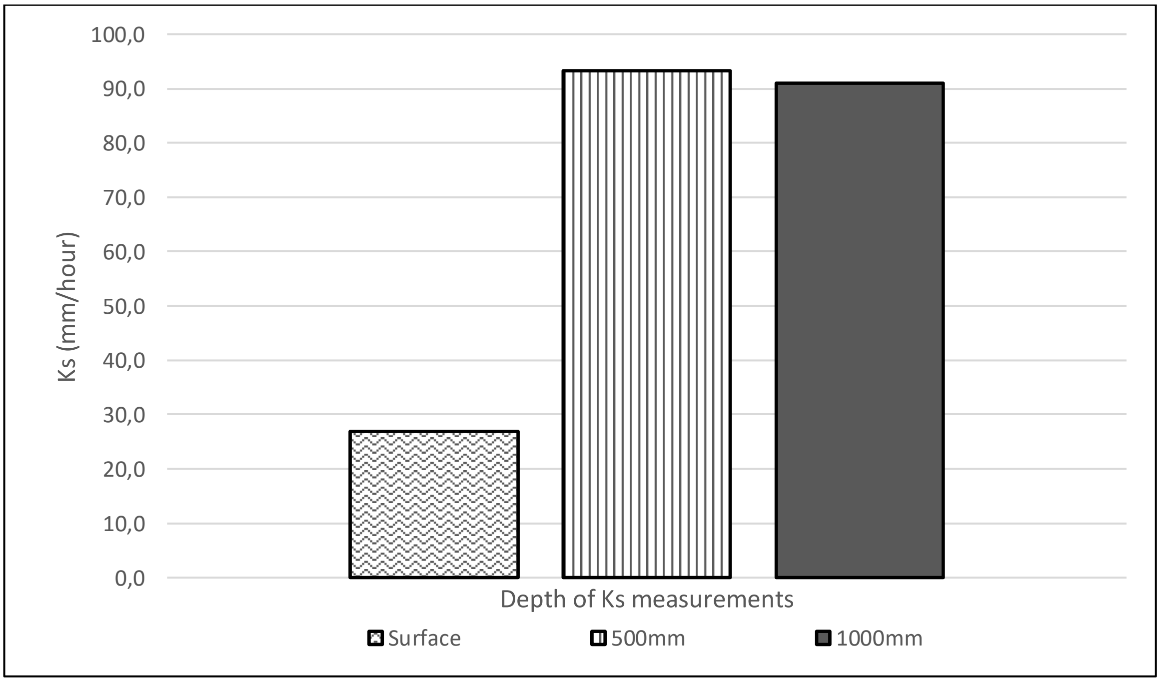

Figure 30: Saturated hydraulic conductivity at various depths for slope component 5

4.5 Volumetric Water Content

The following sections include results from VWC and precipitation on one graph and descriptions thereof. It is worth noting that the precipitation values do not represent daily precipitation, but rather the total precipitation between VWC data accumulation. This set of data, therefore, illustrates the total precipitation before the downloading of the VWC data which can be compared to the VWC data.

4.5.1 Slope Component 1

For the 1st rainfall event, an increase in VWC is recorded for the upper 100 mm. The material at 500 mm is extremely high after this event and decreases up to middle February and is characterised by a constant VWC thereafter. The material at 1 000 mm below the surface has a higher VWC 12 days after the 1st rainfall event and could have spiked between the 5th of January and the 12th given lack of data between those dates.

No significant increases in VWC are recorded during or after the 2nd and 3rd rainfall events. For the 4th rainfall, however, an increase in VWC is recorded on the 22nd and the 27th of February for the upper 100 mm and on the 24th of February for the material at 1 000 mm below the surface. The VWC spike could not be as a result of the 3rd rainfall event due to the fact that a spike in VWC for the upper 100 mm has not been recorded, which ultimately indicates to overland flow being dominant after the 3rd rainfall event. Similarly, no increase in VWC is recorded after the 2nd rainfall event.

Therefore, assumptions can be made that the 2nd and 3rd rainfall events would have been characterised by overland flow rather than infiltration. Even though the 1st rainfall event has a higher intensity than the 3rd rainfall event, 4.6 mm of rainfall is recorded an hour before the high-intensity event, which would have infiltrated the first 100 mm, which has resulted in an increase in VWC. The infiltrated precipitation percolates through the profile, reaching the material 500 mm and 1 000 mm within four to 12 days. The 4th rainfall event results in a rapid increase in VWC for the entire profile. Assumptions can thus be made that vertical seepage occurs within this slope component during and after gentle rainfall events which is described to the high saturated hydraulic conductivity throughout the profile (surface to 1 000 mm below the surface, see Figure 27). The VWC for the material at 500 mm is significantly higher than that of the rest of the material which indicates a high density due to compaction.

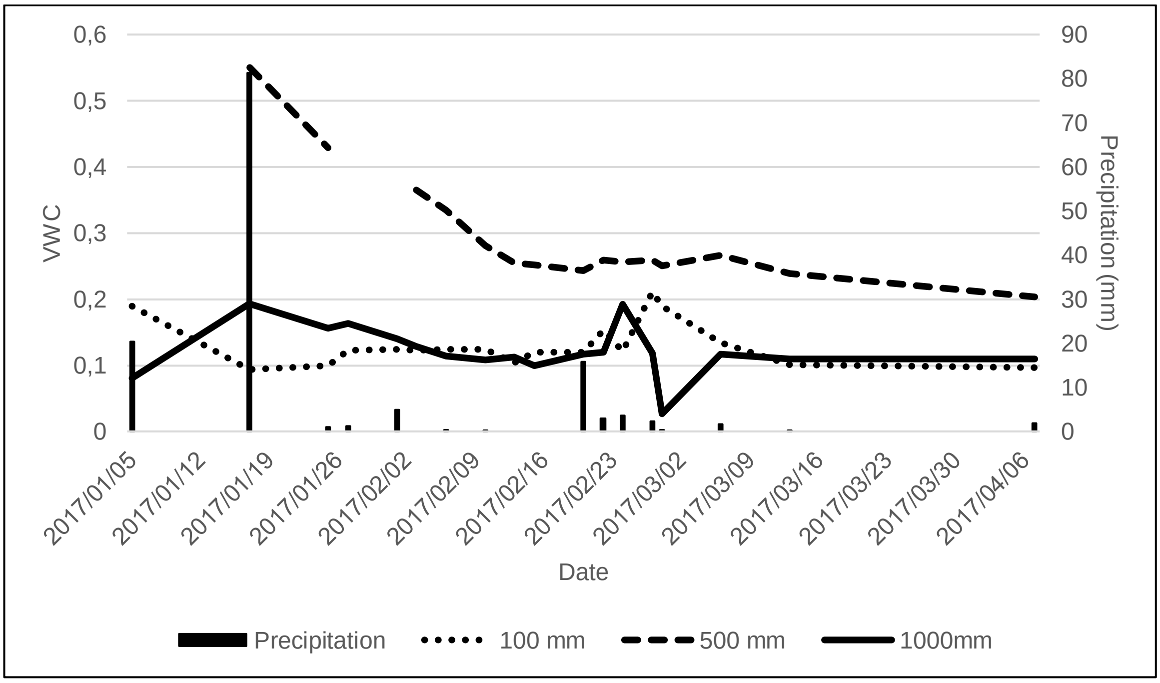

Figure 31: VWC measured at various depths for slope component 1

4.5.2 Slope Component 2

For slope component 2, an increase in VWC is recorded on the 25th of January for the entire profile (surface to 1 000 mm below surface). This phenomenon was deemed to be an outlier dataset given the fact that there is no precipitation recorded for nine days before the spike in VWC. The cover material has a high VWC on the 25th of January and therefore percolation delay cannot be the result of these high VWC values. Alternatively, no abnormal weather events have been recorded for this day, i.e. high wind speeds, high volumes of dew, extreme temperatures etc. Possibilities exist that this event might be caused by human or natural interferences (from animals). No high VWC values are recorded for the 1st significant rainfall event with only a slight increase in VWC on the 27th of February which reacts to the 4th rainfall event. The latter mentioned increase in VWC is recorded for the upper 100 mm and the material at 500 mm below surface with the dataset for the 1 000 mm mark missing due to malfunctioning equipment.

Therefore, assumptions can be made that any high rainfall events (with an intensity of the 3rd rainfall event and higher) will result in overland flow. Low-intensity rainfall events however (as in the case of the 4th rainfall event) will result in rapid infiltration and percolation with very little lateral movement given the fact that an increase in VWC was recorded for the upper 100 mm and the material at 500 mm below surface on the same day during the 4th rainfall event.

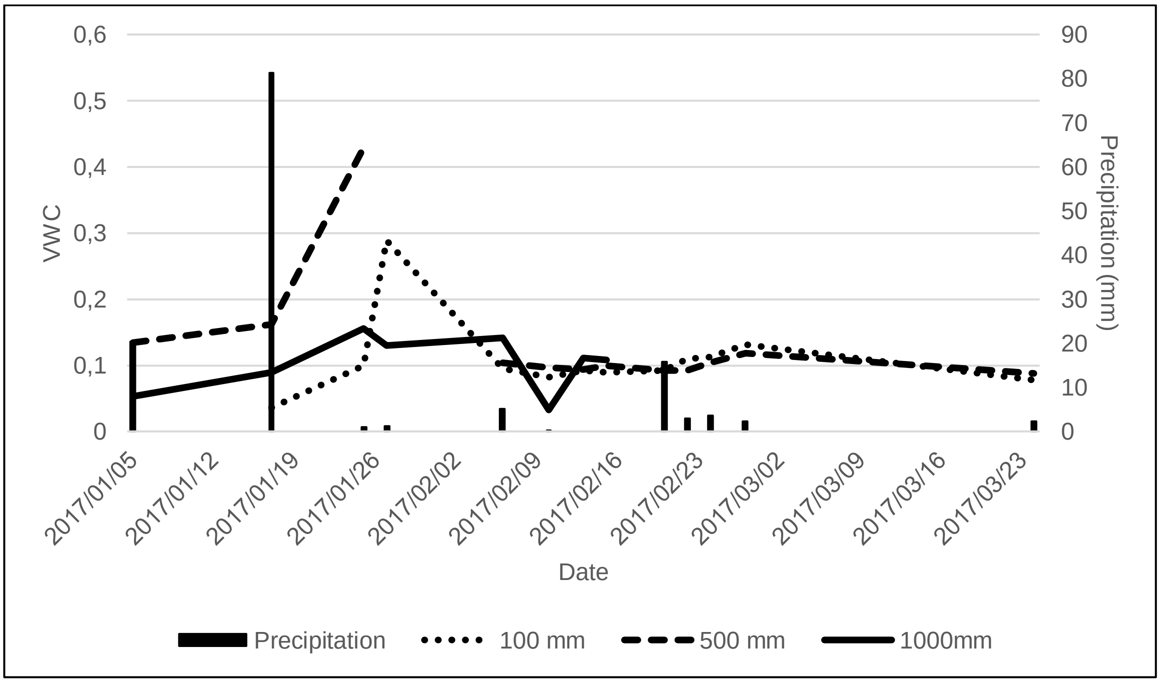

Figure 32: VWC measured at various depths for slope component 2

4.5.3 Slope Component 3

The upper 100 mm of the cover material on slope component 3 as well as the material at 500 mm below surface rapidly reacts to the high-intensity rainfall event on the 3rd and 4th of January. The material at 1 000 mm below surface starts reacting to the first rainfall event between the 5th of January and the 17th of January and peaks on the 25th of January. This phenomenon indicates a low hydraulic conductivity between the 500 mm and the 1 000 mm below surface mark, which is backed by the *Ks* results illustrated in Figure 28. The hydraulic conductivity is approximately three times lower at the 500 mm mark than the hydraulic conductivity at 200 mm, which indicates a substantial decrease in hydraulic conductivity before reaching the 1 000 mm mark. Therefore, percolation is slow and the water holding capacity is higher due to an expected increase in bulk density due to compaction of the material at certain depths. Furthermore, the rest of the datasets indicate peaks after rainfall events with a percolation delay for the material at 1 000 mm below surface.

It is, however, important to notice the VWC values of these datasets. The VWC recorded throughout the study period is very low with increases and spikes only indicating slight increases at all depths. The constant VWC throughout the profile indicates high volumes of overland flow rather than infiltration.

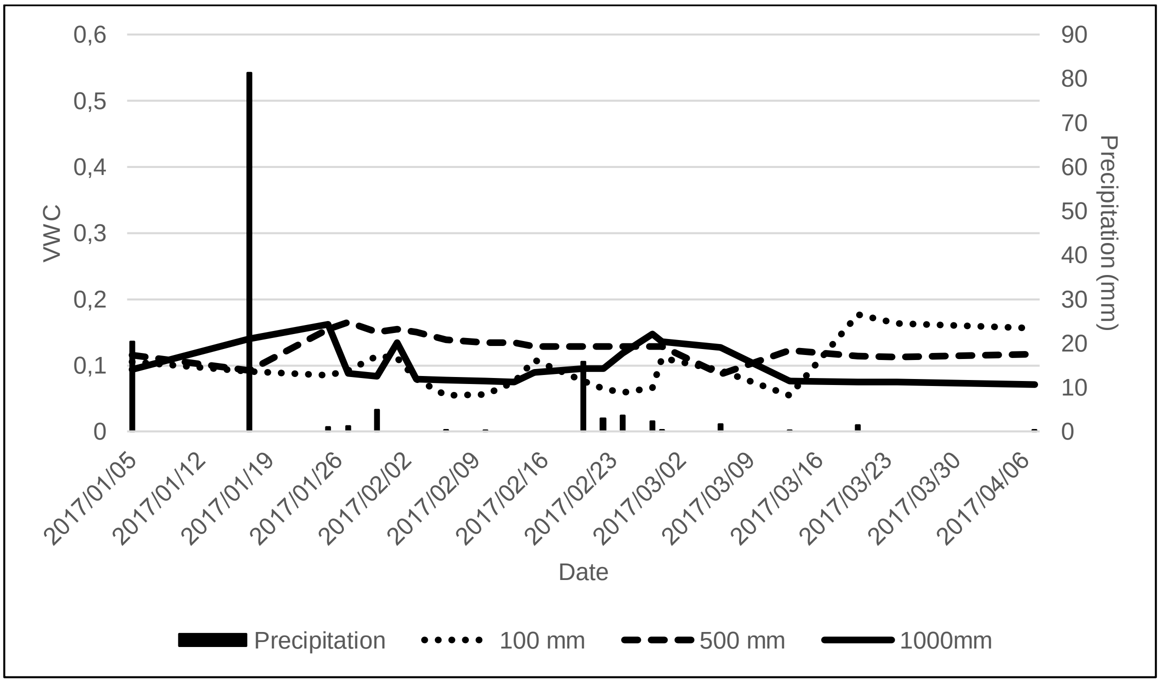

Figure 33: VWC measured at various depths for slope component 3

4.5.4 Slope Component 4

For the 1st rainfall, no high VWC results are recorded. The high VWC of the material at 1 000 mm below the surface is a result of precipitation at the end of January. For this slope component however, a substantial increase in VWC is recorded directly after the 2nd rainfall event for the upper 100 mm material and the material at 500 mm below the surface. A high VWC is recorded for the material at 1 000 mm below the surface on the 25th of January. However, due to the lack of data between the 17th of January and the 25th of January, a percolation delay from the material at 500 mm below surface to the material a 1 000 mm below surface can be expected to be anything between four and 12 days.

A defective reading is then recorded on the 15th of February. This reading illustrates a significant increase in VWC without any precipitation or other abnormal weather events, i.e. cold temperatures, dew, wind speeds etc. An increase is however recorded after the 3rd rainfall event with a four-day percolation delay from the surface to the material at 500 mm below the surface. The material at 1000 mm below the surface does not receive any moisture which indicates lateral movement between the surface and 1 000 mm below the surface for this specific rainfall event or the removal of moisture by means of evaporation and transpiration.

For the 4th rainfall event, the upper 100 mm constantly stays moist. There is no evidence that precipitation reaches the material 500 mm below surface due to the saturation from the 3rd event at this material on the given dates. Due to the four-day delay time however, it is assumed that moisture does not reach the material at 500 mm below surface during and after the 4th rainfall event.

Therefore, overland flow on this slope component is rare and infiltration takes place during and after high rainfall events. Moisture only reaches the material at 1 000 mm below surface after the 2nd rainfall event and not after the 3rd rainfall event. This profile requires very high-intensity rainfall events to reach the material at 1 000 mm below surface, which indicates either severe lateral movement of water (between the 500 mm and 1 000 mm mark) or an efficient cover. The saturated hydraulic conductivity is high throughout the profile, which eliminates a low hydraulic conductivity as an explanation for moisture not reaching the material at 1 000 mm below the surface (Figure 29).

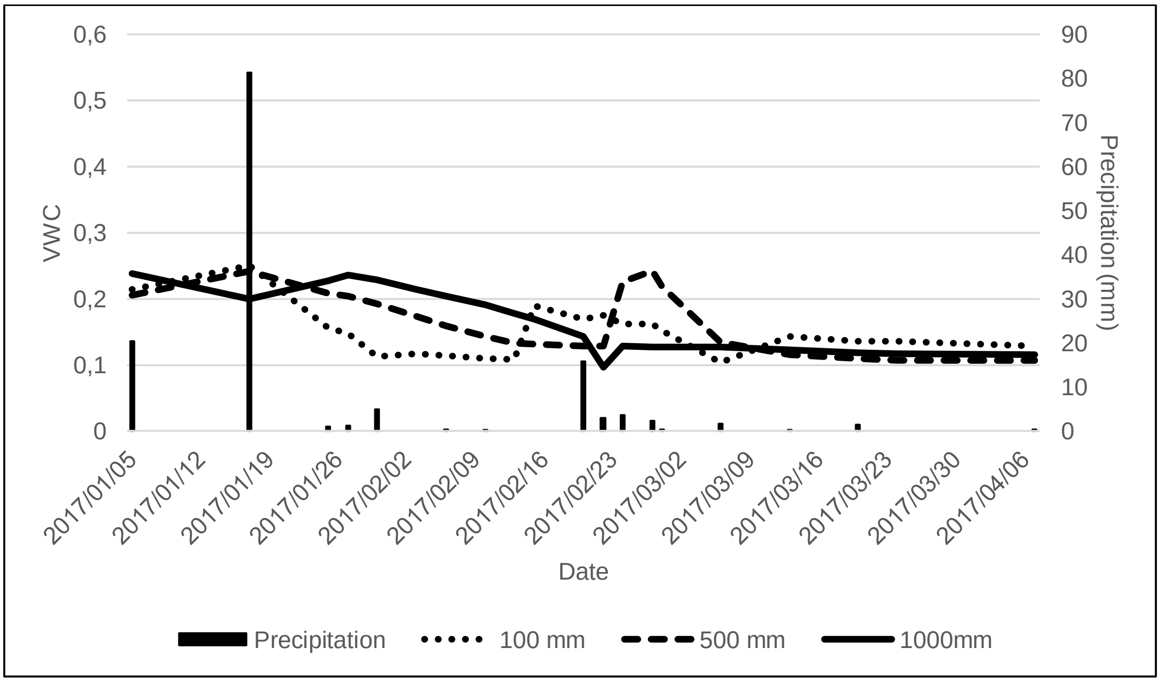

Figure 34: VWC measured at various depths for slope component 4

4.5.5 Slope Component 5

No data exist for the 1st rainfall event regarding the VWC. The VWC does however rapidly increase for the upper 100 mm and the material 1 000 mm below the surface with the material at 500 mm below the surface not spiking but rather staying constant throughout the study period.

A significant increase in VWC is recorded for the upper 100 mm after the 4th rainfall event with no significant increases in VWC for the 3rd rainfall event at any depth. Therefore, assumptions can be made that overland flow occurs seldom due to the high VWC after the very high-intensity rainfall and the gentle rainfall event for the upper 100 mm. The material at 1 000 mm has a high VWC on the same day that an increase is recorded for the upper 100 mm after the 2nd rainfall event. The VWC stays constant at 500 mm below surface and therefore assumptions can be made that vertical seepage is dominant and rapid, which is backed by the high saturated hydraulic conductivity values below the first 100 mm, see Figure 30.

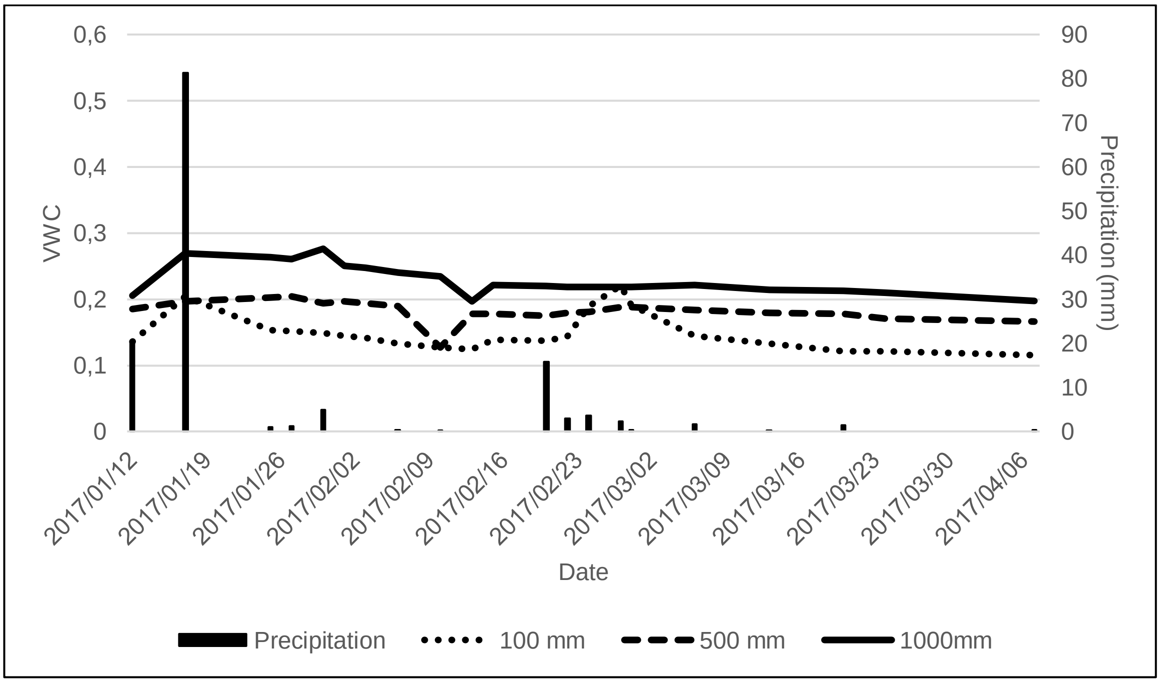

Figure 35: VWC measured at various depths for slope component 5

4.6 Overland Flow

As can be seen in Figure 36, Slope Component (SC) 5 is characterised by the most overland flow during and after rainfall events with the least overland flow recorded for SC 2. No overland flow was recorded for SC 1 due to faulty equipment. It is however the opinion of the researcher that many of these data sets illustrate false recordings. The tipping buckets tip over as soon as they have accumulated up to 1,3 L and will not tip over before accumulating this volume of water. It is however a possibility that animals drink water from these buckets when the tipping buckets are only half full, which will result in too much weight being placed on the bucket by the animal, ultimately allowing the bucket to tip even though 1,3 L has not accumulated. For slope component 5 for instance, an extremely high number of tips have been recorded even though the ROP on this slope component is on a flat surface. Simulations will predict accurate volumes of overland flow given the parameterisation of measured VWC and other parameters.

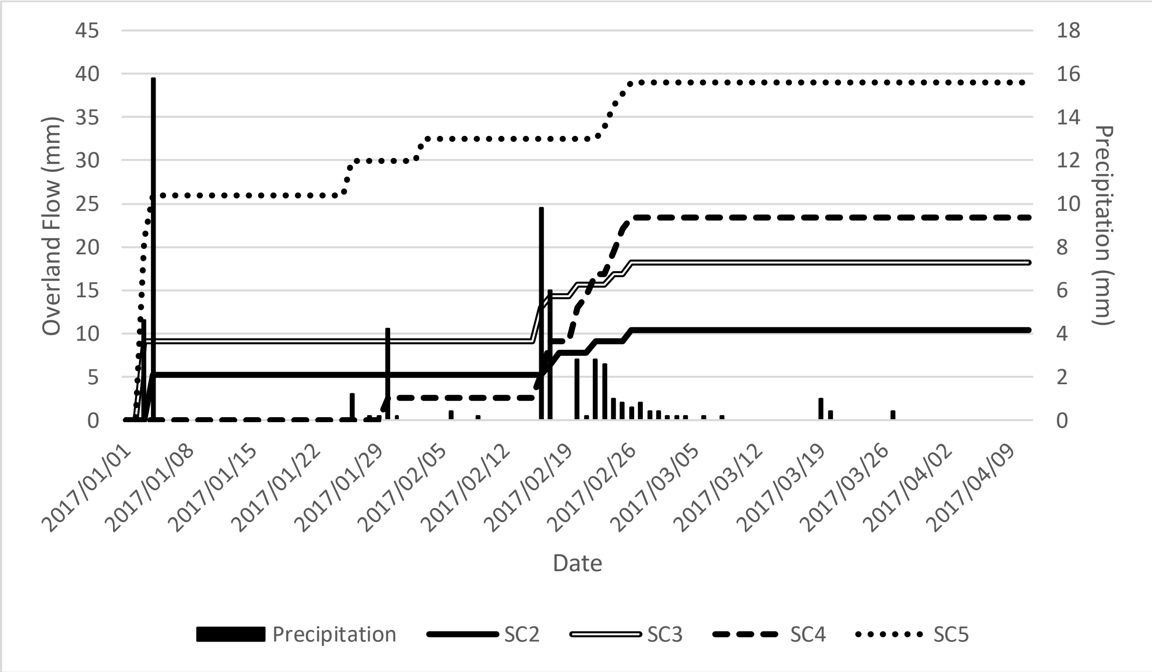

Figure 36: Overland flow and precipitation during the survey period

Chapter 5: Simulated Results

The results derived from simulations have been divided into five sections, each section representing an individual slope component. These simulations have been carried out by means of the descriptions provided in Section 3.2.4- “Predictions” in the *HYDRUS-2D* tool. The *Ks* values for the vermiculite cover material was adjusted after the initial simulation for all of the slope components due to a significant difference between simulated overland flow and measured overland flow. For *Ks* values similar to those measured *in-situ*, no overland flow is recorded due to high infiltrations accompanied by high *Ks*. It is the opinion of the researcher that results from the *in-situ* measurements for the cover material’s *Ks* is inaccurate due to various potential complications. The *Ks* values has been adjusted according to the description in Section 3.2.4.8- “Water Flow Parameters”.

Due to the large scale of the x-axis and the vast amount of data exported from the simulated results into the graph illustrated in Figure 47, the spike in rainfall events have been highlighted only for the VWC simulations from slope component 2 onwards after in-depth study of the trends in Figure 37 and Figure 38 for slope component 1.

5.1 Slope Component 1

The following sections describe simulated results for slope component 1 relevant to infiltration, overland flow and the direction of fluxes compared to the recorded precipitation. No overland flow data was recorded for slope component 1 due to faulty equipment. Therefore, the overland flow vs infiltration results could not be compared to measured data. Even though the accuracy of these results could not be proved, these results still add value given the fact that they do correlate well with the measured VWC.

5.1.1 Simulations for Entire Study Period

The simulated VWC results for the observation nodes during the entire study period (in hours) is illustrated in Figure 37. For slope component 1, the Observation Node (ON) at a 500 mm below the surface was removed given the abnormal reading from this ON. It is noticeable from this figure that a moderate increase in VWC is recorded at the ON a 100 mm below the surface after the rainfall event around the 60th hour (1st high-intensity rainfall event) with an increase in VWC approximately double that of the latter mentioned around the 300th hour due to a high-intensity rainfall event (2nd high-intensity rainfall event). An even larger increase is recorded after the second significant rainfall event around the 360th hour for the ON at 100 mm below the surface, even though the rainfall recorded for the spike in VWC is approximately a third of that of the previously mentioned. Thereafter, a gradual low-intensity rainfall event is recorded for a long period between the 1100th hour and the 1200th hour which has resulted in a small spike in the VWC reading for the ON at 100 mm below the surface.

As for the ON at 1 000 mm below the surface, the only spike in VWC reading is recorded after the 2nd significant rainfall event (15th-17th January or around the 300th hour) approximately 150 hours after the rainfall event that exceeded 25 mm/hour. With the exception of rainfall events, the simulated VWC is higher at a depth of 1 000 mm than at 100 mm.

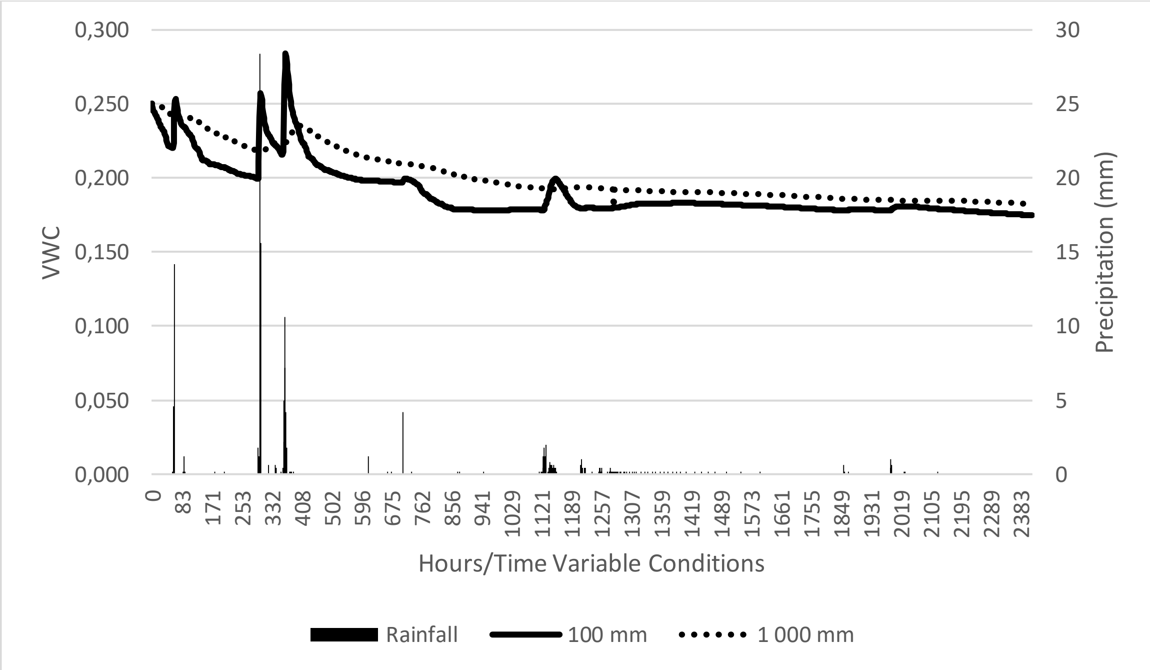

Figure 37: Simulated VWC results vs rainfall during the study period for slope component 1

The simulated pressure head results are illustrated in Figure 38 and similarly to Figure 37, is presented with the recorded rainfall data. Even though these results directly correlate with that of the VWC results in Figure 37, the spikes in pressure head results seem to be much more sensitive than the spikes in VWC. The sensitivity of this dataset has therefore indicated an additional spike in pressure head for an extremely small rainfall event on the 1989th and the 1990th hour worth one mm rainfall in total after a prolonged period without precipitation.

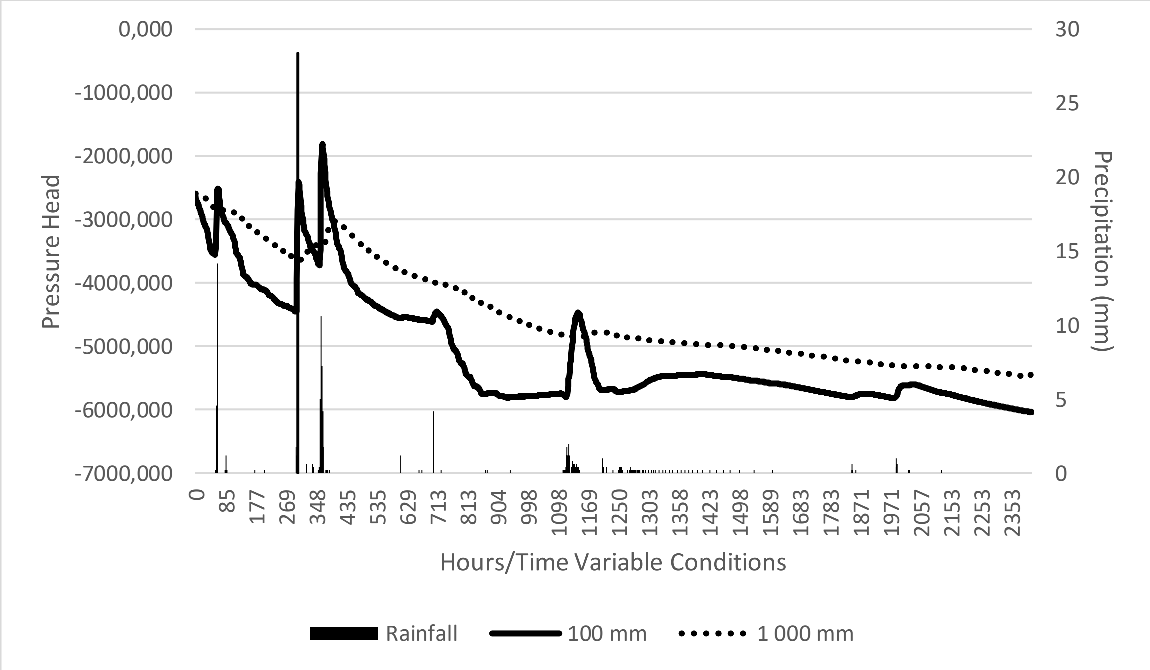

Figure 38: Simulated pressure head results vs rainfall during the study period for slope component 1

5.1.2 Overland Flow and Infiltration

Figure 39 and Figure 40 illustrate the simulated infiltration and overland flow results vs precipitation for the first and second high-intensity rainfall event respectively. For the first high-intensity rainfall event (Figure 39), the majority of precipitation is infiltrated with only a fraction (2.074 mm) being transported via overland flow. A small rainfall event is then recorded on the 85th hour totalling 3.112 mm which of which the total volume is infiltrated.

As for the second rainfall event (Figure 40), a higher intensity rainfall event is recorded of which the majority is transported via overland flow. A large volume of overland flow was simulated which totals 21.22 mm after the 303rd hour following a 28.4 mm rainfall event on the 303rd hour. Thereafter, a rainfall event with approximately a third the intensity of the latter is recorded on the 356th hour to the 361st hour, after which the majority infiltrates with only 4.92 mm being carried off via overland flow.

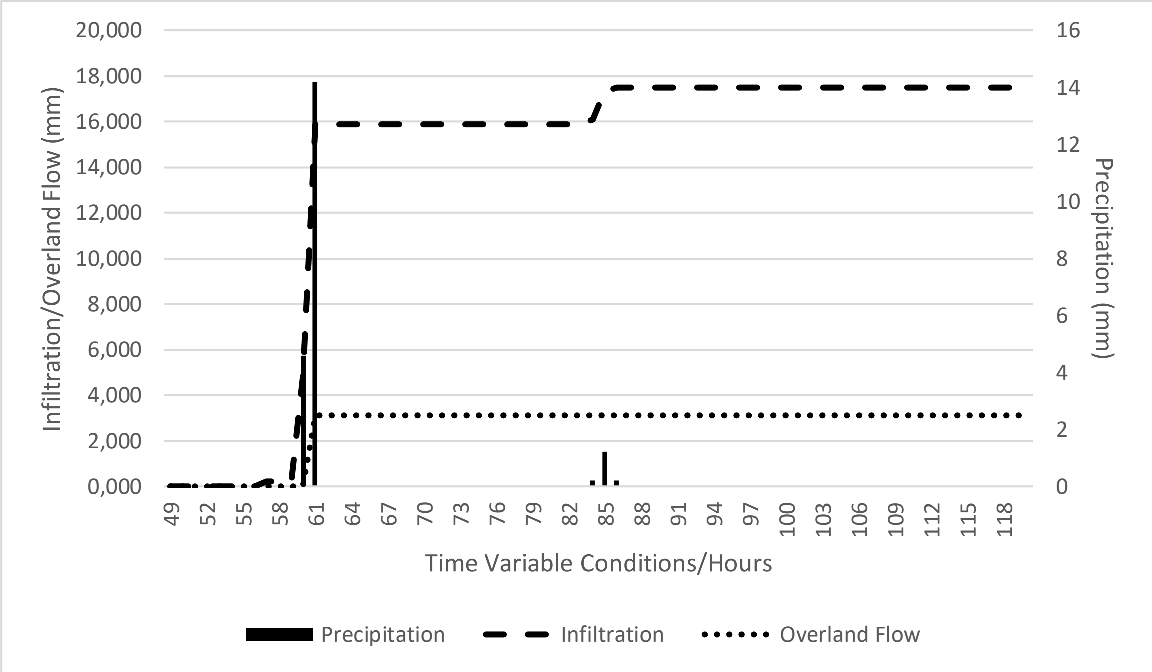

Figure 39: Simulated infiltration/overland flow vs precipitation for the 1st high-intensity rainfall event

Figure 40: Simulated infiltration/overland flow vs precipitation for the 2nd high-intensity rainfall event

5.1.3 Results simulated via Cross-Section Auxiliary Objects

The following sections contain illustrations and descriptions of results obtained from the vertical- and horizontal cross-sections inserted into simulations, as was discussed in Section 3.2.4.16- “Auxiliary Objects”.

5.1.3.1 Vertical Cross-Section

The simulated VWC results from the vertical cross-section auxiliary object through the first and second high-intensity rainfall events are illustrated in Figure 41 and Figure 42 respectively. The results simulated in Figure 41 indicates a spike in VWC at a depth of 100 mm on the hour of the high-intensity rainfall event (14.2 mm/hour on the 62nd hour) with a slighter increase in VWC recorded for at a depth of 200 mm an hour later. A slight increase in VWC is recorded at a depth of 500 mm three hours after the rainfall event with no increase in VWC recorded at depths of 1 000 mm and 2 000 mm. It is, however, worth noting that the VWC at a depth of 2 000 mm below the surface is higher than that of the 1 000 mm mark.

The simulated results from the second high-intensity rainfall event indicate a similar trend to that of the first rainfall event in regard to spikes in VWC after rainfall events at certain depths. The only difference can be noticed at a depth of 500 mm, where a larger increase in VWC was recorded due to the larger rainfall event.

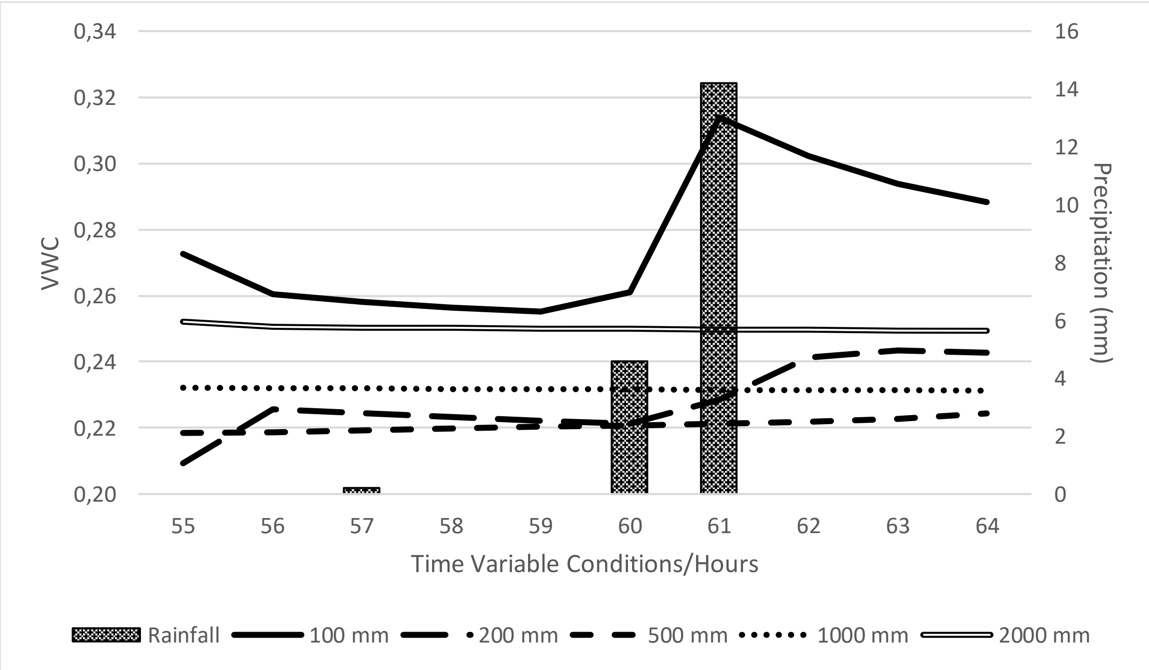

Figure 41: Simulated VWC through the vertical cross section for the first high-intensity rainfall event

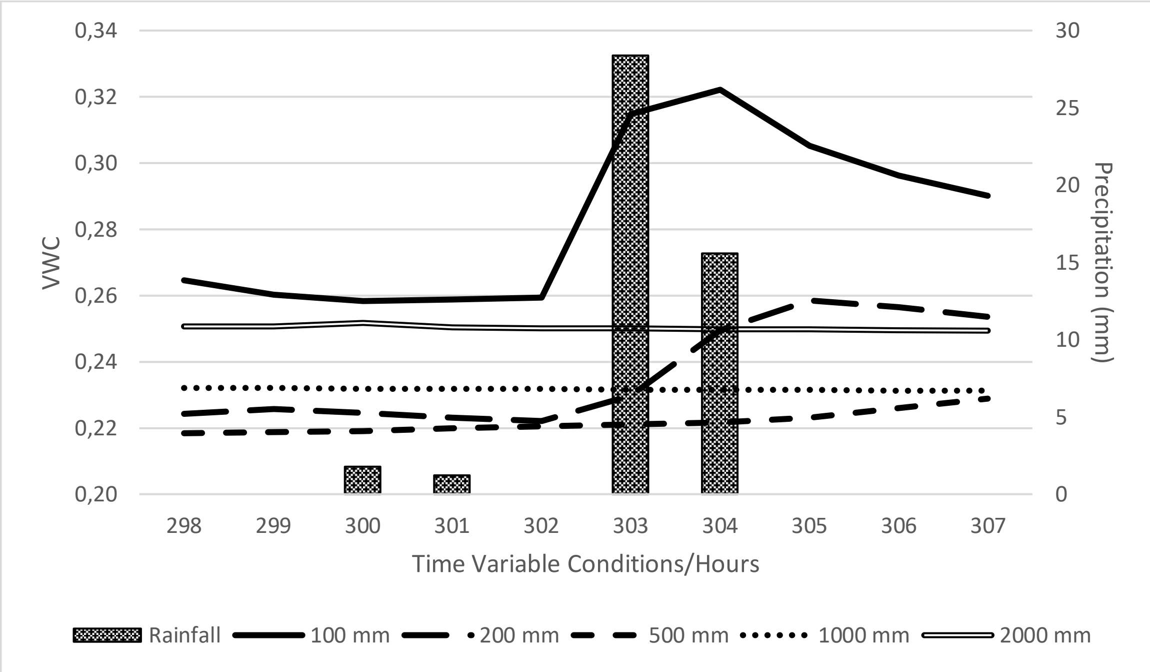

Figure 42: Simulated VWC through the vertical cross section for the second high-intensity rainfall event

5.1.3.2 Horizontal Cross-Section

The simulated VWC results from the horizontal cross-section auxiliary object through the first and second high-intensity rainfall events are illustrated in Figure 43 and Figure 44 respectively. Figure 43 indicates spikes in VWC on the 100 mm length mark starting from the hour of the high-intensity rainfall event (61st hour) with the 500 mm mark's spike starting an hour later. Thereafter, a slight increase in VWC can be noticed three hours later. The 2 000 mm mark is characterised by an increase in VWC seven days after the high-intensity rainfall event on the 62nd hour. As for the 5 000 mm mark, a steady decrease was noticed up to fourteen days after rainfall. It is worth noting that the VWC for the mark at a length of 5 000 mm is higher than that of the 2 000 mm mark. Therefore, some lateral movement could occur within the profile given higher VWC at the seepage face.

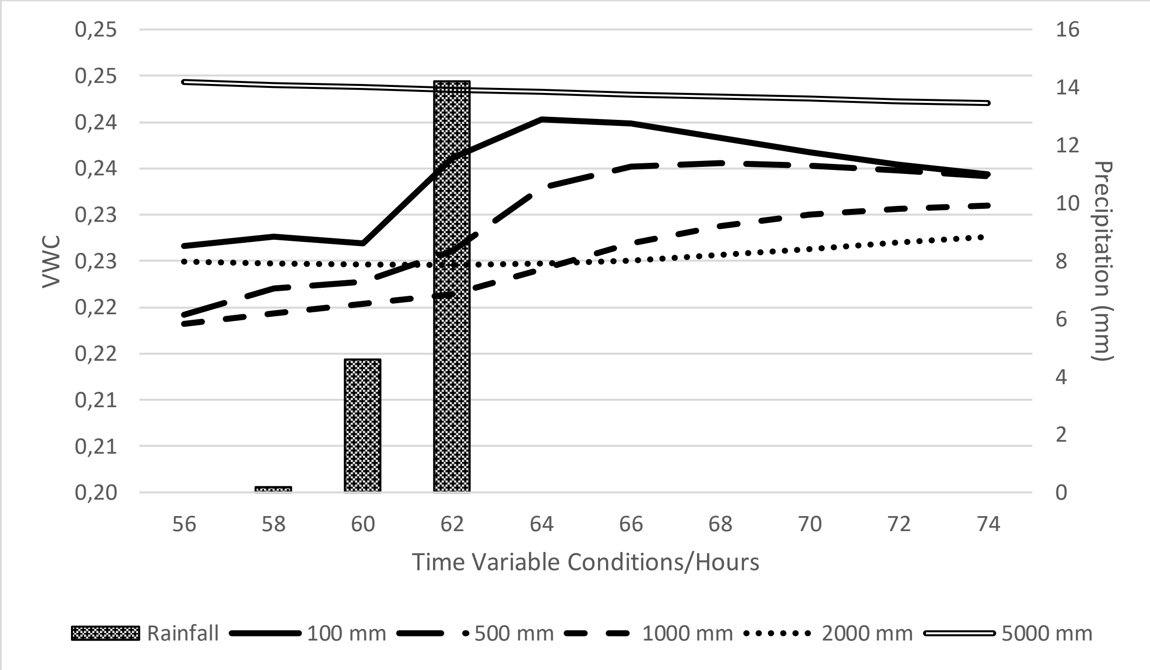

Figure 43: Simulated VWC through the horizontal cross section for the first high-intensity rainfall event

The simulated results through the horizontal cross-section during the second high-intensity rainfall event is similar to that described for the first high-intensity rainfall event. The only noticeable difference in results from the second high-intensity rainfall event is the VWC itself due to much more rainfall recorded during the second event. The spikes for all the relevant distances are higher than that of the first event. It is worth noting that even with 28 mm more rainfall during a four day-period, no increase in VWC in the 5 000 mm length mark was recorded.

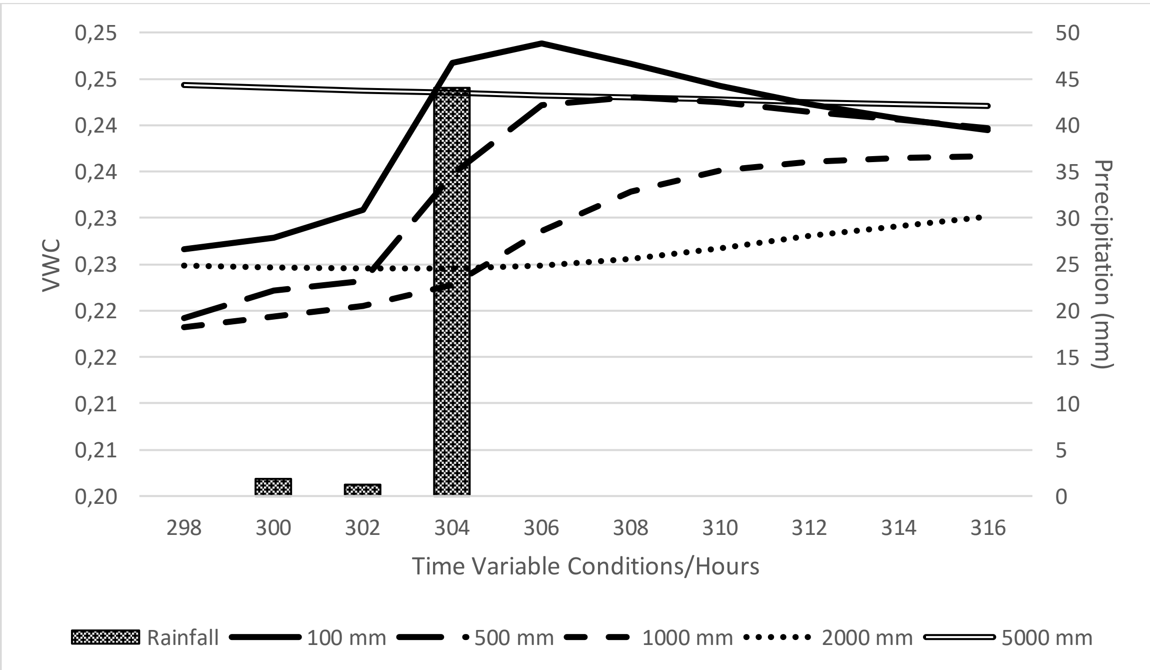

Figure 44: Simulated VWC through the horizontal cross section for the second high-intensity rainfall event

5.1.4 Velocity Vectors

The velocity vector results from the first rainfall event are illustrated in Figure 45. The direction of the velocity vectors indicates a dominant vertical movement of infiltrated water with a velocity of generally less than 0.875 mm/hour. The upper 200 mm dries up before the rainfall event due to percolation of water and continues evaporation and transpiration during the day (hence the upward direction of the velocity vectors before the rainfall event indicated at hour 61). During the rainfall events (62^{nd} and 63^{rd} hour), the velocity of infiltration increases up to 8 mm/hour during the infiltration of high volumes of precipitation. The surface stays saturated for the next three hours with ongoing vertical percolation at a velocity smaller than 0.875 mm/hour.

For the second high-intensity rainfall event illustrated in Figure 46. The difference between the velocity vectors illustrating percolation and infiltration between the first and second high-intensity rainfall event lies in the depth and velocity of the velocity vectors. The velocity vectors for the second high-intensity rainfall event has a higher velocity (0.622-2.487 mm/hour) deeper depths for longer periods than that of the first rainfall event. The surface was saturated slightly more prior to the second rainfall event. In both examples, the velocity vectors indicate the dominance of lateral movement within the cover material with a dominant vertical movement of water deeper than that. During high infiltration events, the little lateral movement there is within the profile changes into dominant vertical movement.

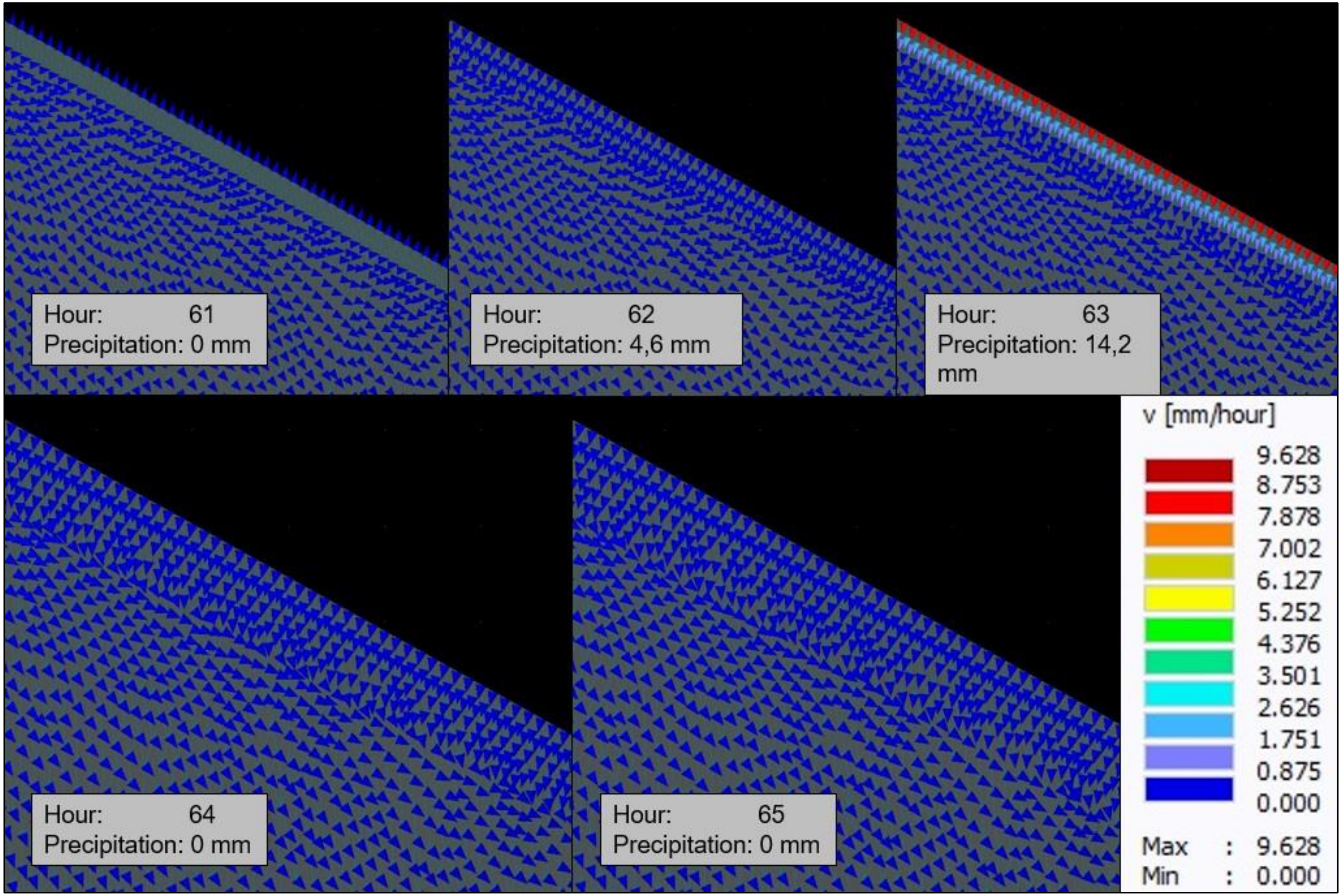

Figure 45: Velocity vectors simulated by the HYDRUS-2D tool during the 1st high-intensity rainfall event

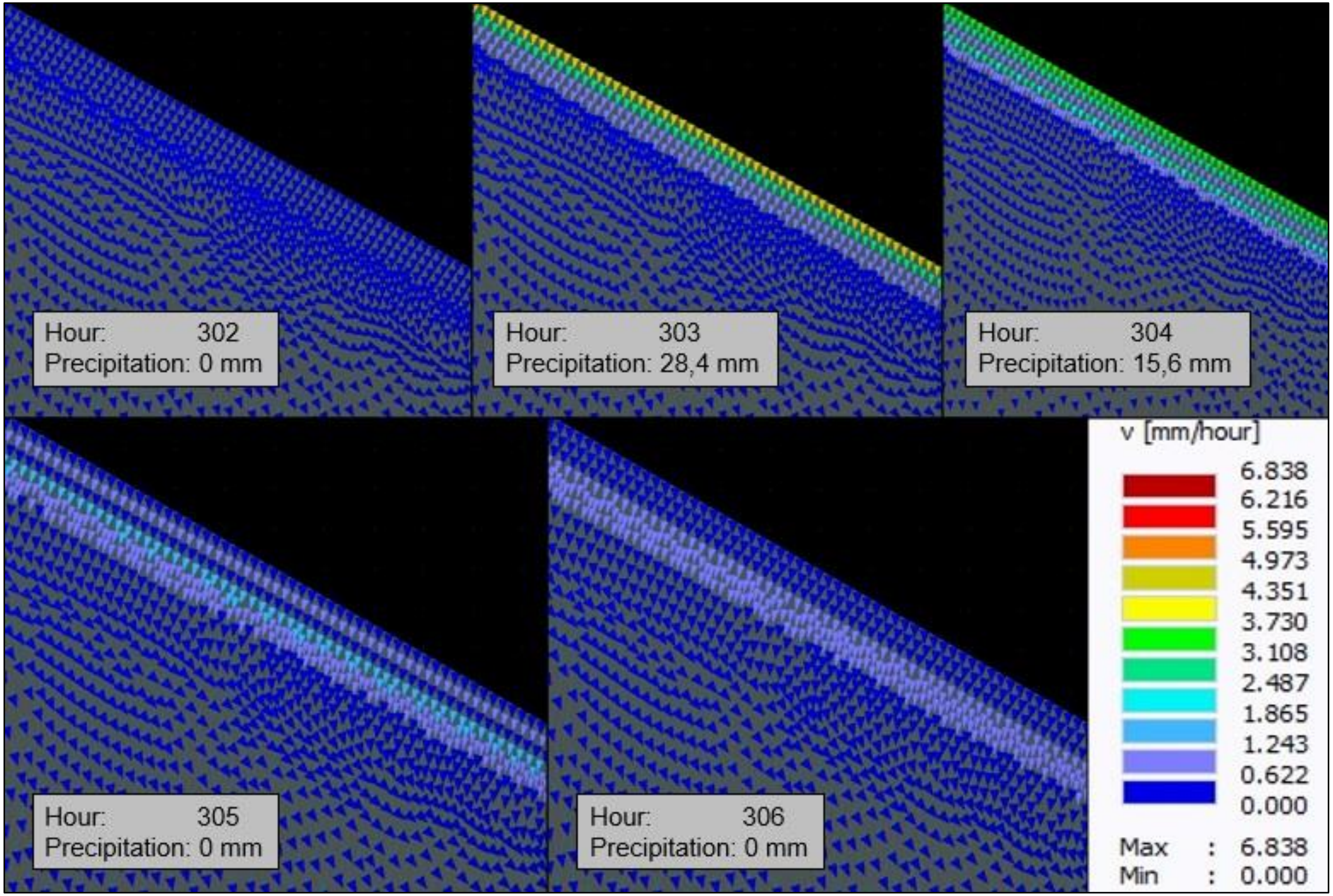

Figure 46: Velocity vectors simulated by the HYDRUS-2D tool during the 2nd high-intensity rainfall event

5.2 Slope Component 2

The following sections describe simulated results for slope component 2 relevant to infiltration, overland flow and the direction of fluxes compared to the recorded precipitation. The *Ks* for the cover material was fitted by means of inverse modelling and decreased to a recommended 1,35 mm/h according to the description in 3.2.4.8- "Water Flow Parameters".

5.2.1 Simulations for Entire Study Period

The simulated VWC results for the observation nodes during the entire study period (in hours) is illustrated in Figure 47 to Figure 49. For slope component 2, the Observation Node (ON) at a 100 mm below the surface immediately records an increase in VWC during the rainfall event on the 60^{th} and 61^{st} hour, closely followed by spikes at a depth of 500 mm and 1 000 mm, with decreasing magnitudes. This trend can be noticed for the rest of the rainfall events following in Figure 47 with the largest peak in VWC simulated during the highest rainfall event in Figure 48 and the lowest in Figure 49.

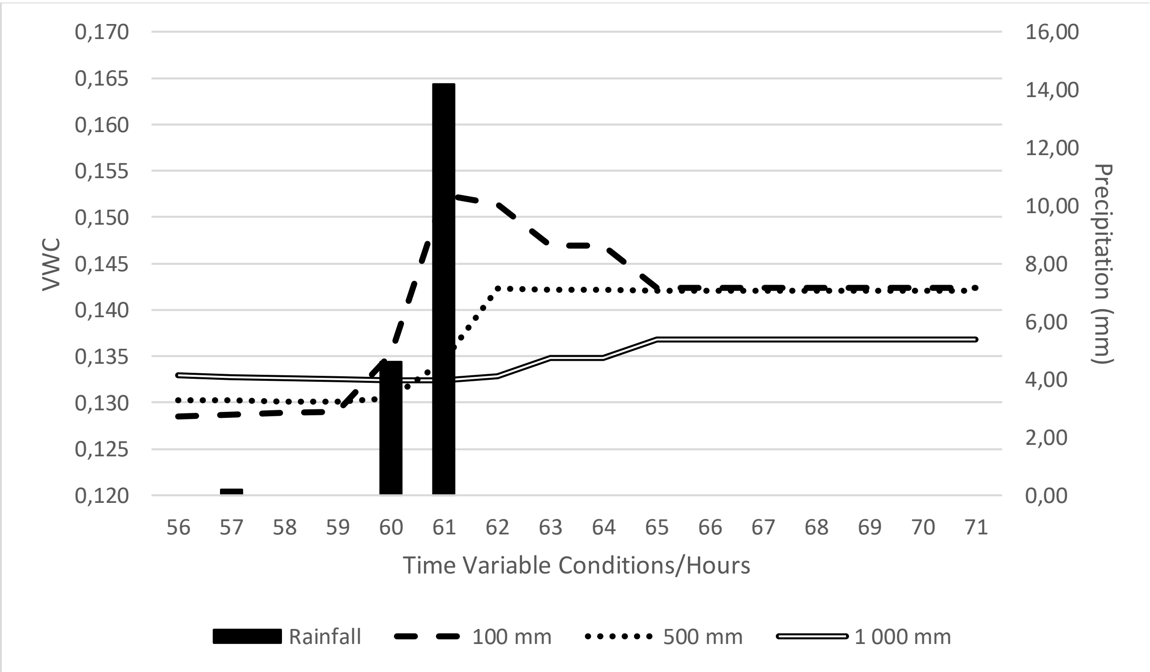

Figure 47: Simulated VWC results vs rainfall for slope component 2

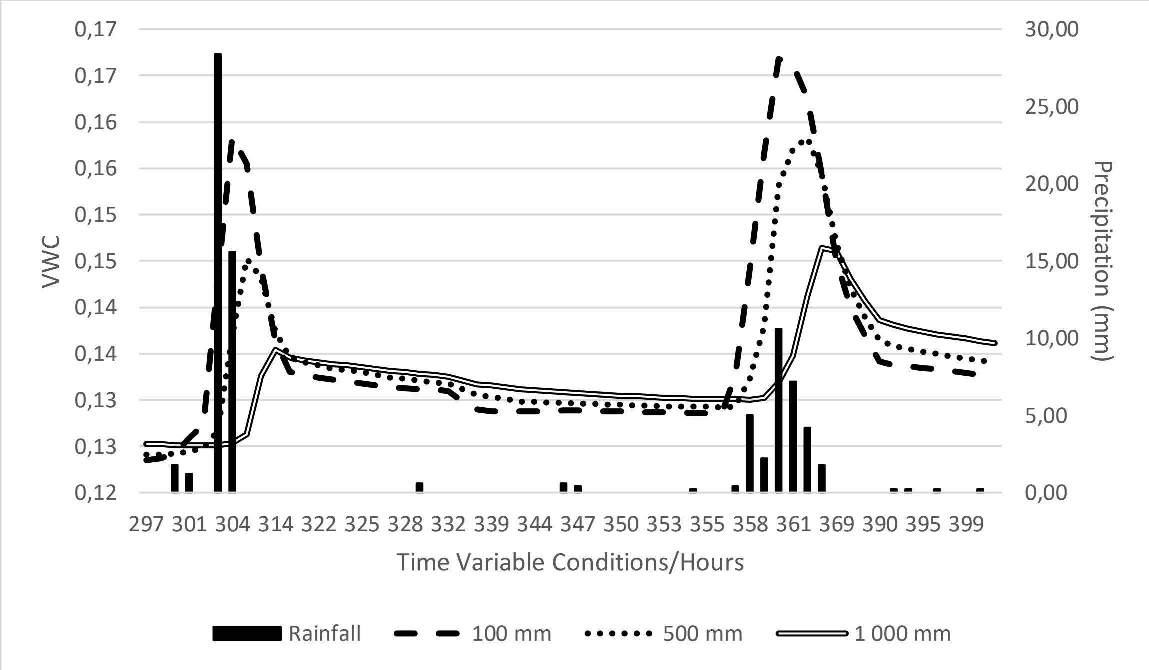

Figure 48: Simulated VWC results vs rainfall for slope component 2

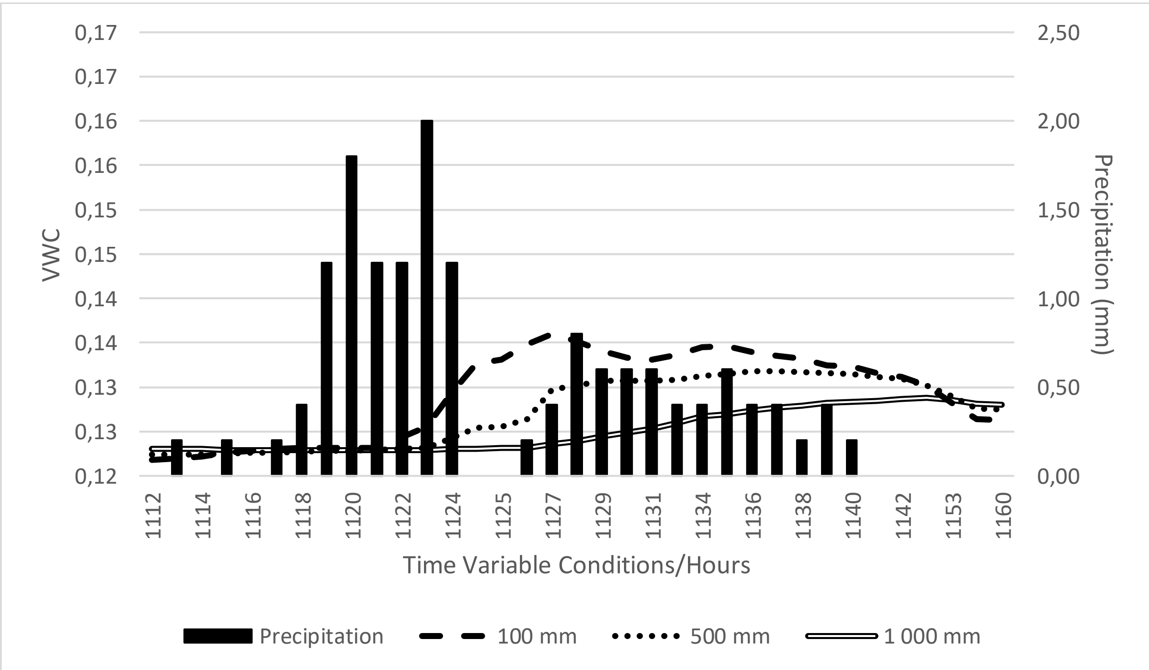

Figure 49: Simulated VWC results vs rainfall for slope component 2

5.2.2 Overland Flow and Infiltration

Figure 50 indicates the dominance of infiltration over overland flow with the *Ks* fitted to 1.35 mm/hour to match recorded overland flow values and to reach conditions closely resembling the recorded VWC at various depths. Figure 51, however, indicates the dominance of overland flow over infiltration after the rainfall event totalling over 30 mm with the cumulative infiltrated volume surpassing that of the cumulated volume of overland flow due to various low-intensity rainfall events during which no overland flow was simulated.

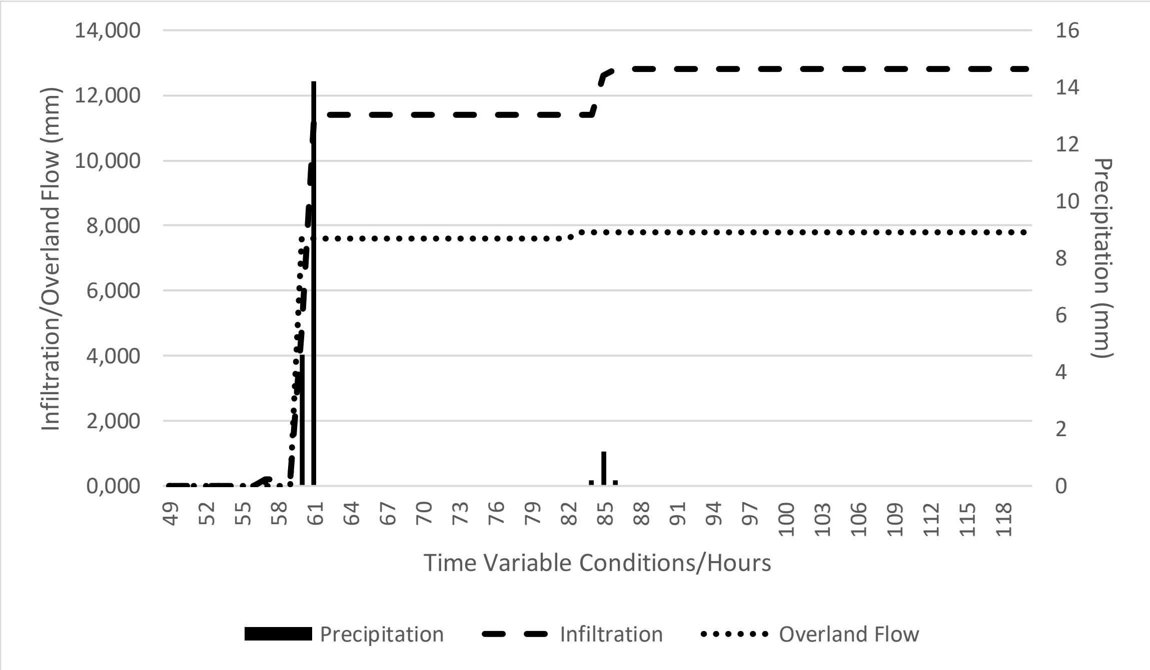

Figure 50: Simulated infiltration/overland flow vs precipitation for the 1st high-intensity rainfall event

Figure 51: Simulated infiltration/overland flow vs precipitation for the 2nd high-intensity rainfall event

5.2.3 Results Simulated Through Cross-Section Auxiliary Objects

The following sections contain illustrations and descriptions of results obtained from the vertical- and horizontal cross-sections inserted into simulations, as was discussed and illustrated in Section 3.2.4.16- “Auxiliary Objects”.

5.2.3.1 Vertical Cross-Section

The simulated VWC results from the vertical cross-section auxiliary object through the first and second high-intensity rainfall events are illustrated in Figure 52 and Figure 53 respectively. For the first high-intensity rainfall event, a high VWC is simulated at a depth of a 100 mm below the surface. The rest of the depths (in order from shallow to deep) receive moisture from the rainfall event at delayed intervals and at lower magnitudes with the depth at 2 000 mm below the surface not receiving any moisture from the rainfall event within seven hours' time. For the second high-intensity rainfall event, the same trends follow that of the first high-intensity rainfall event only with larger peaks in VWC due to a higher volume of water infiltrated from the larger rainfall event, as can be seen in Figure 50 and Figure 51.

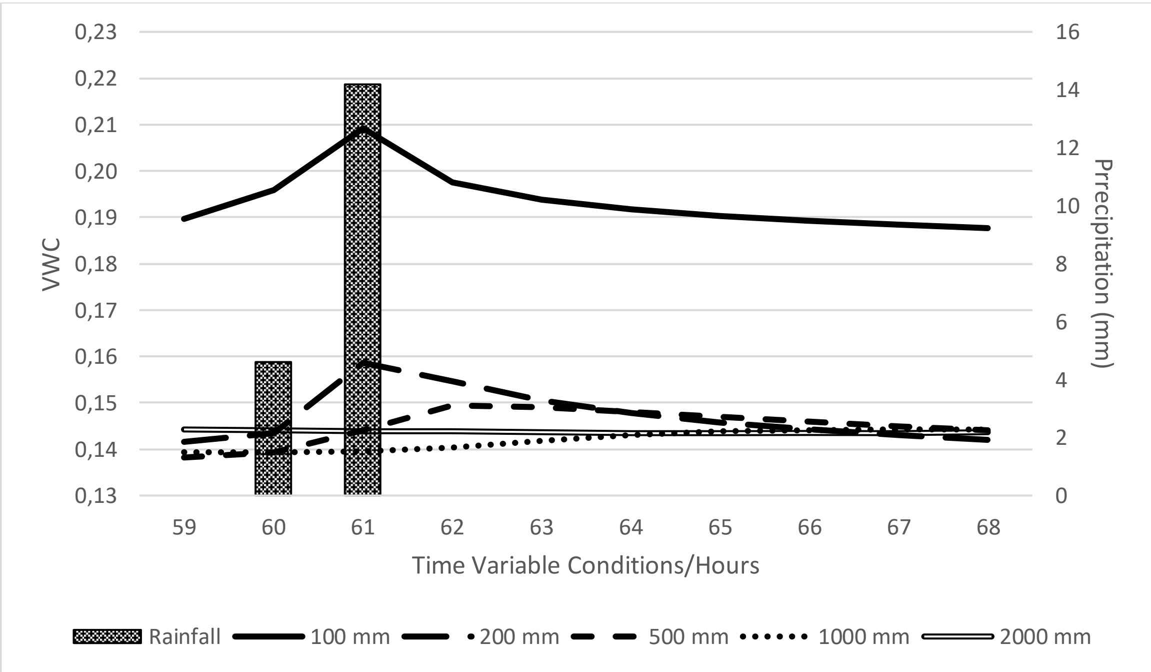

Figure 52: Simulated VWC through the vertical cross section for the first high-intensity rainfall event

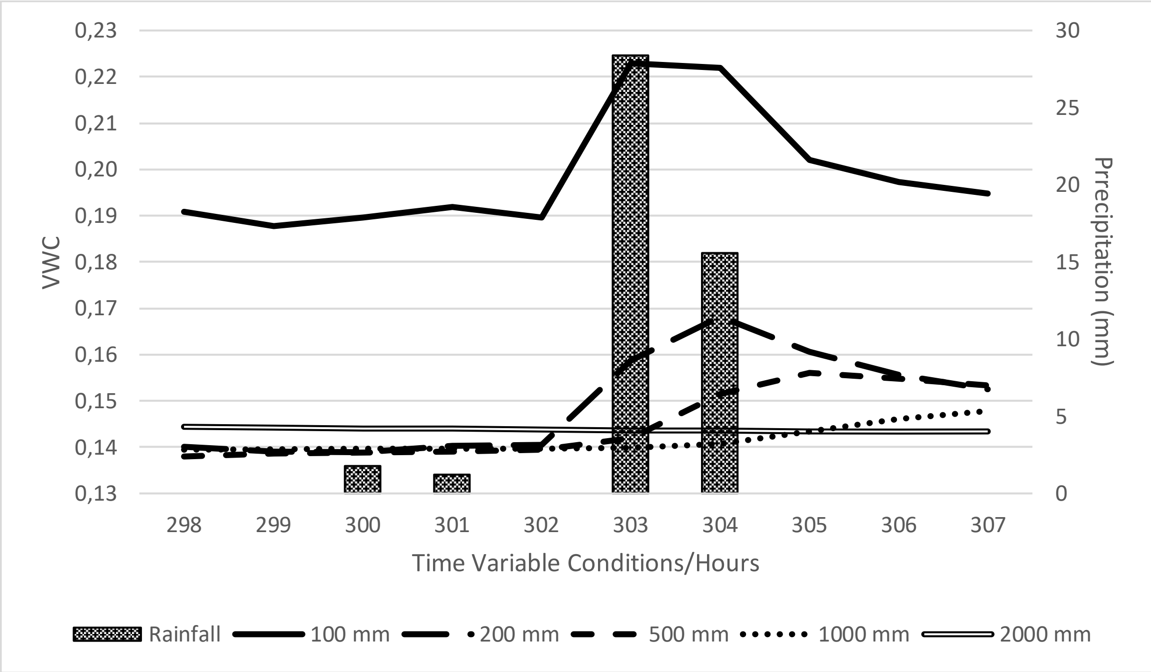

Figure 53: Simulated VWC through the vertical cross section for the second high-intensity rainfall event

5.2.3.2 Horizontal Cross-Section

The simulated VWC results from the horizontal cross-section auxiliary object through the first and second high-intensity rainfall events are illustrated in Figure 54 and Figure 55. After the first intensity rainfall event, a slight increase in VWC is simulated from the start of the cross-sectional profile up to the 5 000 mm in length mark, which indicates a lateral seepage flux up to the 5 000 mm mark, which is expected to be negligible given the extremely low increase in VWC over the horizontal cross-sectional profile up to seven hours after the rainfall period. The rest of the lengths decrease in VWC which indicate the dominance of vertical seepage at the relevant depths. The opposite is simulated for the second high-intensity rainfall event with the horizontal movement being more dominant than that of the first high-intensity rainfall event. Even though this might be the case, the vertical movement is much more dominant than that of lateral movement, which is backed by the negative values in seepage fluxes simulated by the *HYDRUS-2D* tool.

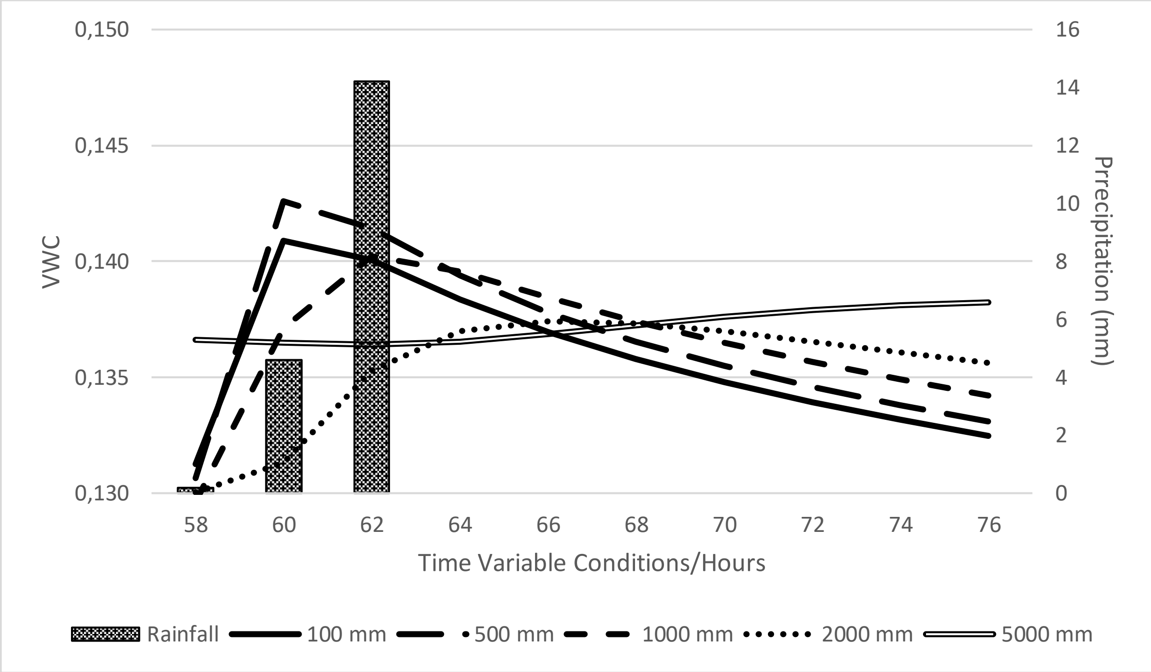

Figure 54: Simulated VWC through the horizontal cross section for the first high-intensity rainfall event

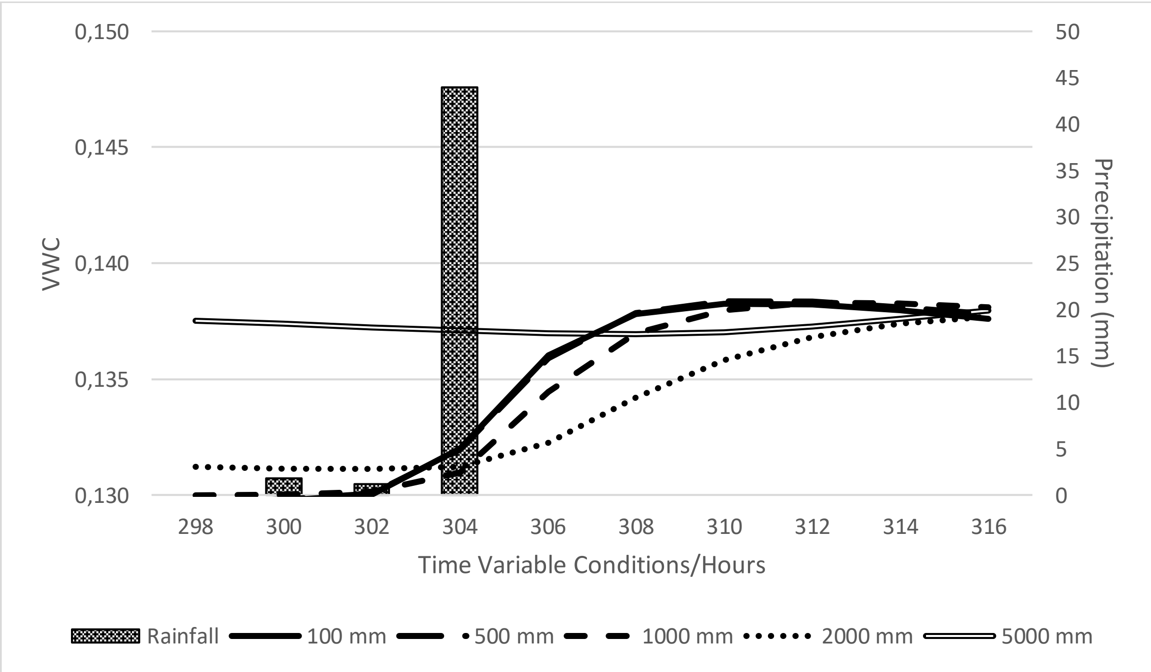

Figure 55: Simulated VWC through the horizontal cross section for the second high-intensity rainfall event

5.2.4 Velocity Vectors

The velocity vector results from the first and second high-intensity rainfall event are illustrated in Figure 56 and Figure 57. The highest velocities recorded for infiltration and percolation for the simulations are similar with the second high-intensity rainfall event being characterised by deeper percolation of with a higher velocity at deeper depths.

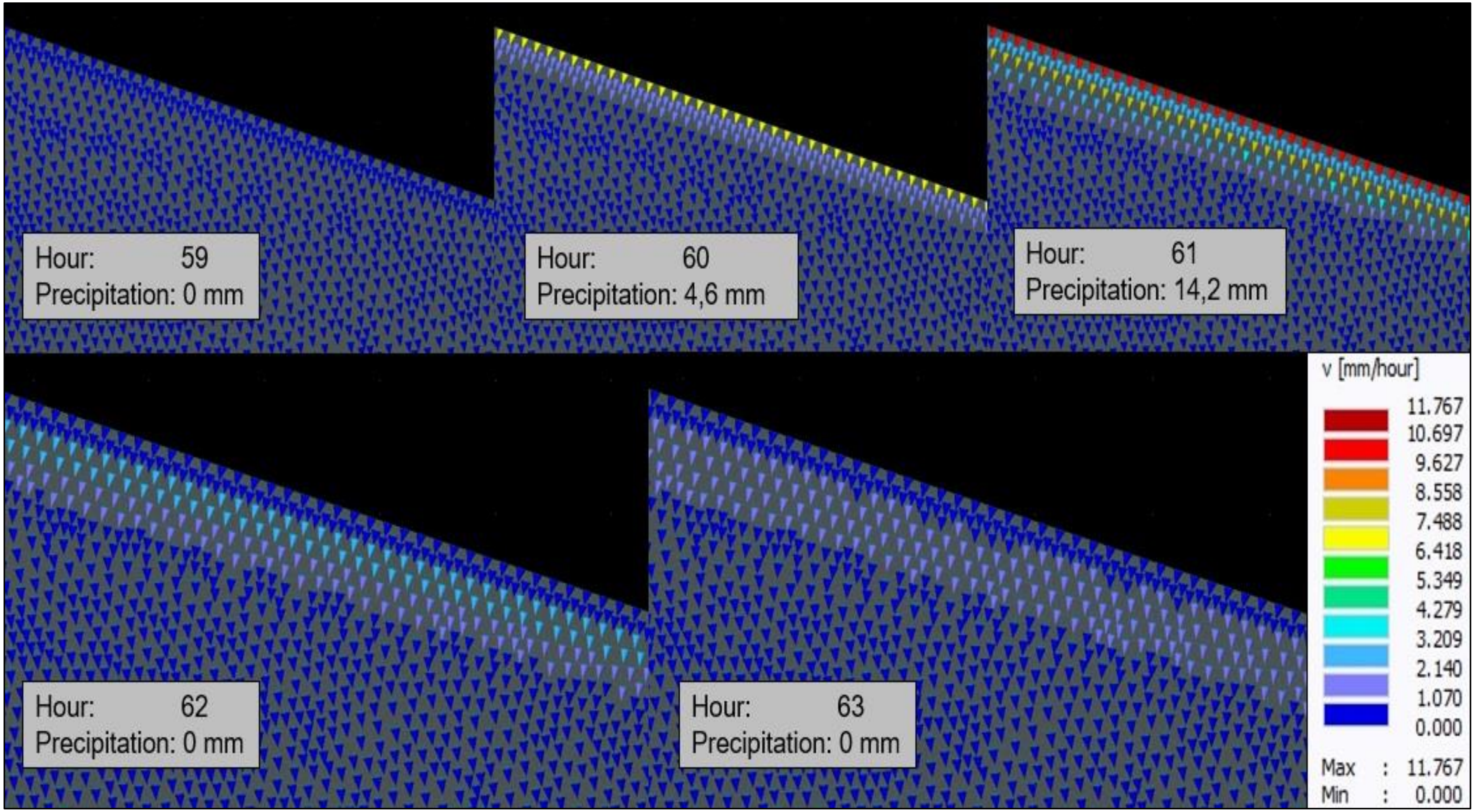

Figure 56: Velocity vectors simulated by the HYDRUS-2D tool during the 1st high-intensity rainfall event

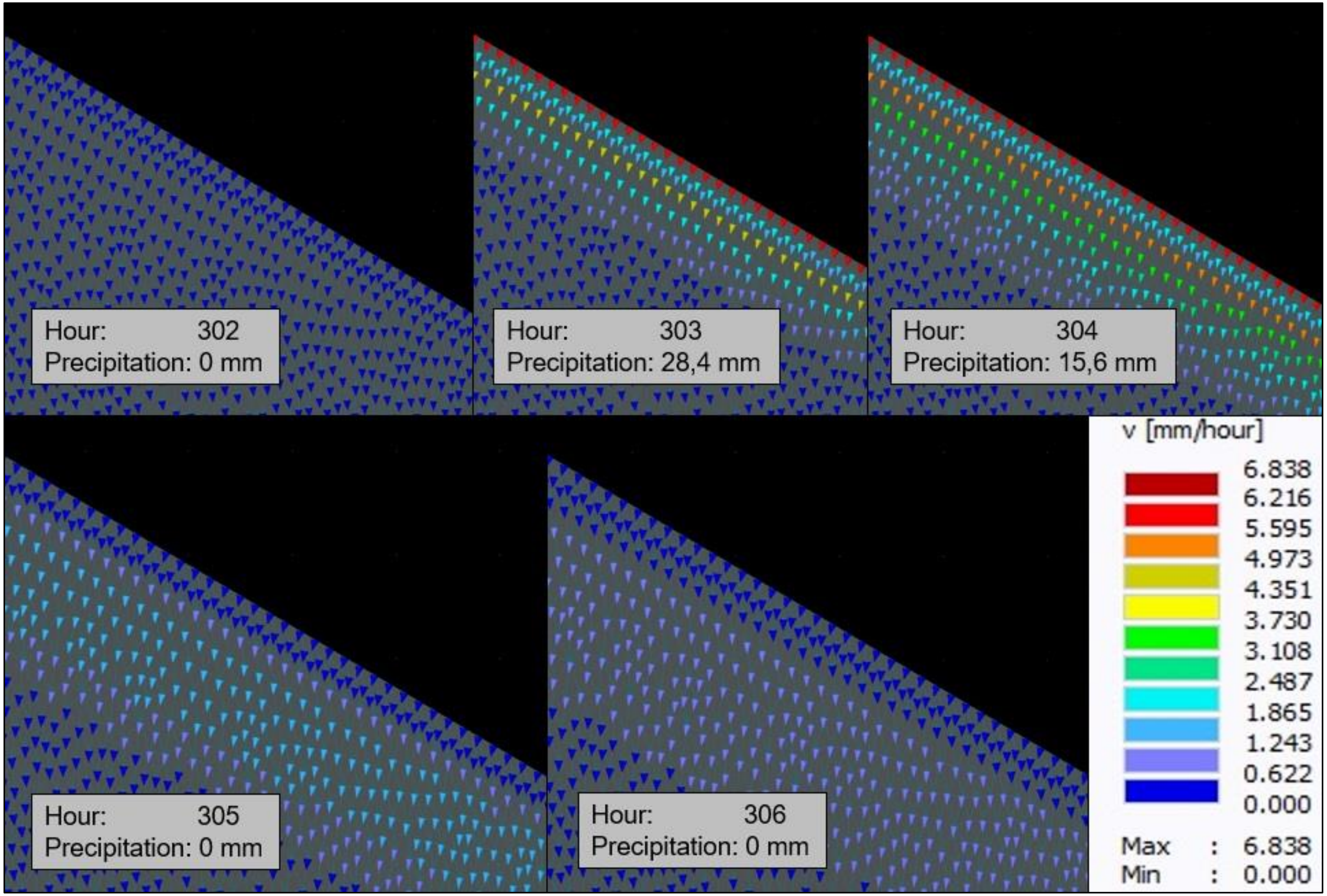

Figure 57: Velocity vectors simulated by the HYDRUS-2D tool during the 2nd high-intensity rainfall event

5.3 Slope Component 3

The following sections describe simulated results for slope component 3 relevant to infiltration, overland flow and the direction of fluxes compared to the recorded precipitation. The *Ks* for the cover material was decreased to 1,5 mm/h to closely resemble the measured overland flow during and after rainfall events to improve the accuracy of predictions. θs has been fitted as part of inverse modelling to combine simulated data and observed data for accurate predictions.

5.3.1 Simulations for Entire Study Period

The simulated VWC results for the observation nodes during the entire study period (in hours) is illustrated in Figure 58 to Figure 60. The peaks in VWC is gradual for depths of 100 mm and 500 mm and characterised by a delay of four hours and seven hours respectively for these two depths during the first high-intensity rainfall event. After fourteen hours, no increase in VWC was simulated at a depth of 1 000 mm.

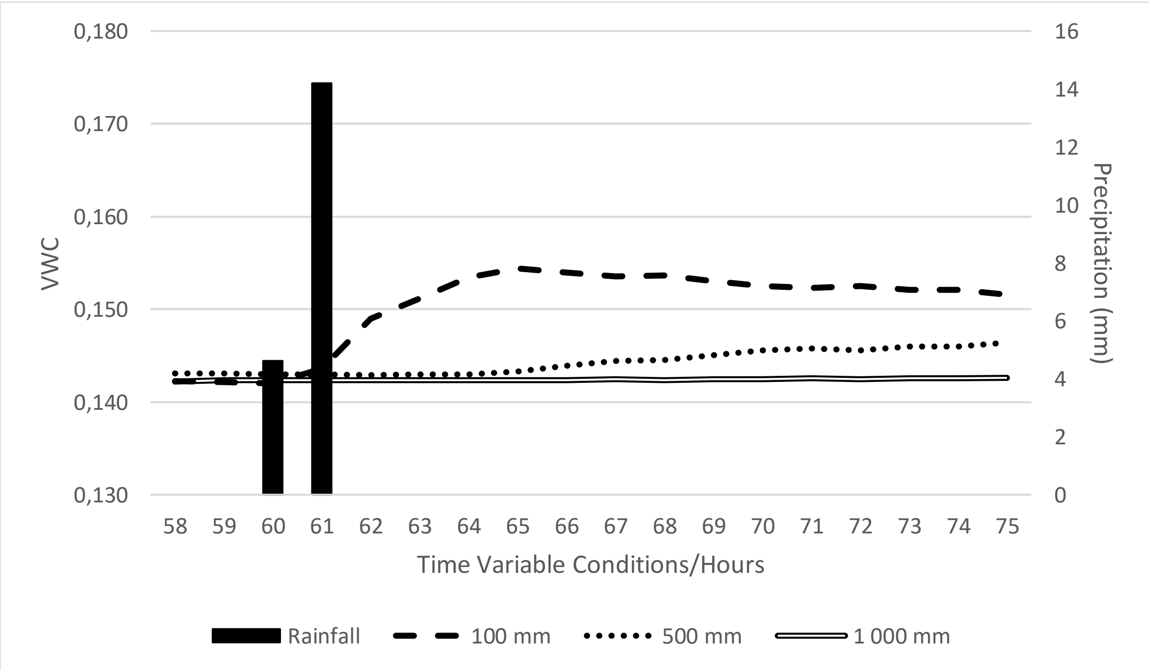

Figure 58: Simulated VWC results vs rainfall for slope component 3

During the second high-intensity rainfall event (Figure 59), higher peaks in VWC in simulated due to higher rainfall with the rainfall event at 360 hours resulting in VWC much higher at all three depths than for the rainfall event around the 300th hour with a much lower rainfall event. A minimal increase in VWC is simulated during the rainfall events illustrated in Figure 60.

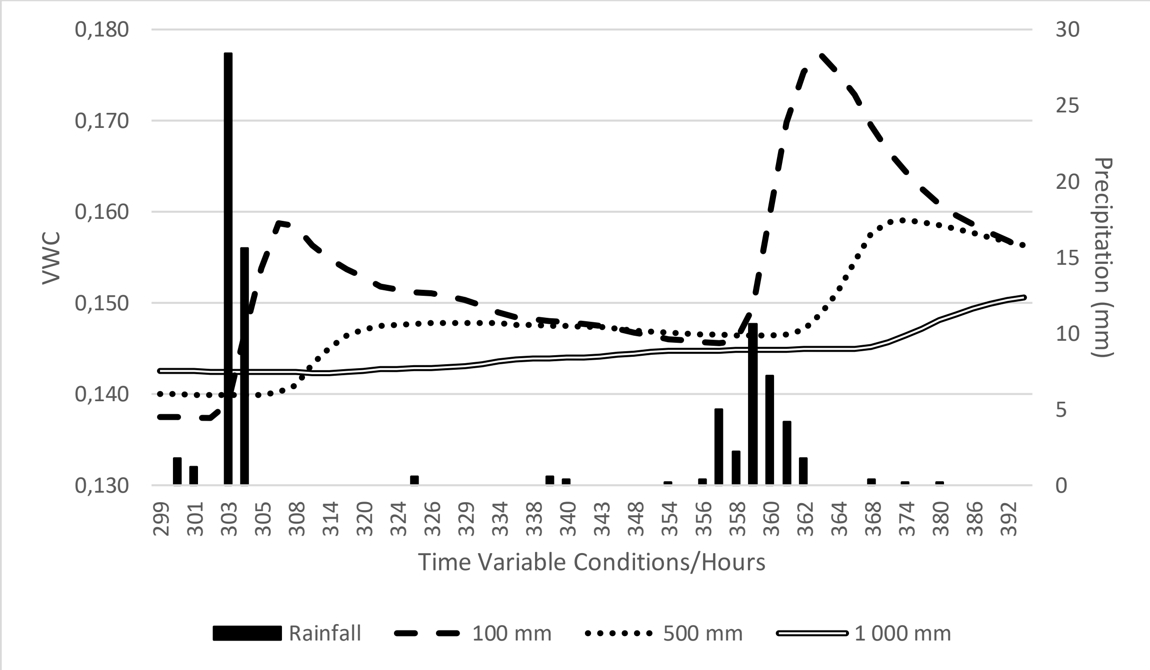

Figure 59: Simulated VWC results vs rainfall for slope component 3

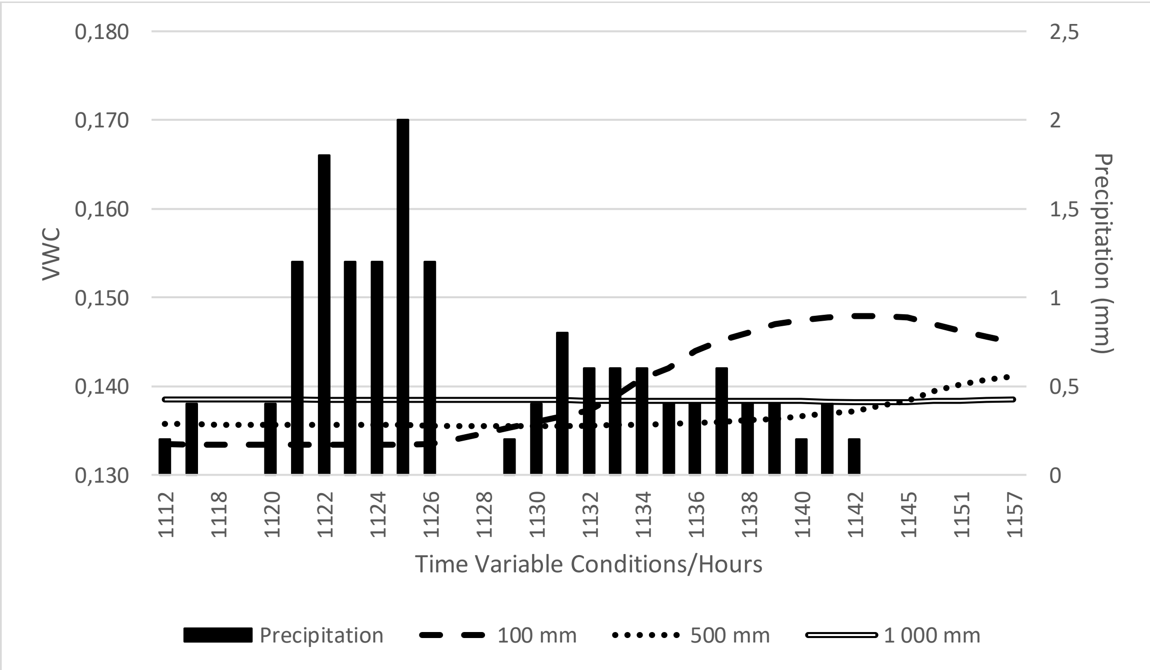

Figure 60: Simulated VWC results vs rainfall for slope component 3

5.3.2 Overland Flow and Infiltration

Figure 61 and Figure 62 illustrate the dominance of overland flow during both rainfall events. Double the volume of infiltration is simulated during the rainfall event on the 360th hour than the rainfall event around the 300th hour, hence the difference of VWC at all three depths illustrated in

Figure 59. A *Ks* of 1 mm/hour was selected to match recorded overland flow values and to reach conditions closely resembling the recorded VWC at various depths.

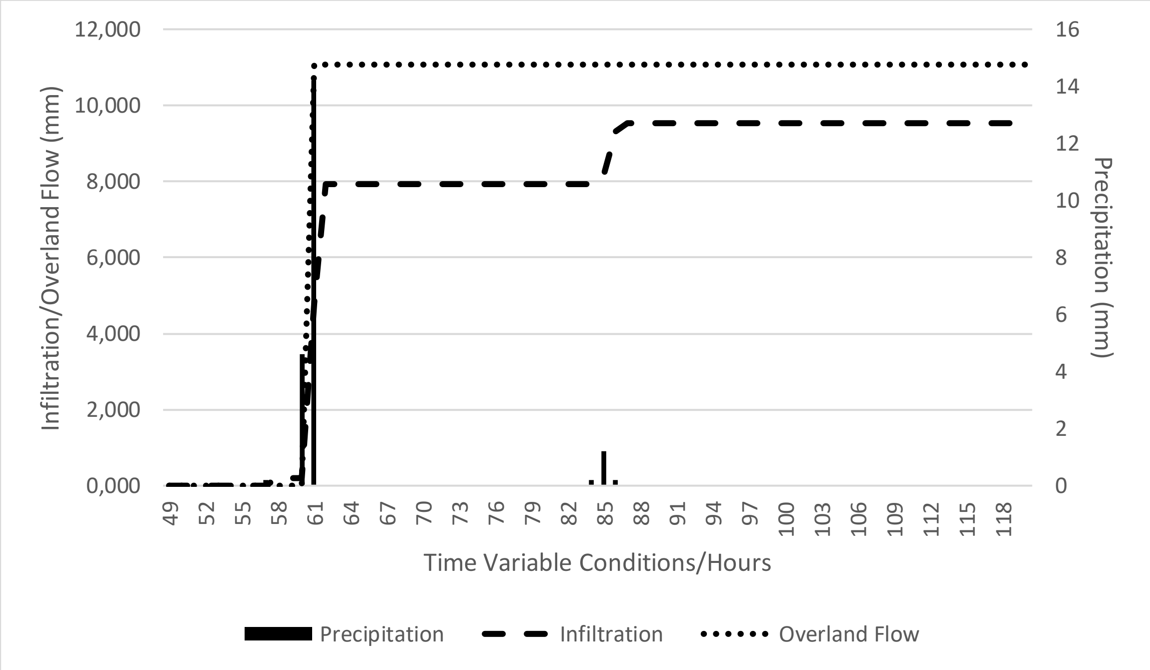

Figure 61: Simulated infiltration/overland flow vs precipitation for the 1st high-intensity rainfall event

Figure 62: Simulated infiltration/overland flow vs precipitation for the 2nd high-intensity rainfall event

5.3.3 Results simulated via Cross-Section Auxiliary Objects

The following sections contain illustrations and descriptions of results obtained from the vertical- and horizontal cross-sections inserted into simulations, as was discussed in Section 3.2.4.16- "Auxiliary Objects".

5.3.3.1 Vertical Cross-Section

The simulated VWC results from the vertical cross-section auxiliary object through the first and second high-intensity rainfall events are illustrated in Figure 63 and Figure 64. For both rainfall events, only an increase in VWC was recorded from simulations at depths of 100 mm and 500 mm below the surface, it is worth noting that the VWC before the rainfall events is lower than the rest of the depths and increases with the infiltration of water.

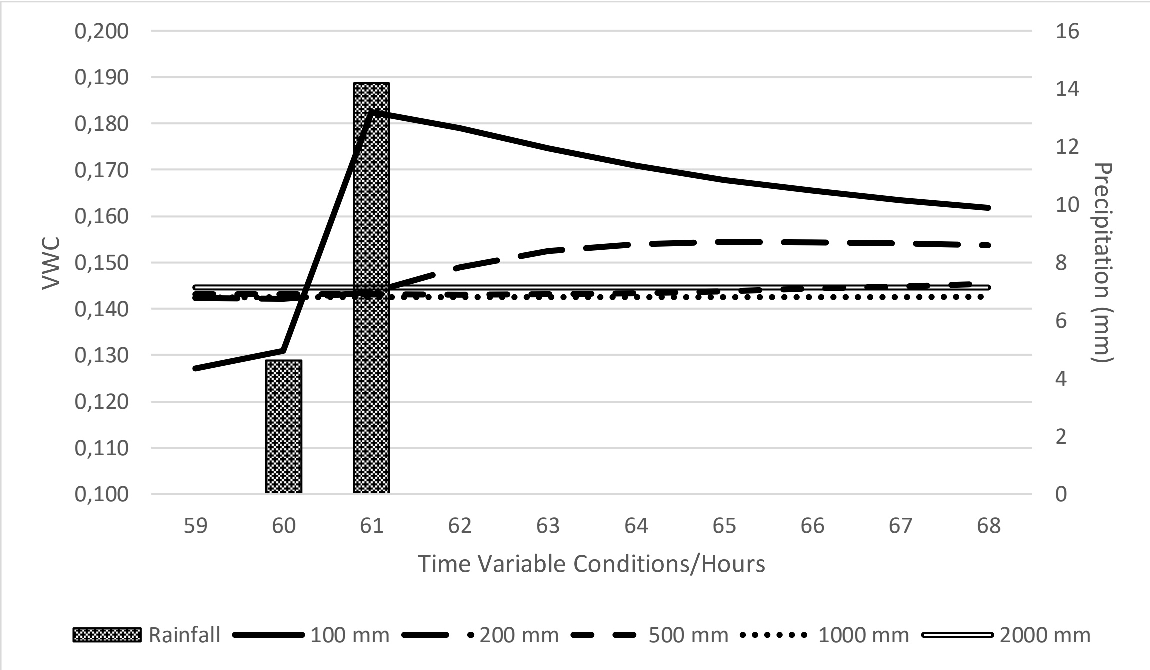

Figure 63: Simulated VWC through the vertical cross section for the first high-intensity rainfall event

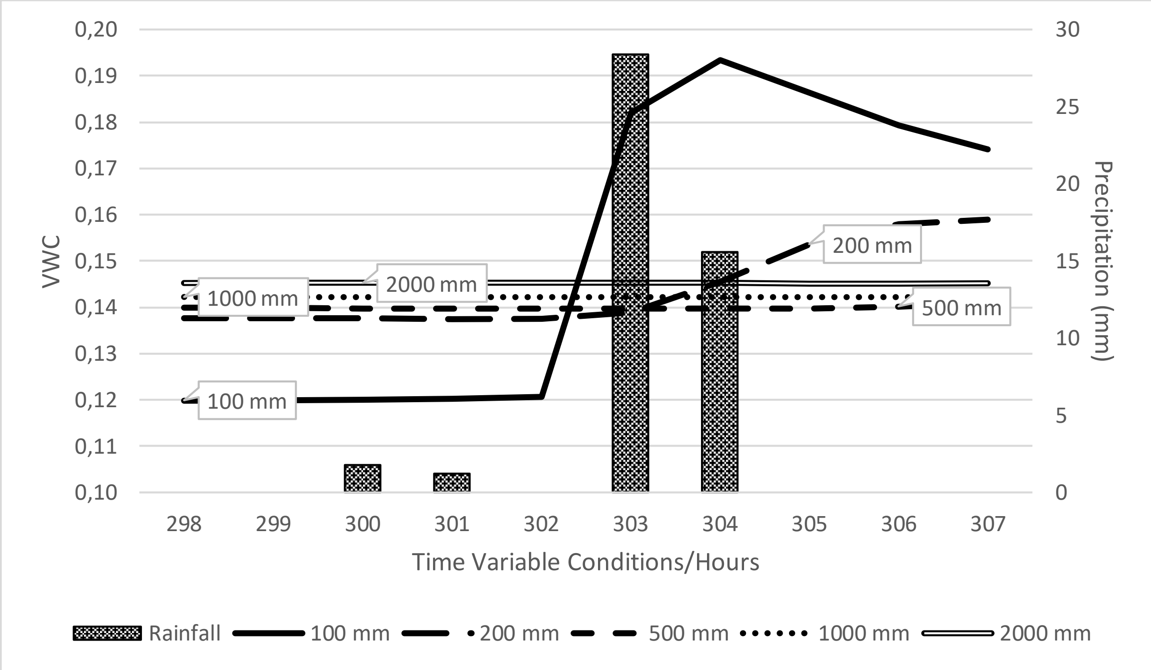

Figure 64: Simulated VWC through the vertical cross section for the second high-intensity rainfall event

5.3.3.2 Horizontal Cross-Section

For the first high-intensity rainfall event, very little lateral movement is recorded after the rainfall event due to the shallow depths having a higher VWC than the deeper depths. As for the second rainfall event, no lateral movement is recorded directly after the rainfall event, however, given the fact that the 5 000 mm mark has a higher VWC than the shallower depths. This high VWC value is, however, a result of pervious rainfall events, including the rainfall event around the 60th hour.

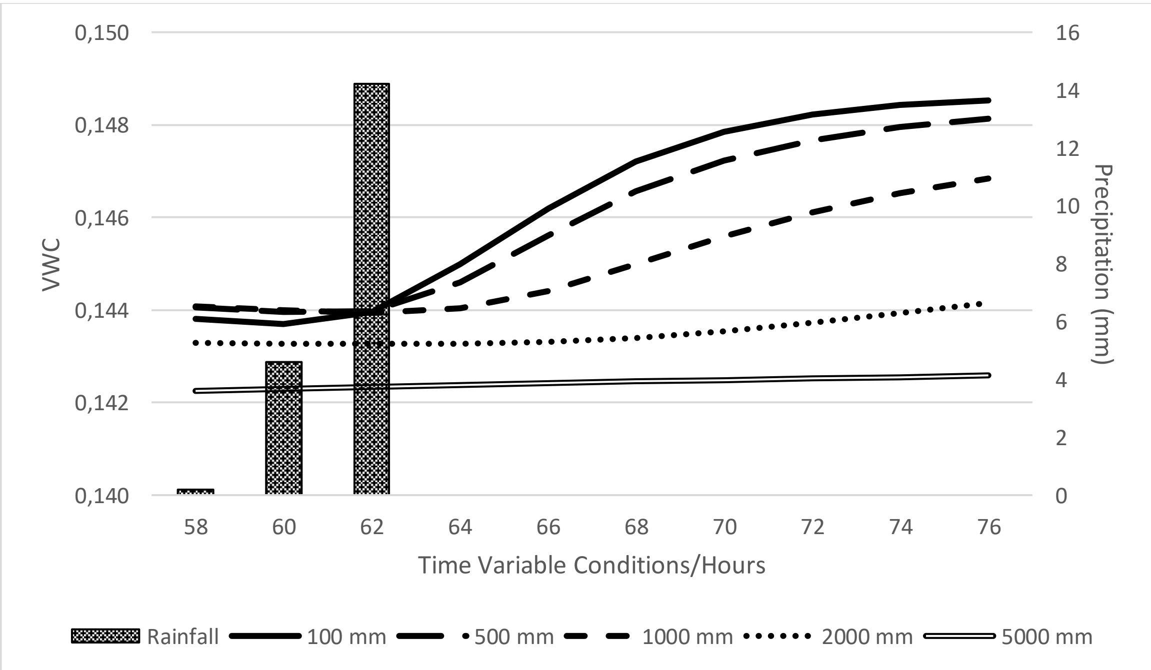

Figure 65: Simulated VWC through the horizontal cross section for the first high-intensity rainfall event

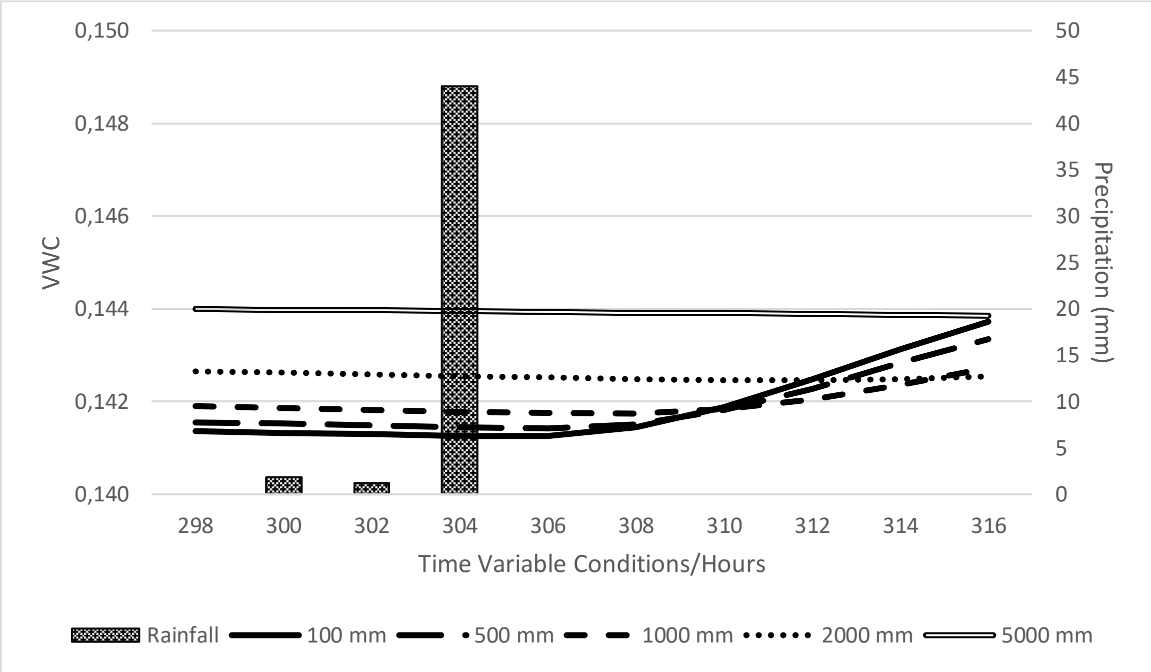

Figure 66: Simulated VWC through the horizontal cross section for the second high-intensity rainfall event

5.3.4 Velocity Vectors

The velocity vector results from the first rainfall event are illustrated in Figure 67 with that of the second rainfall event illustrated in Figure 68. The velocity of the infiltration following the second rainfall event is slightly higher than that of the first rainfall event with the direction of the velocity vectors dominantly facing downward. The velocity vectors do however tend to slightly face in a horizontal direction during dry periods (before rainfall periods). The high volumes of water infiltrated into the cover material promote a vertical percolation of water at increased velocities. The percolation of water continues deeper into the tailings material after the second rainfall event than after the first rainfall event due to a higher volume of water infiltrated (as can be seen in Figure 61 and Figure 62.

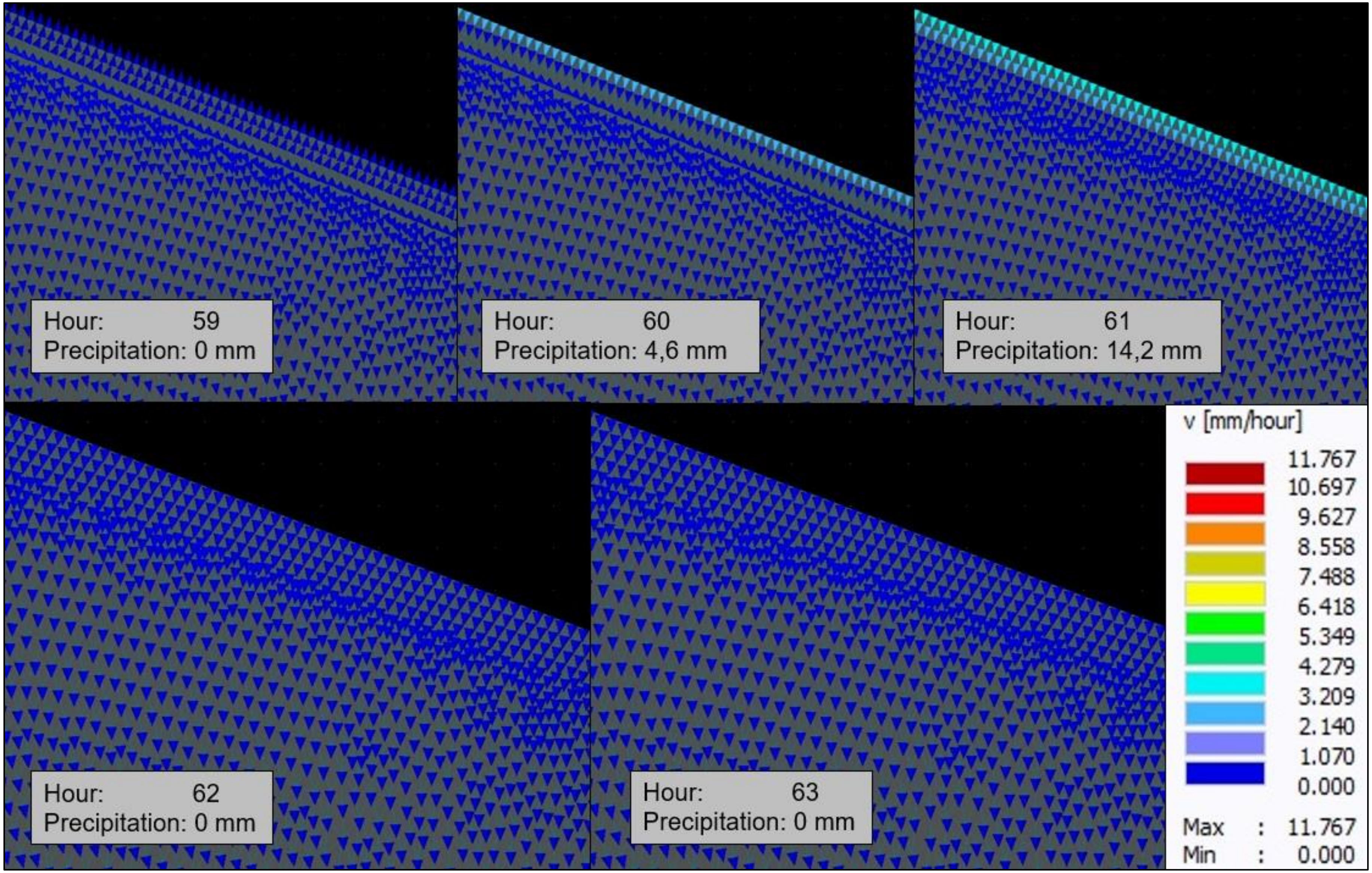

Figure 67: Velocity vectors simulated by the HYDRUS-2D tool during the 1st high-intensity rainfall event

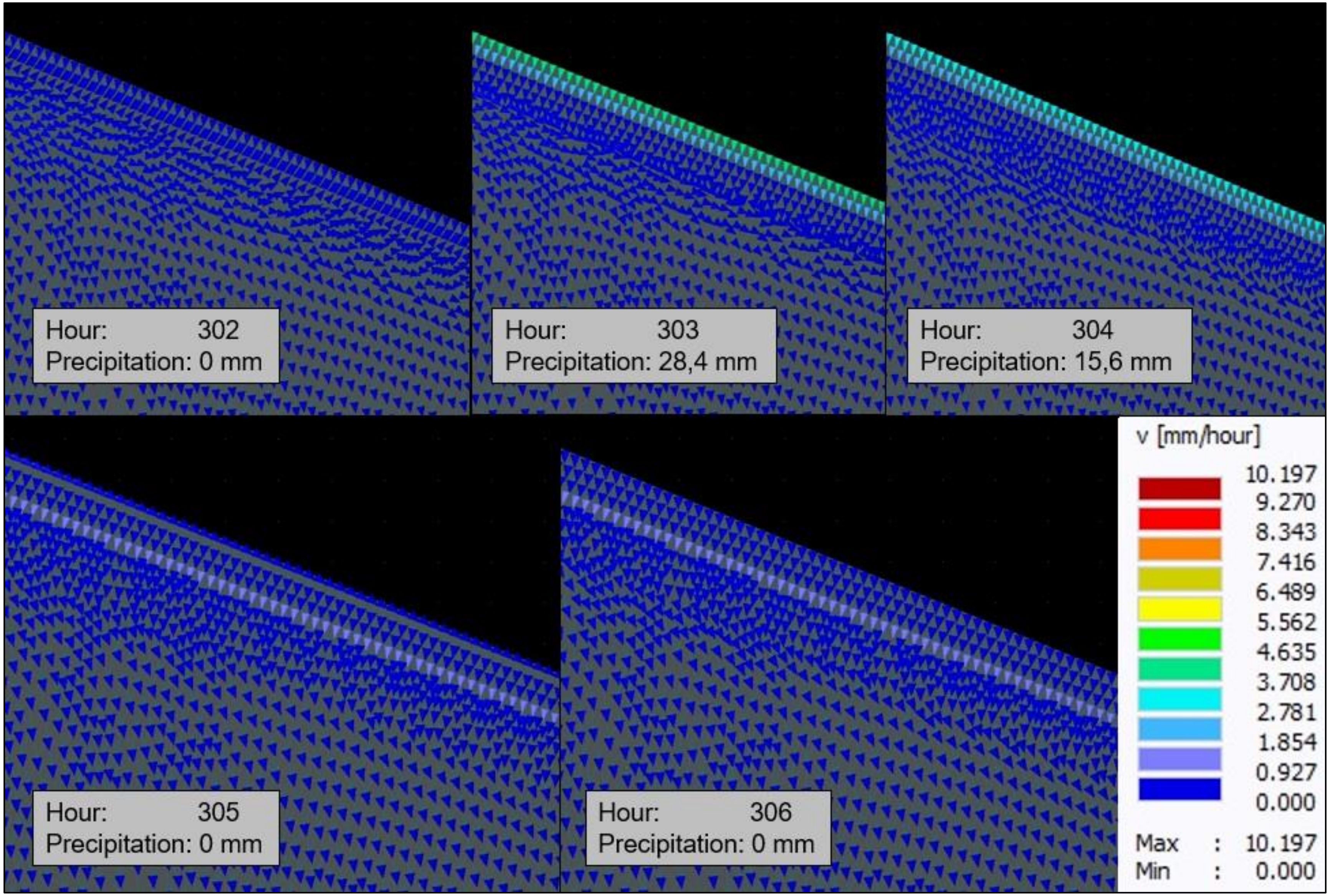

Figure 68: Velocity vectors simulated by the HYDRUS-2D tool during the 2nd high-intensity rainfall event

5.4 Slope Component 4

The following sections describe simulated results for slope component 4 relevant to infiltration, overland flow and the direction of fluxes compared to the recorded precipitation. The *Ks* for the cover material was decreased to 1,5 mm/h to closely resemble the measured overland flow during and after rainfall events to improve the accuracy of predictions.

5.4.1 Simulations for Entire Study Period

The simulated VWC results for the observation nodes during the entire study period (in hours) is illustrated in Figure 69 to Figure 71. An increase in VWC at a depth of 100 mm is recorded from the simulations within three hours of the rainfall events, with an increase in VWC recorded at a depth of 500 mm at approximately 15 hours after the second rainfall event with an delay in percolation up to a depth of 1 000 mm recorded at 80 hours, see Figure 70.

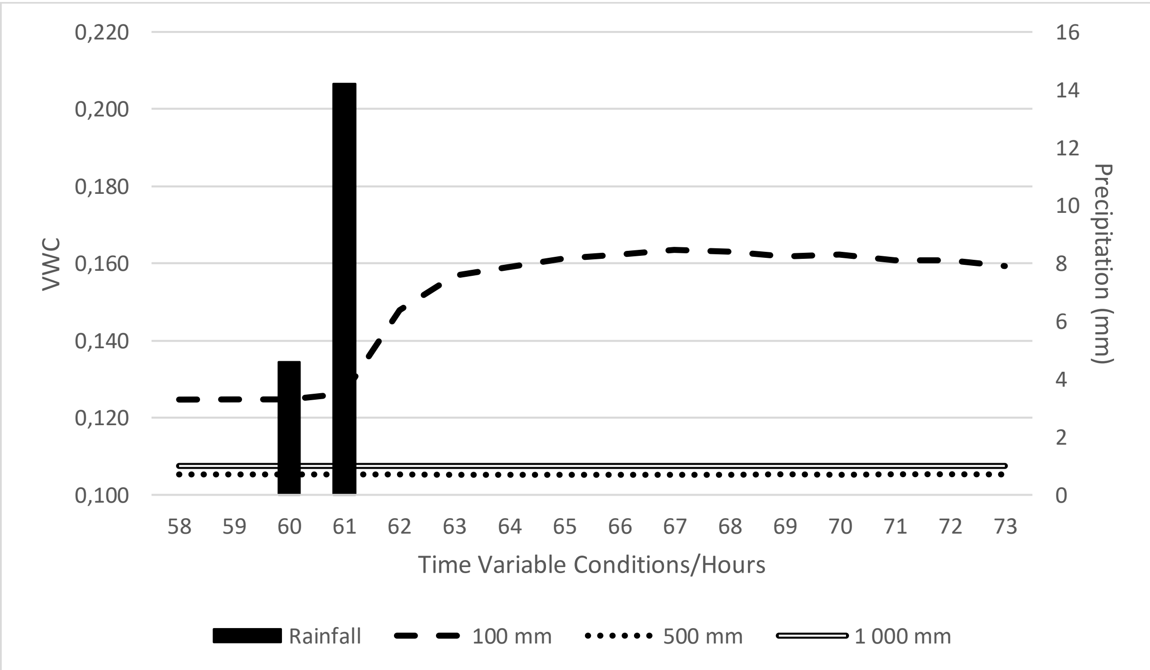

Figure 69: Simulated VWC results vs rainfall during the study period for slope component 4

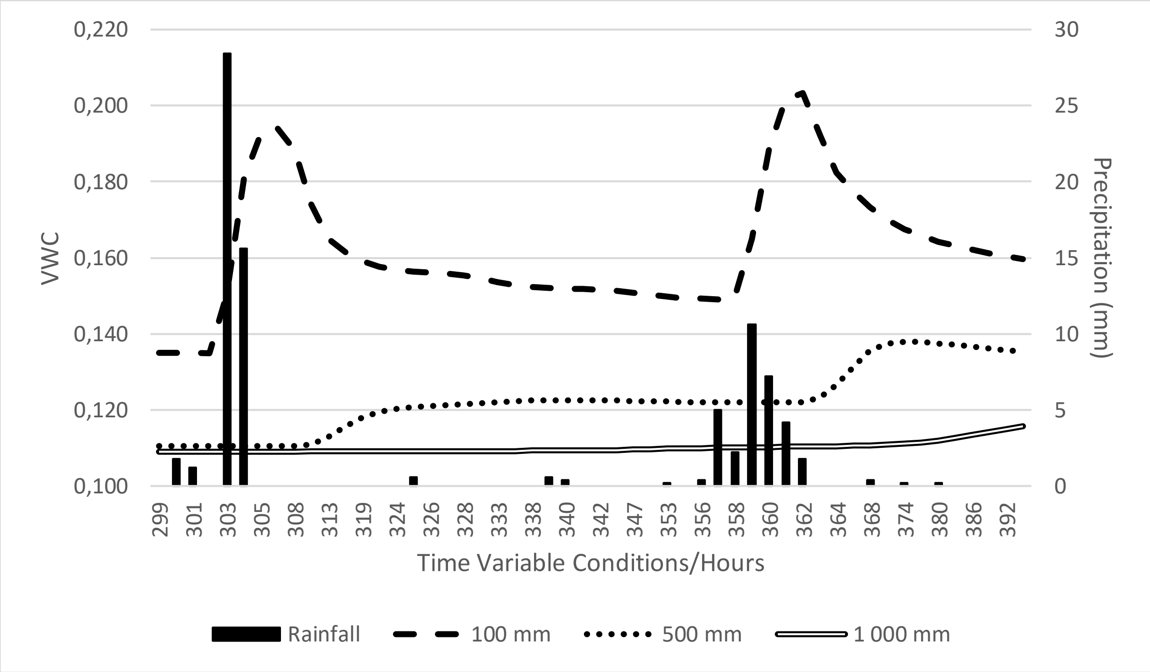

Figure 70: Simulated VWC results vs rainfall during the study period for slope component 4

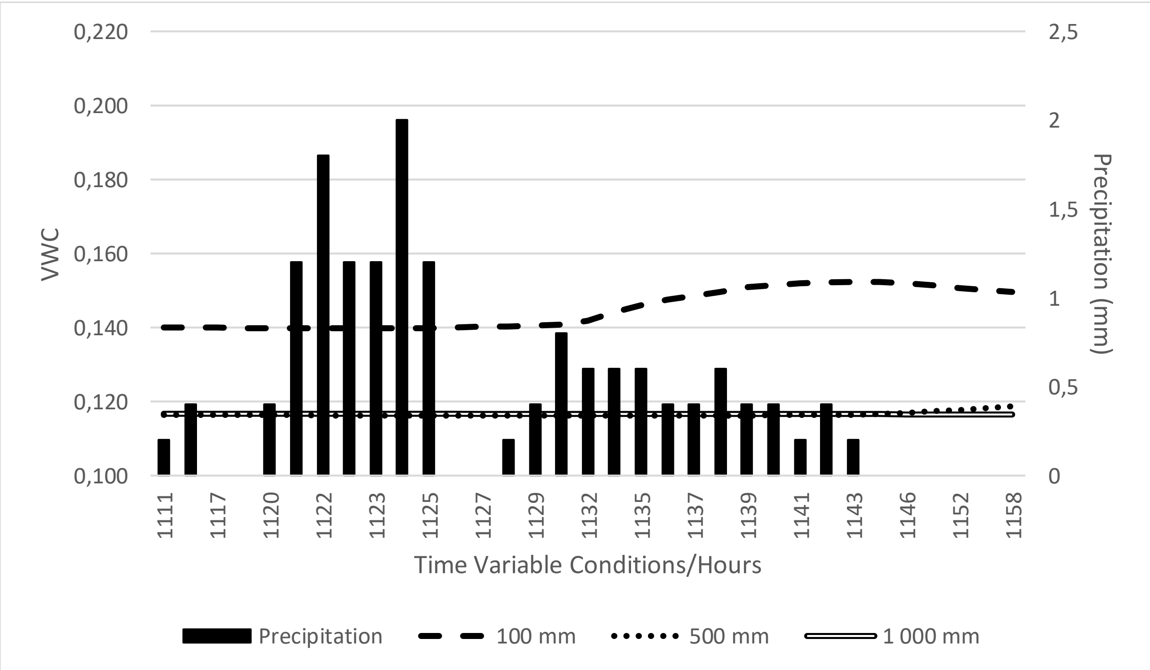

Figure 71: Simulated VWC results vs rainfall during the study period for slope component 4

5.4.2 Overland Flow and Infiltration

Figure 72 and Figure 73 illustrates the overland and infiltration volumes recorded for the simulations of the first and second high-intensity rainfall events respectively. Infiltration is dominant over overland flow during the first rainfall event with overland flow being dominant during the second rainfall event.

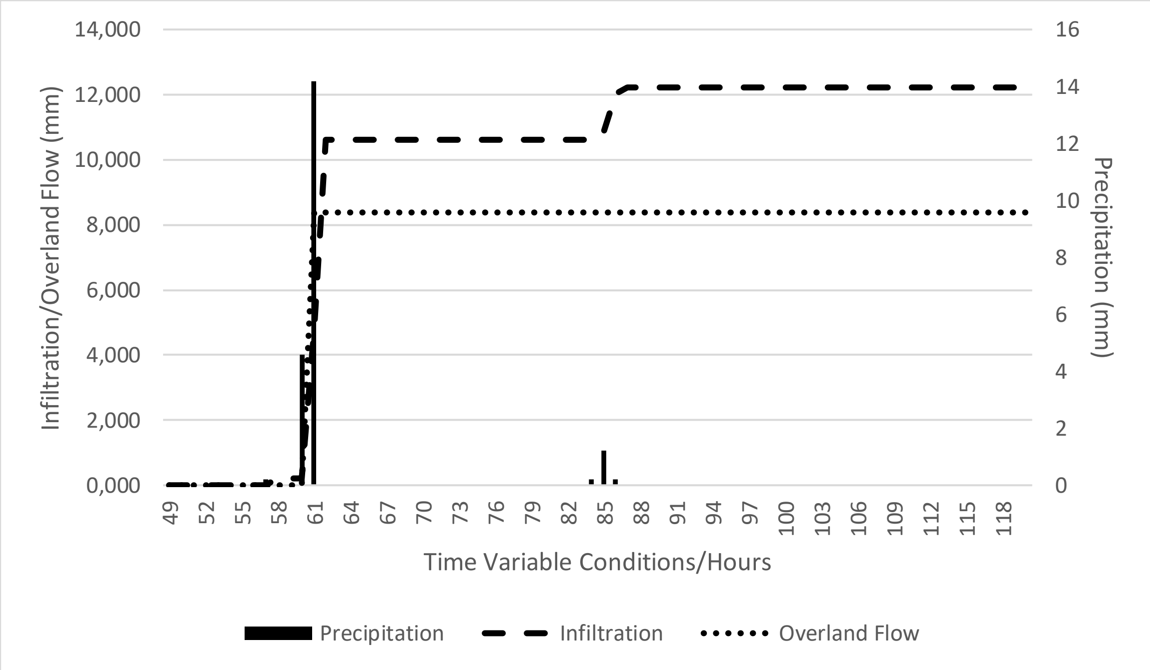

Figure 72: Simulated infiltration/overland flow vs precipitation for the 1st high-intensity rainfall event

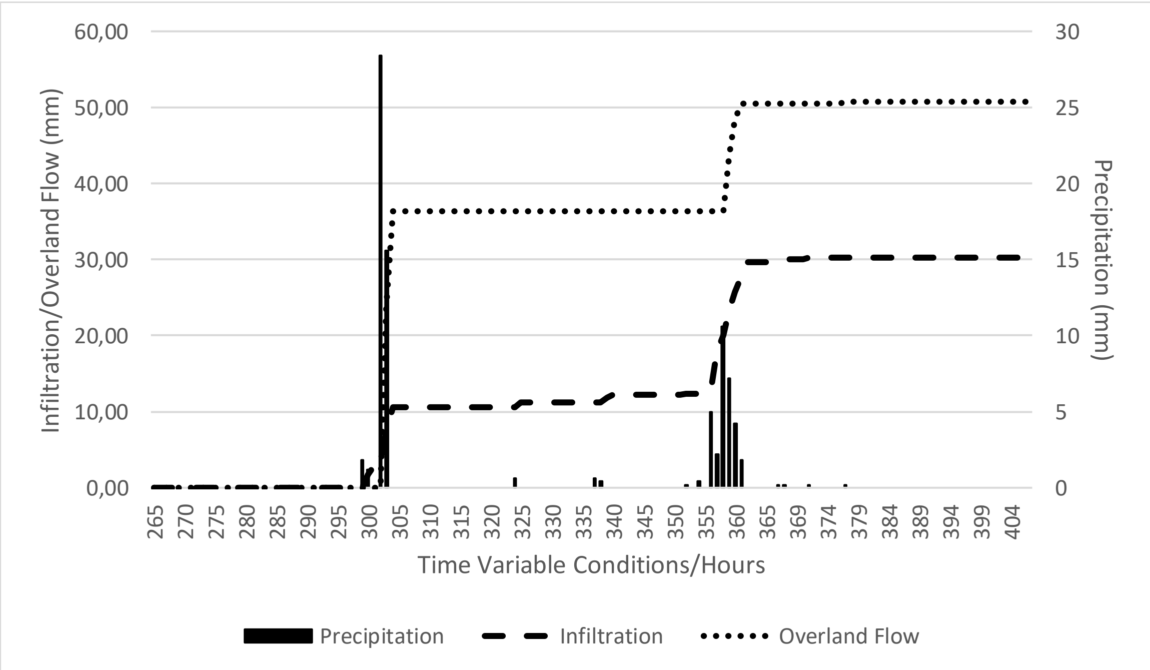

Figure 73: Simulated infiltration/overland flow vs precipitation for the 2nd high-intensity rainfall event

5.4.3 Results simulated via Cross-Section Auxiliary Objects

The following sections contain illustrations and descriptions of results obtained from the vertical- and horizontal cross-sections inserted into simulations, as was discussed in Section 3.2.4.16- “Auxiliary Objects”.

5.4.3.1 Vertical Cross-Section

The simulated VWC results from the vertical cross-section auxiliary object through the first and second high-intensity rainfall events are illustrated in Figure 74 and Figure 75. Vertical movement of water through the profile is slow but noticeable from the illustrations in Figure 74. The upper 100 mm within the cover material reacts immediately to the rainfall events with the material at 500 mm below the surface receiving moisture from the rainfall event approximately three hours after the rainfall event. The VWC for the upper 100 mm is lower than the deeper depths before rainfall. The cover material is however characterised by a rapid increase in VWC during and after rainfall events with depths deeper than 500 mm not receiving any moisture up to seven hours after the rainfall event.

Similar trends can be noticed during the second high-intensity rainfall event with a significant increase in VWC at a depth of 2 000 mm following rainfall events prior to the second high-intensity rainfall event.

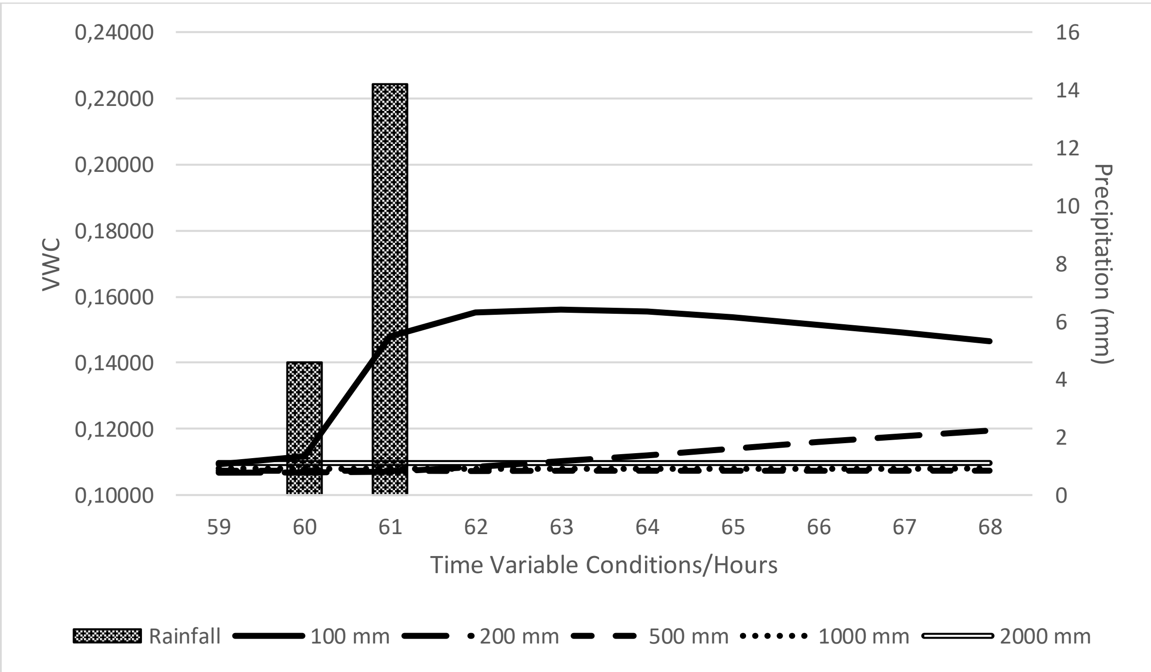

Figure 74: Simulated VWC through the vertical cross section for the first high-intensity rainfall event

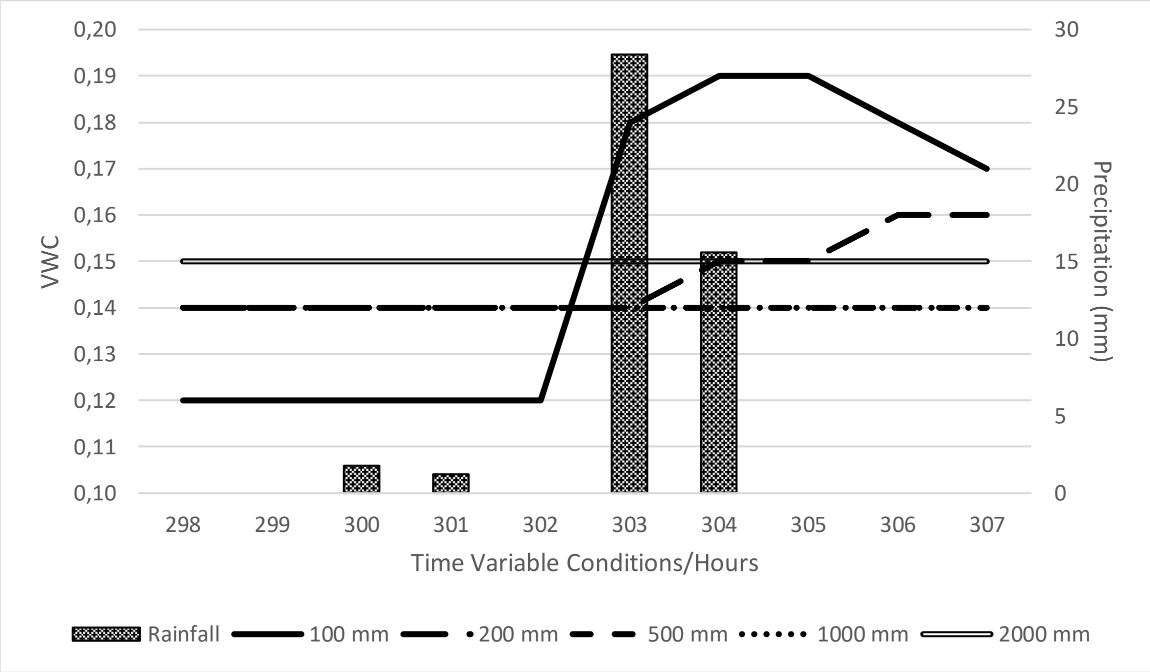

Figure 75: Simulated VWC through the vertical cross section for the second high-intensity rainfall event

5.4.3.2 Horizontal Cross-Section

The higher VWC at a distance of 5 000 mm (Figure 76) in comparison to shallower depths indicates the possibility of lateral flows within this profile ultimately seeping out in the seepage face boundary. This phenomenon is backed by previous statements that vertical percolation is delayed up to the 1 000 mm mark. As for the conditions during the second high-intensity rainfall event Figure 77, vertical fluxes are more likely than lateral fluxes due to a low VWC at farther distances from the beginning of the profile and higher VWC at the start of the profile (horizontally).

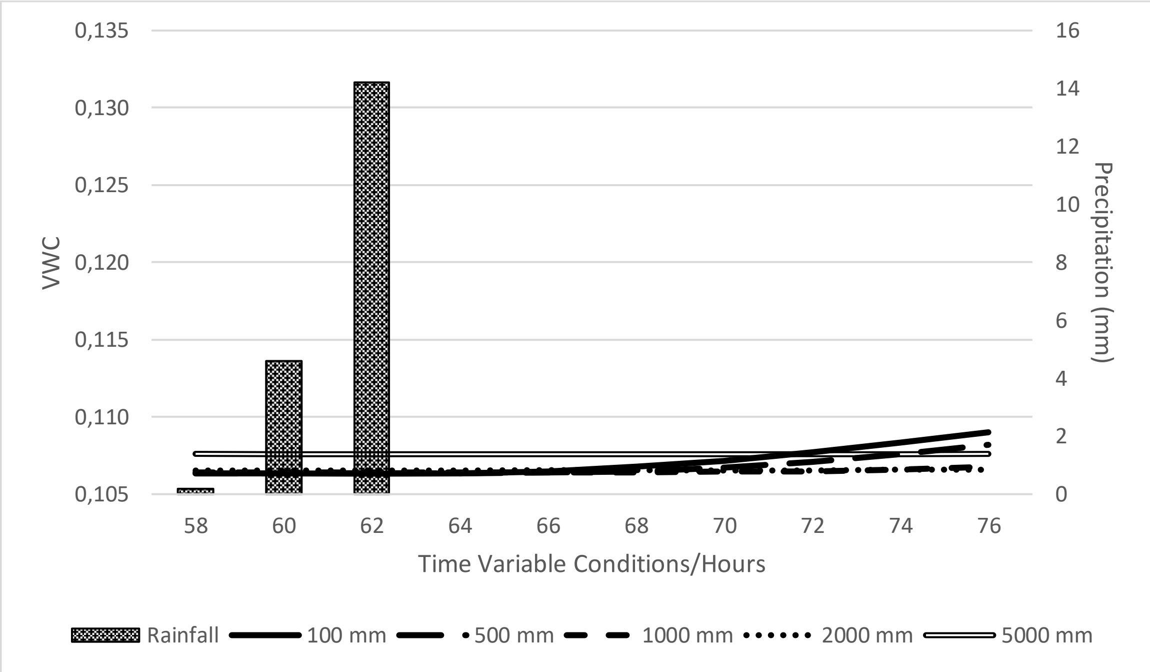

Figure 76: Simulated VWC through the horizontal cross section for the first high-intensity rainfall event

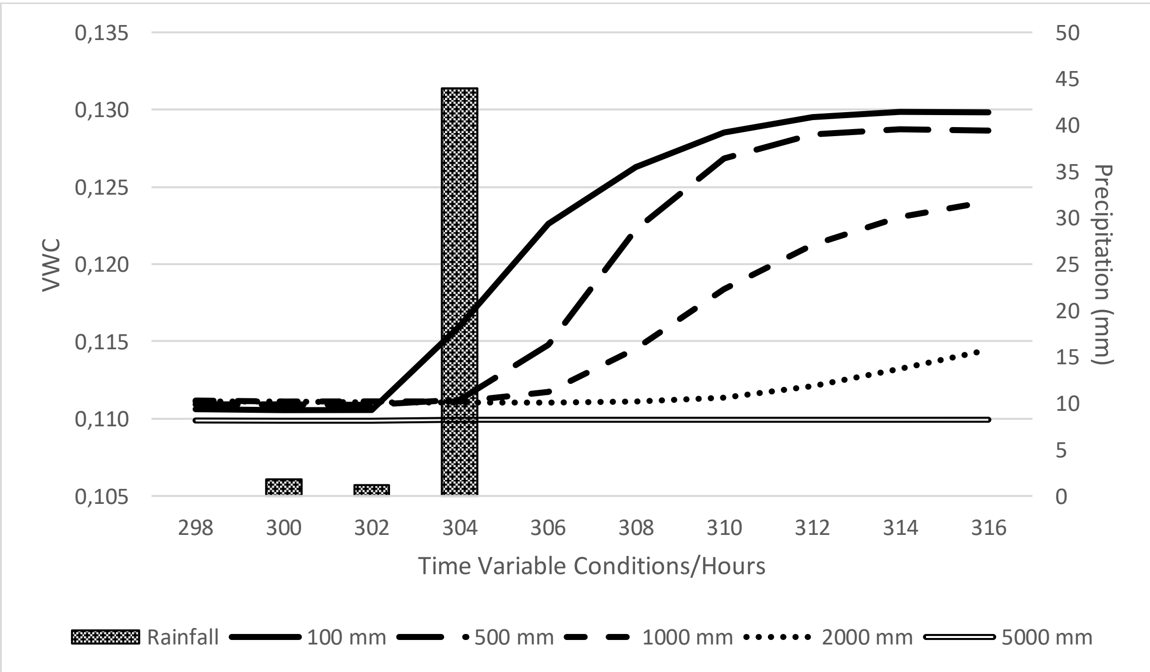

Figure 77: Simulated VWC through the horizontal cross section for the second high-intensity rainfall event

5.4.4 Velocity Vectors

The velocity vector results from the first and second rainfall event is illustrated in Figure 78 and Figure 79. Previous statements that lateral movement occurs before rainfall events are backed by the direction of velocity vectors during the first rainfall event which changes into dominant vertical movement during and after rainfall events. Similar trends are illustrated for the velocity vectors pertaining to sub-surface fluxes during the second high-intensity rainfall event only with deeper percolation and higher velocities even though the same volume of infiltration is recorded during rainfall events, see Figure 72 and Figure 73. The lower velocities recorded from simulations during the first event can be described to the level of saturation prior to the rainfall event as opposed to the dry conditions within the cover material prior to the second rainfall event.

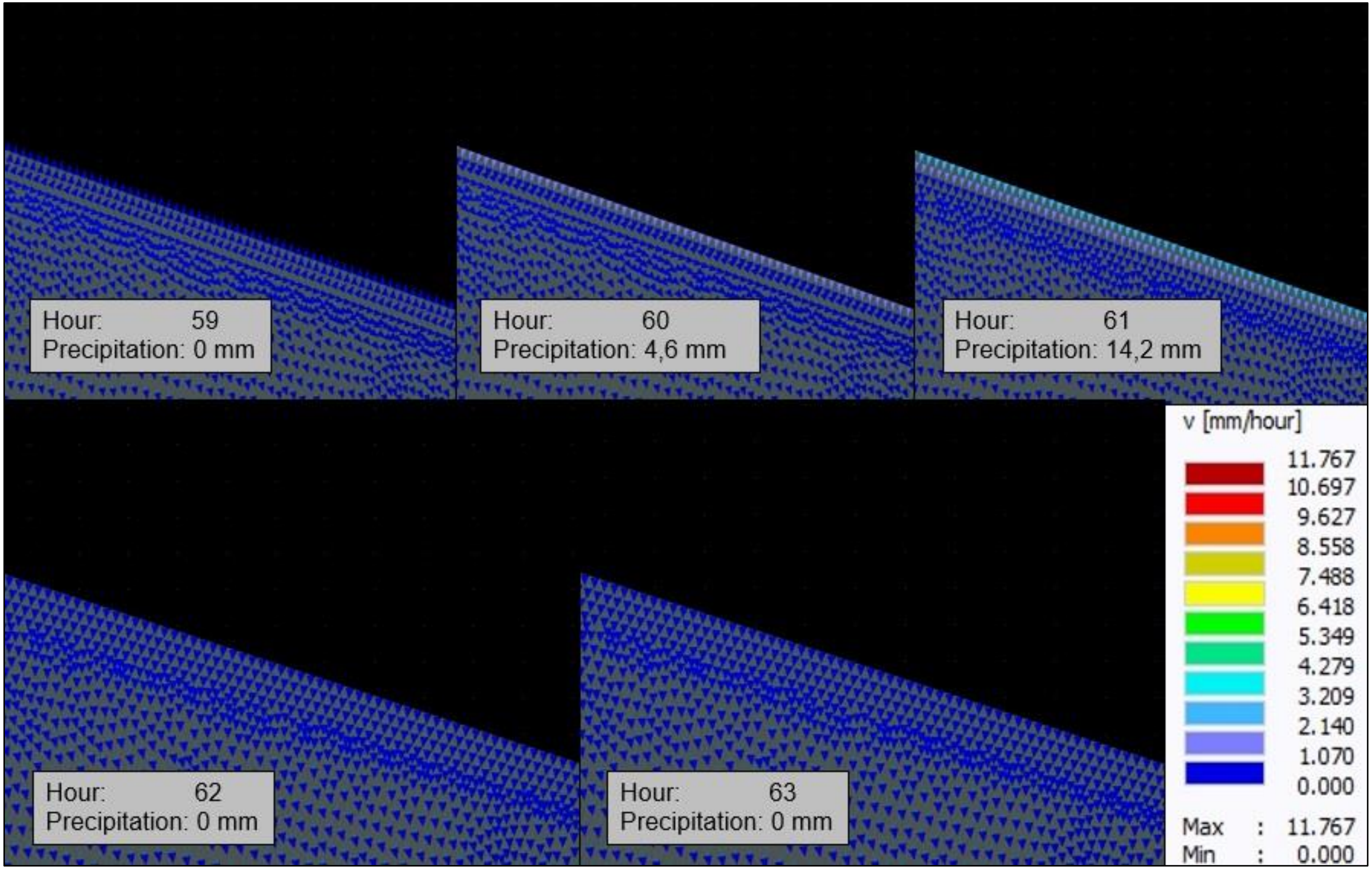

Figure 78: Velocity vectors simulated by the HYDRUS-2D tool during the 1st high-intensity rainfall event

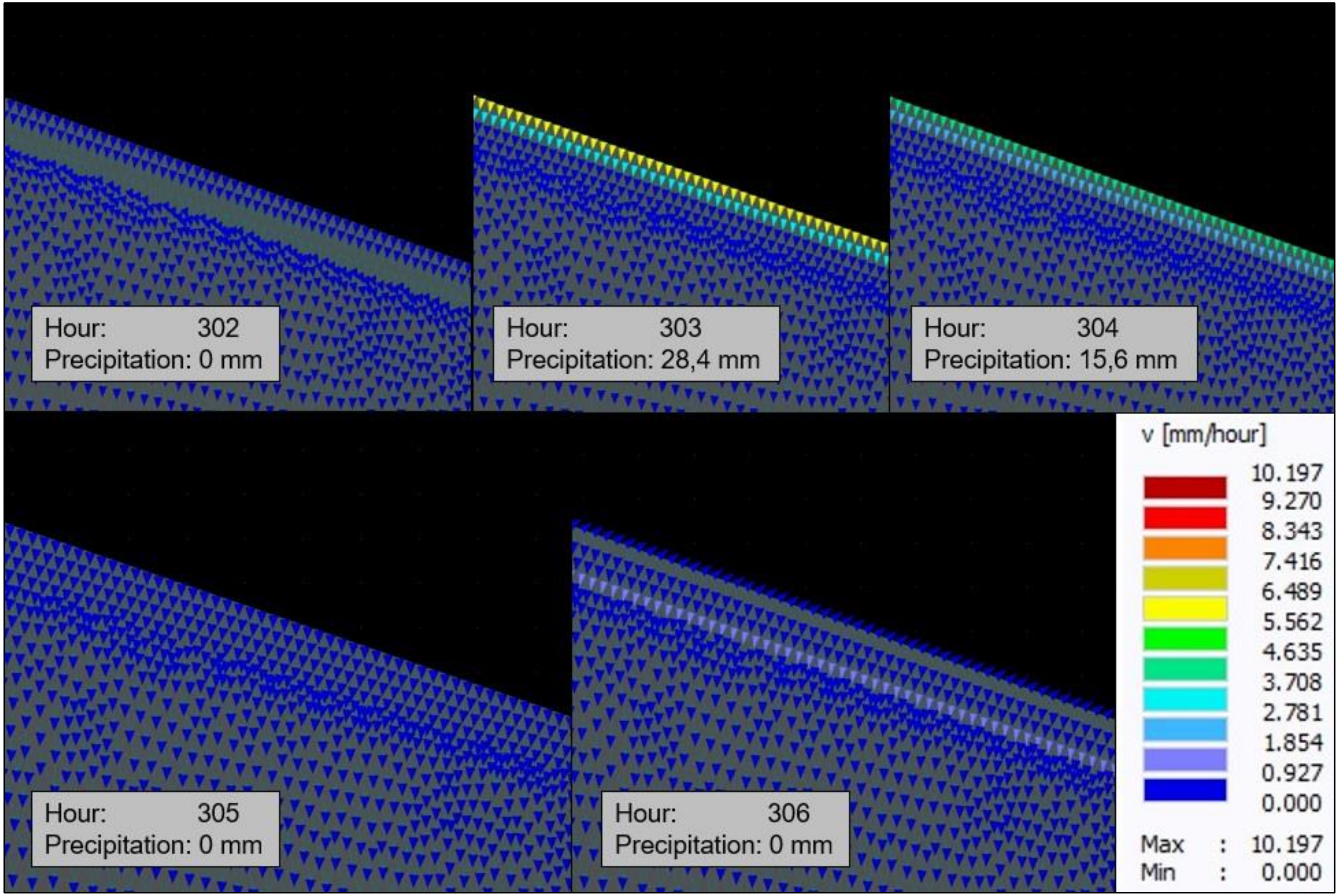

Figure 79: Velocity vectors simulated by the HYDRUS-2D tool during the 2nd high-intensity rainfall event

5.5 Slope Component 5

The following sections describe simulated results for slope component 2 relevant to infiltration, overland flow and the direction of fluxes compared to the recorded precipitation. The *Ks* measured *in-situ* for the cover material on slope component 5 was deemed to be accurate given simulations closely resembling measured VWC and overland flow from run-off plots.

5.5.1 Simulations for Entire Study Period

The simulated VWC results for the observation nodes in slope component 5 are unique and differs significantly from that of the previous slope components. Slope component 5 is the only slope component that's *Ks* has not been adjusted by means of recommended values from the inverse modelling solution. Slope component 5 has a unique geometry in the sense that the observation nodes are situated on top of the TSF and not on the TSF's slope (as in the case with slope components 1-4). For the first rainfall event, an increase in VWC is only recorded from simulations at a depth of 100 mm below the surface with measurements at 500 mm and 1 000 mm unchanged and constant, see Figure 80.

As for the second rainfall event, an immediate response in VWC readings is noticed during the rainfall event, followed by a spike in VWC at a depth of 500 mm below the surface approximately 20 hours after the rainfall event. Due to the flat geometry and high infiltration, a high volume of water reaches a depth of 500 mm below the surface, ultimately resulting in a significant increase in VWC. The VWC readings at 1 000 mm below the surface, however, stay unchanged and constant, see Figure 81.

During the third rainfall event illustrated in Figure 82 however, a constant but increased VWC is recorded from simulations at a depth of 1 000 mm below the surface. An even higher (and constant) VWC is recorded from simulations at a depth of 500 mm below the surface as well.

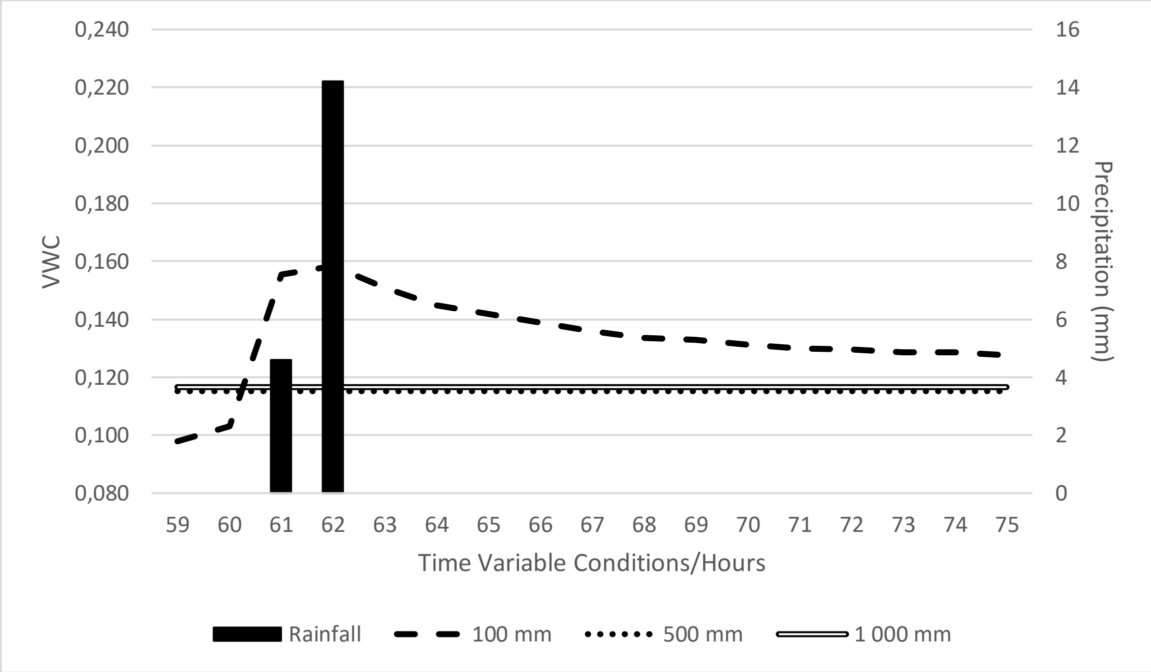

Figure 80: Simulated VWC results vs rainfall during the study period for slope component 4

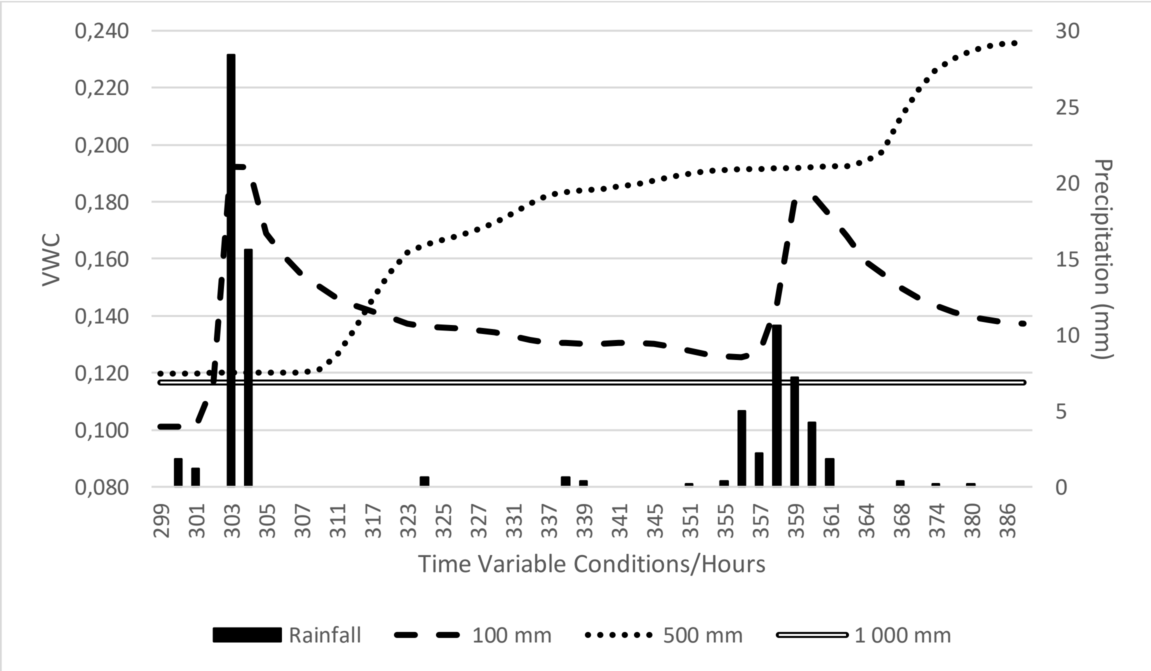

Figure 81: Simulated VWC results vs rainfall during the study period for slope component 4

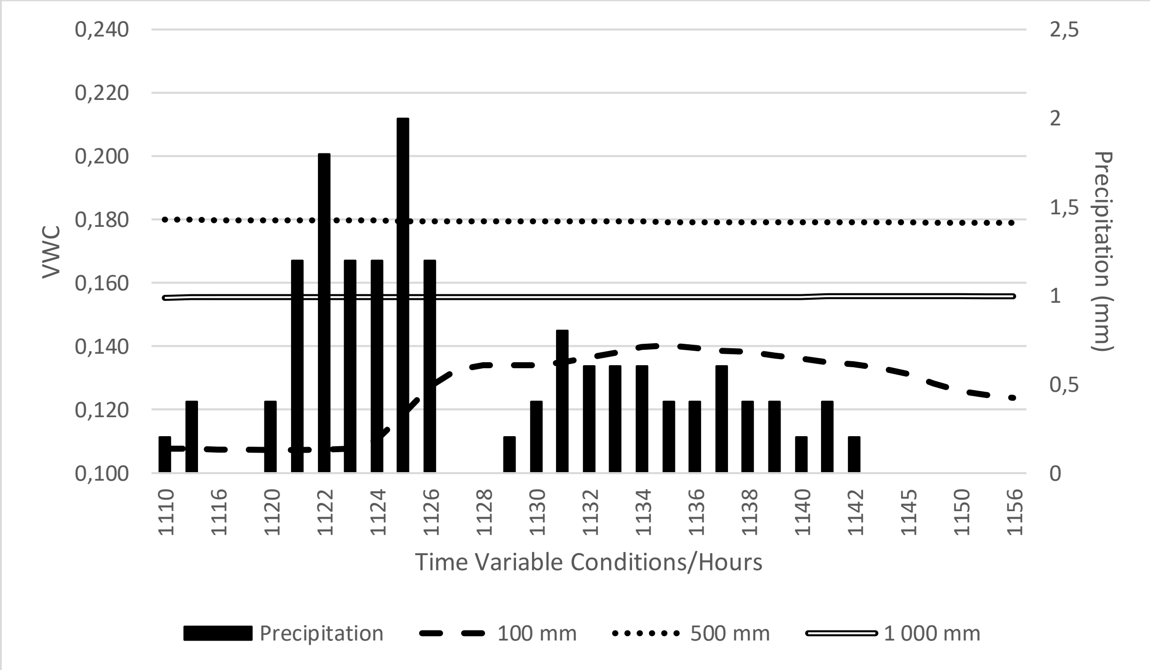

Figure 82: Simulated VWC results vs rainfall during the study period for slope component 4

5.5.2 Overland Flow and Infiltration

Figure 83 and Figure 84 indicate zero overland flow due to the high *Ks* at the surface and the flat geometry. During rainfall events, the total volume of precipitation will be infiltrated, ultimately increasing the VWC throughout the profile.

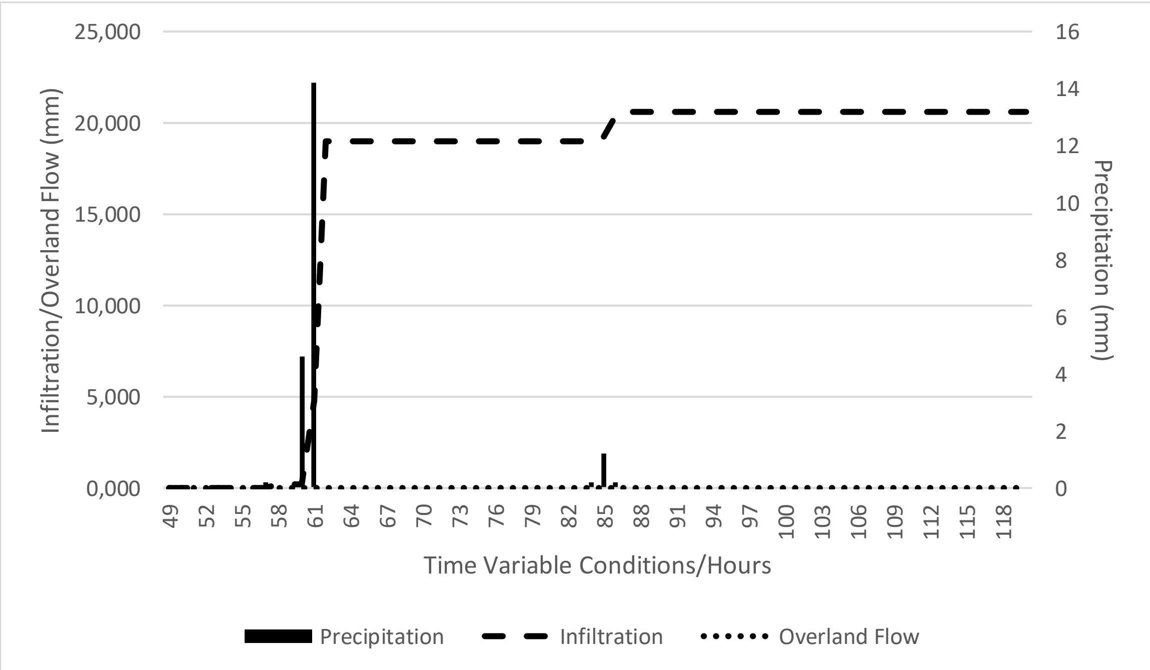

Figure 83: Simulated infiltration/overland flow vs precipitation for the 1st high-intensity rainfall event

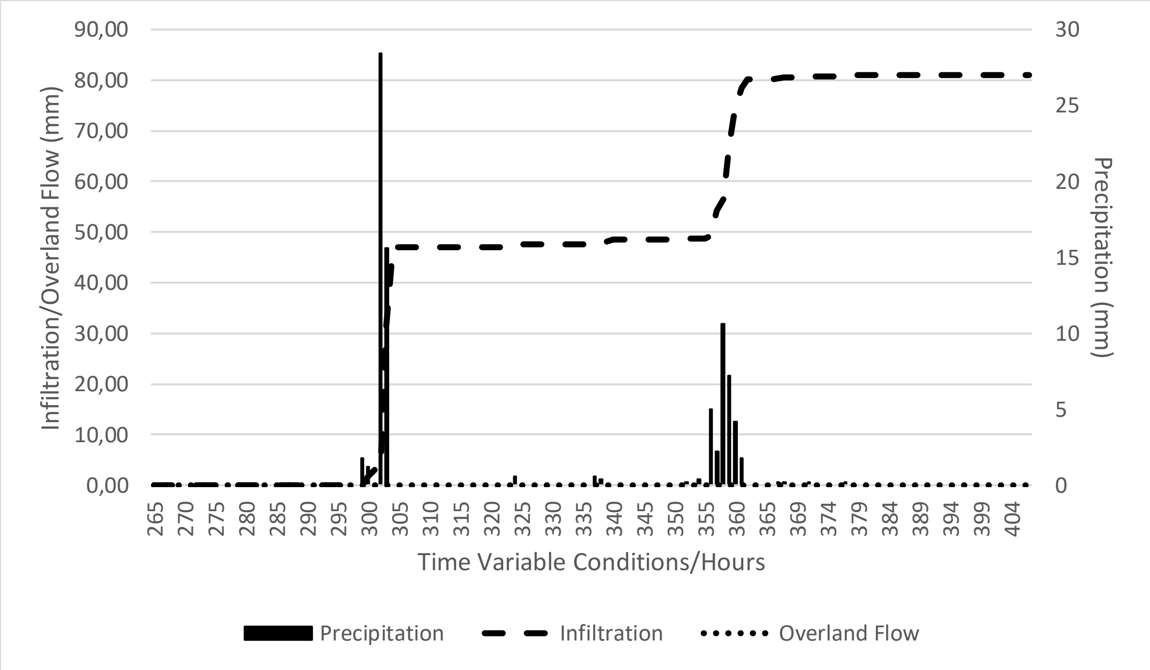

Figure 84: Simulated infiltration/overland flow vs precipitation for the 2nd high-intensity rainfall event

5.5.3 Results simulated via Cross-Section Auxiliary Objects

The following sections contain illustrations and descriptions of results obtained from the vertical- and horizontal cross-sections inserted into simulations, as was discussed in Section 3.2.4.16- "Auxiliary Objects".

5.5.3.1 Vertical Cross-Section

The simulated VWC results from the vertical cross-section auxiliary object through the first and second high-intensity rainfall events are illustrated in Figure 85 and Figure 86. The results from simulations for the first high-intensity rainfall event indicate a higher VWC (as has been illustrated in Figure 80) at a depth of 100 mm below the surface with lower values at deeper depths. As for the second high-intensity rainfall event, depths at 200 mm and 500 mm generally have higher VWCs with the 500 mm depth having a delay in a VWC increase.

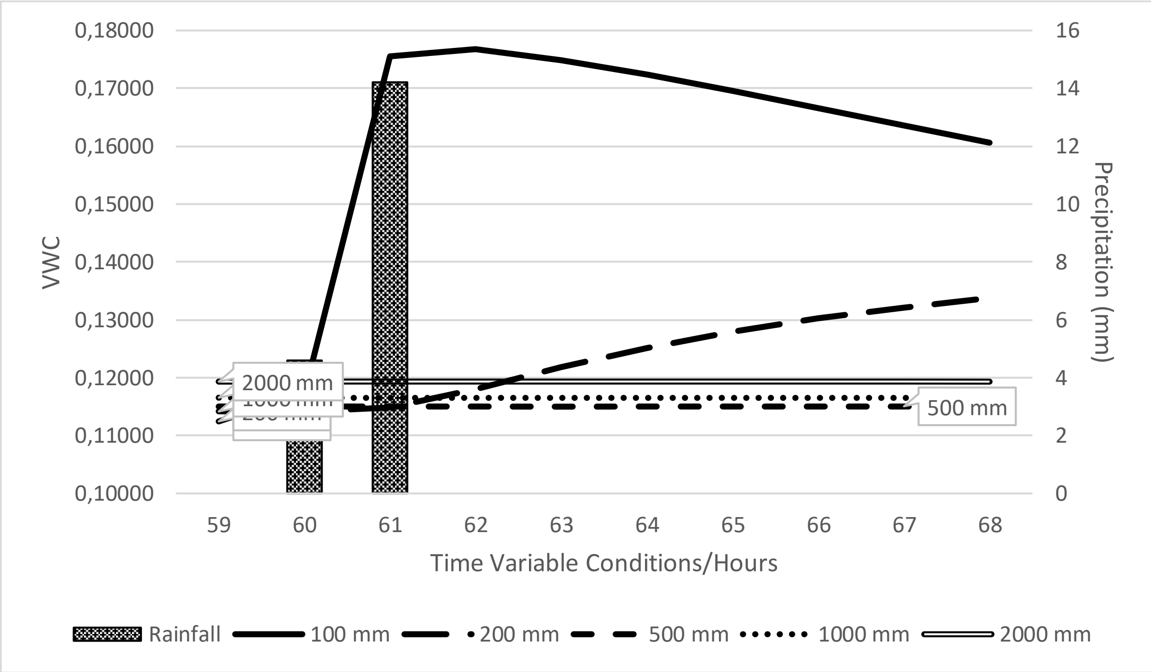

Figure 85: Simulated VWC through the vertical cross section for the first high-intensity rainfall event

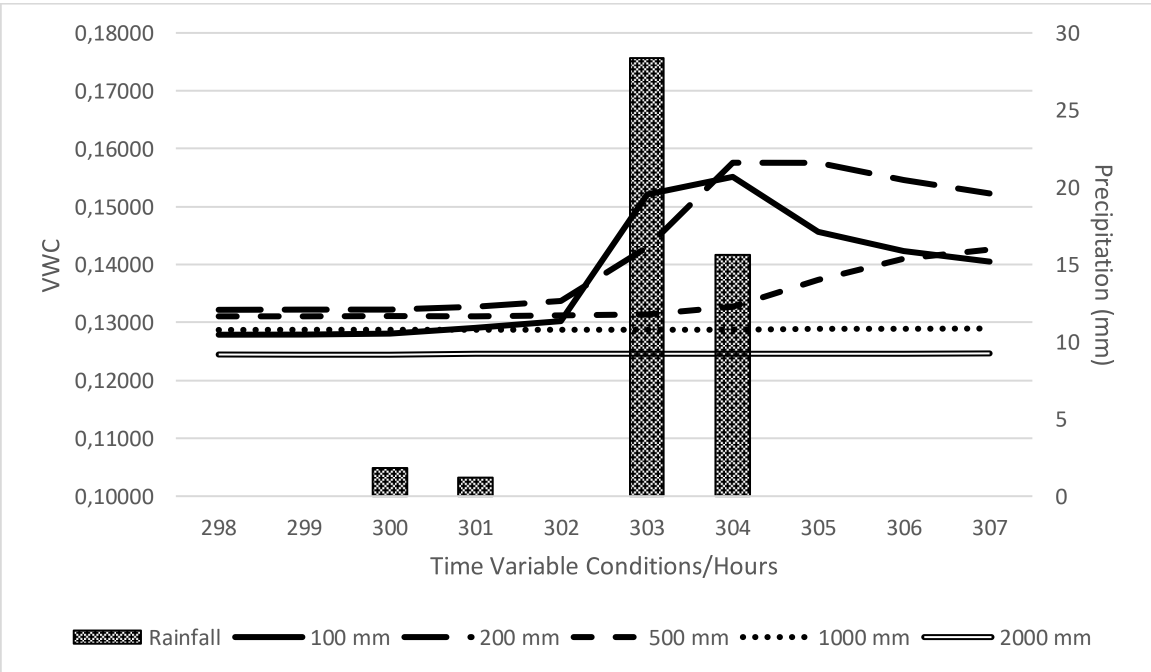

Figure 86: Simulated VWC through the vertical cross section for the second high-intensity rainfall event

5.5.3.2 Horizontal Cross-Section

No sign of lateral movement can be noticed from the simulated results in Figure 87 and Figure 88 due to the widest distances being characterised by the least VWC, which indicates a loss in VWC on a horizontal cross-section. During the second high-intensity rainfall event, the VWC at all lengths increase during and after the rainfall event and slowly dissipated shortly thereafter.

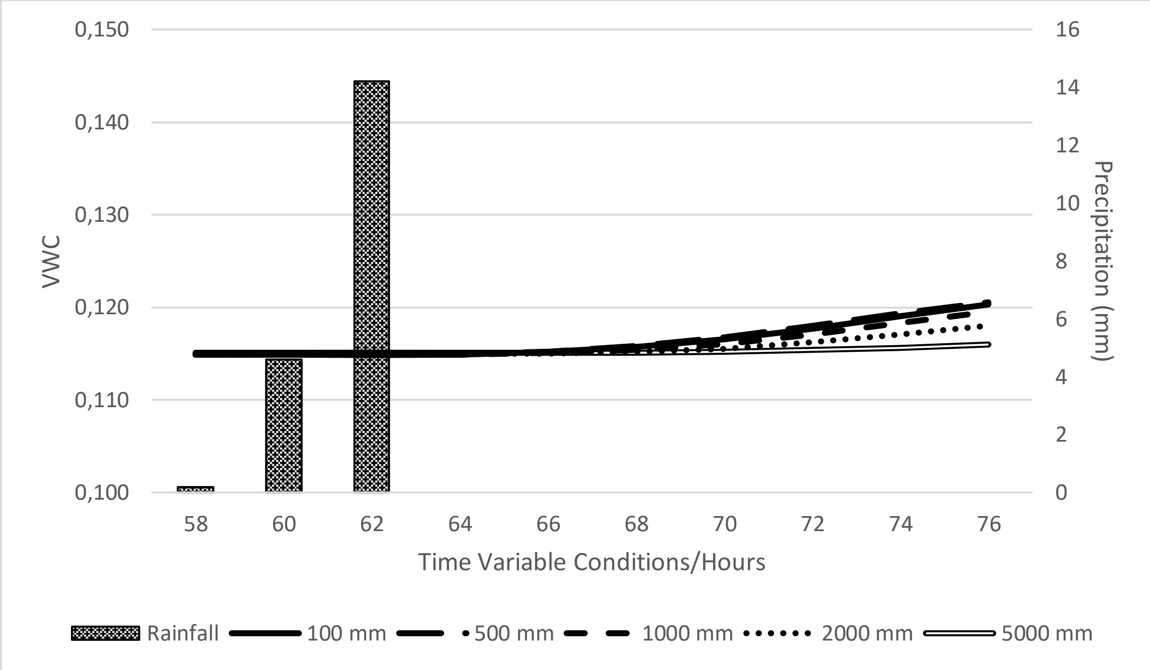

Figure 87: Simulated VWC through the horizontal cross section for the first high-intensity rainfall event

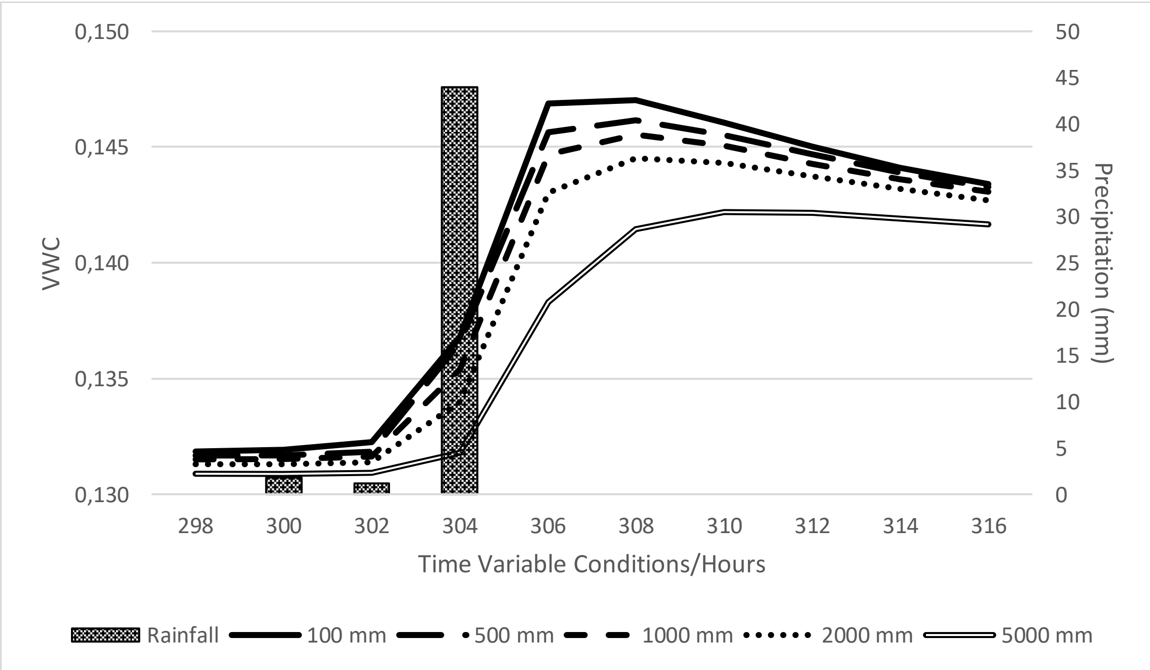

Figure 88: Simulated VWC through the horizontal cross section for the second high-intensity rainfall event

5.5.4 Velocity Vectors

The velocity vector results from the first rainfall event are illustrated in Figure 89 and Figure 90. The velocity vectors during both rainfall events indicate a complete dominant vertical movement of water through the profile at moderate velocities. The dominant vertical movement of water through the profile backs all statements made prior to this section in regard to high infiltration and vertical percolation.

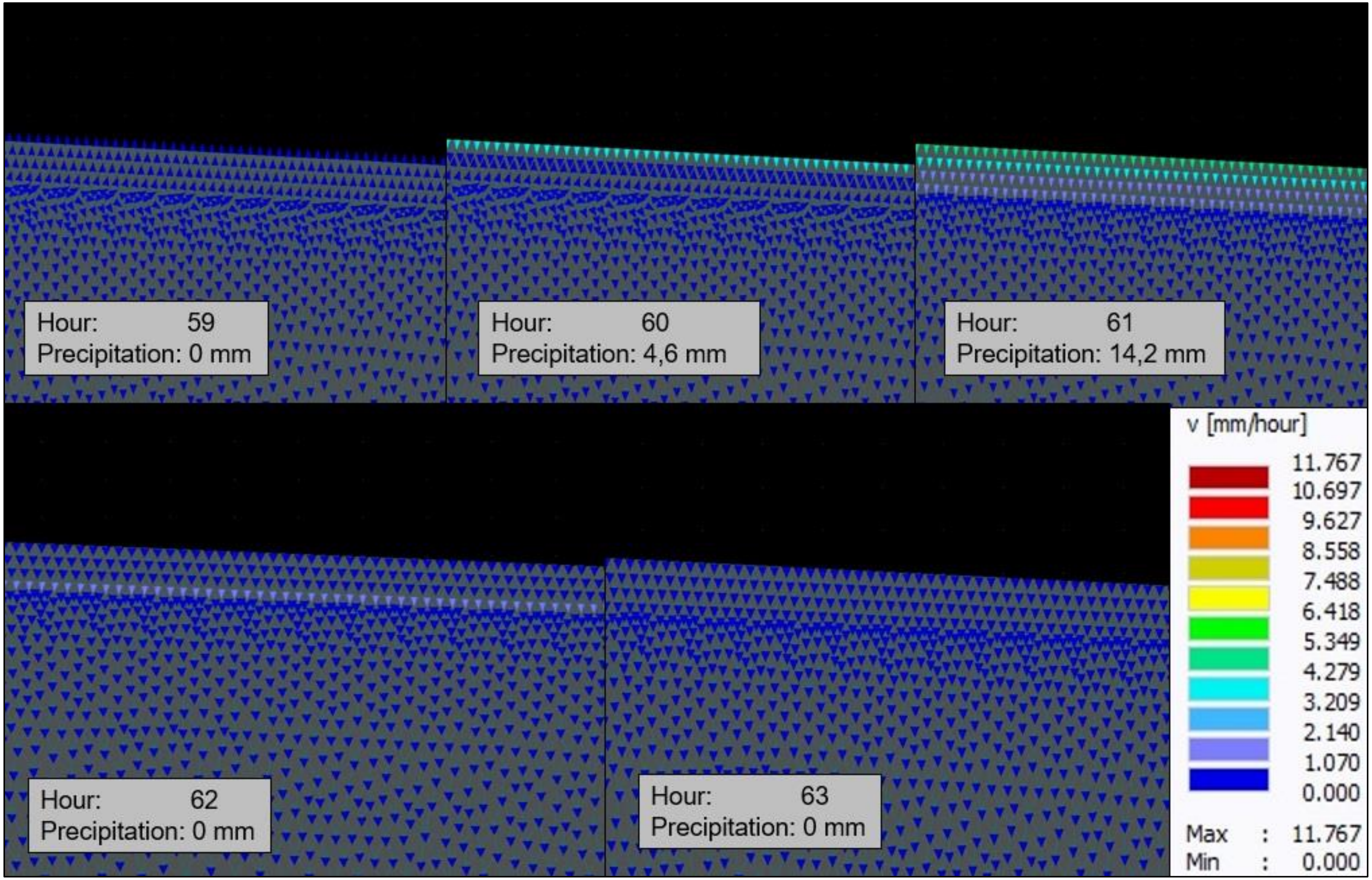

Figure 89: Velocity vectors simulated by the HYDRUS-2D tool during the 1st high-intensity rainfall event

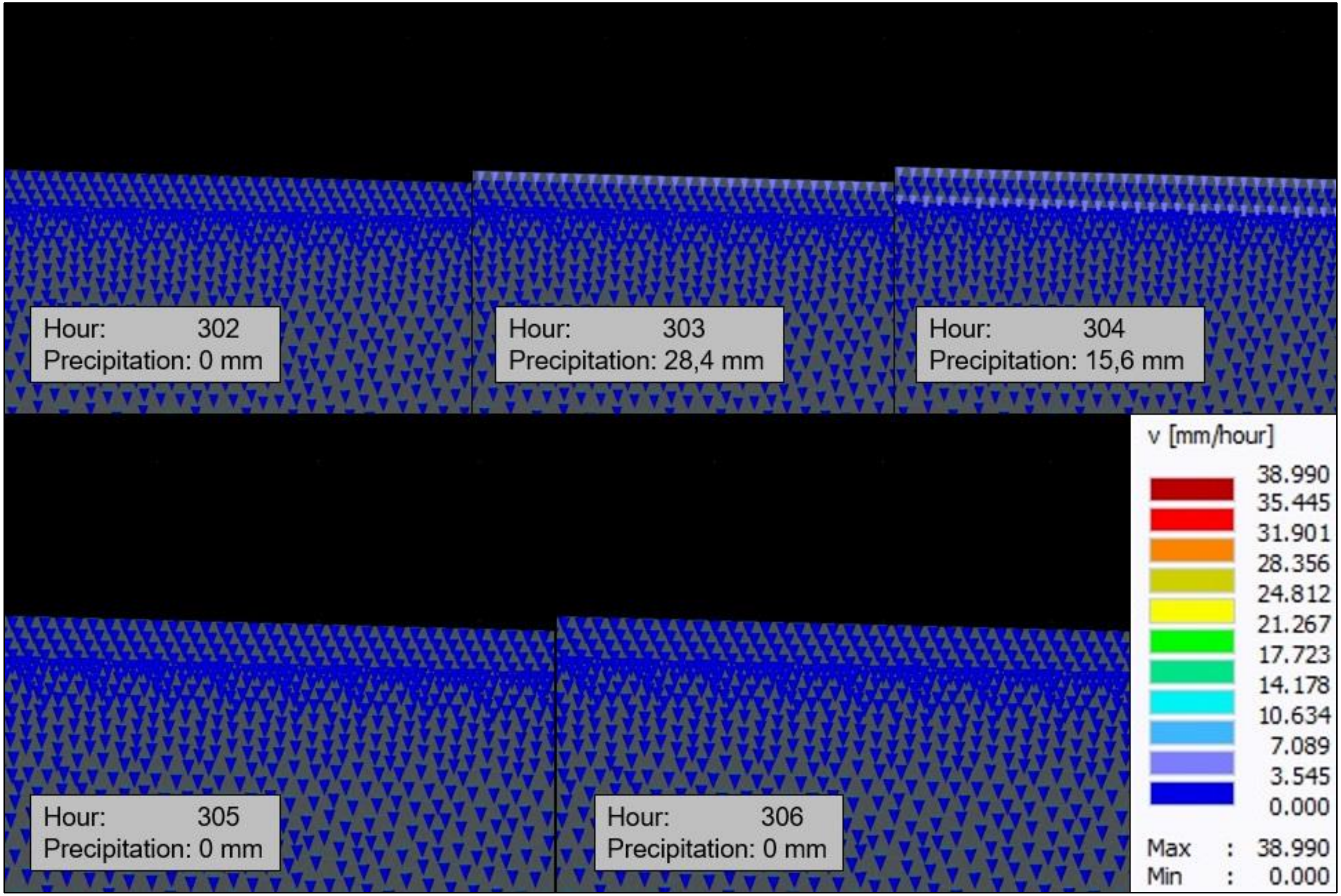

Figure 90: Velocity vectors simulated by the HYDRUS-2D tool during the 2nd high-intensity rainfall event

Chapter 6: Conclusions

To conclude the findings of the simulations relevant to each slope component, the VWC of the deeper tailings material is generally higher than that of the cover material, except during and after rainfall periods, during which the cover material reacts rapidly to incoming moisture with VWC recordings from simulations peaking.

Slope component 1 is characterised by high volumes of infiltration during all of the rainfall events except for the highest intensity rainfall event around the 300th hour. The VWC of the deeper tailings material is generally higher than that of the cover material, except for rainfall periods, during which the cover material reacts rapidly to incoming moisture with VWC recordings from simulations peaking. Incoming precipitation infiltrates and percolates up to depths of 500 mm below the surface, after which vertical percolation is too small to recognise. Even though VWC values at lengths of 5 000 mm is characterised by a higher VWC than the other shorter lengths (on the horizontal cross-section), which indicates the possibility of lateral movement, which is again emphasises by the direction of velocity vectors in the lateral direction. The vertical movement however still remains dominant over lateral movements which are backed by the absence of fluxes through the seepage face boundary. The velocity of infiltration is higher during the first rainfall event than during the second rainfall event due to higher volumes of infiltration during the first rainfall event than the second rainfall event. Overland flow is therefore dominant during the high-intensity rainfall event on the 300th hour (which is the highest intensity rainfall event).

Similarly to the conclusions made for slope component 1, the VWCs of all three depths spike after rainfall events. This slope component's *Ks* has been fitted and reduced to 1,35 mm/hour to ensure a simulation closely resembling the measured overland flow data and the VWCs at all three observation nodes. The magnitudes decrease the deeper the observation node is and increases in delay time accordingly. VWC readings after the rainfall event on the 360th hour is much higher than those readings after the 300th hour. It is worth noting that the rainfall event on the 300th hour is double that of the rainfall event on the 360th hour. Therefore, in this case, the higher the intensity of the rainfall event, the lower the volume of infiltration and the higher the volume of overland flow. A slight increase in VWC is recorded at lengths close to the seepage face, which indicates the possibility of lateral movement. It is, however, worth noting that vertical seepage still remains dominant according to the velocity vectors and the auxiliary vertical cross-sections. No lateral seepage fluxes have been simulated for this slope component.

For slope component 3, the *Ks* has been fitted and reduced to 1 mm/hour. Percolation ensures spikes in VWC at the depth of 100 mm below the surface two hours after rainfall events and approximately 11 hours after rainfall events. An increase in VWC at a depth of 1 000 mm below the surface only starts 30 hours after rainfall events and peaks at approximately 100 hours after rainfall events, subsequently indicating slow percolation and infiltration (hence the low *Ks* of the cover material). Overland flow is dominant on this slope component and is the only slope component which is characterised by simulations indicating overland flow during the rainfall event on the 360th hour, which was labelled as a rainfall event of a gentle nature. The vertical cross-section auxiliary objects indicate infiltration and percolation only up to 500 mm below the surface and very little lateral movement after the 1st rainfall event. It is, however, worth noting that lateral movement only occurs slightly around the 300th hour (as a result of rainfall events prior to the second rainfall event) and quickly dissipates due to the dominance of vertical movement, which is emphasises once again by the velocity vectors.

The *Ks* values for slope component 4's cover material has been fitted and reduced to 1.5 mm/hour which has resulted in a gradual increase in VWC after rainfall events with no increase in VWC at depths of 500 and 1 000 mm below the surface after the 1st high-intensity rainfall event. Increases in VWC is however recorded at a depth of 500 mm below the surface approximately 10 hours after the 1st significant rainfall event. Similarly to the trends described for slope component 2, this slope component has lower infiltration rates during the high-intensity rainfall events with high infiltration rates after the gentle rainfall events after the 360th hour. Vertical movement, as in the case of the previous slope components has been determined to be characterised by vertical movement through the profile and no seepage face fluxes.

For slope component 5, the *Ks* measured *in-situ* for the cover material has been determined to be accurate. Due to the high *Ks* for the cover material and the flat geometry, high infiltration rates have been simulated. A dry cover material ensures an increase only at a depth of 100 mm below the surface. As for the high-intensity rainfall event, an extremely high increase in VWC is recorded at a depth of 500 mm below the surface due to every drop being infiltrated due to high *Ks* and a flat geometry. 800 hours after the second high-intensity rainfall event, it can be noticed that the observation node at 1 000 mm below the surface has increased by 0.2 due to prior rainfall events, yet remains constant at the time. Thereafter, the observation node at 500 mm below the surface has the highest VWC, followed by the observation node at 1 000 mm below the surface and then by the observation node at 100 mm below the surface, these values stay relatively constant after the second high-intensity rainfall event. This phenomenon can be described to a higher *Ks* at 1 000 mm below the surface which would result in the profile draining at 1 000 mm below the surface at quicker rates than that of the material at 500 mm below the surface.

To summarise all findings, the *Ks* for slope components 1-4 have been fitted and significantly decreased to ensure simulations closely resembling the measured overland flow values and the measured VWC values at all three depths. As in the case of this study, the only slope component that's cover material *Ks* has not been fitted is that of slope component 5. The rest of the slope component's Ks had to be amended to resemble accurate representations of the profile's hydraulic conductivity properties by comparing the simulated and observed VWC and overland flow results. Possibilities exist that the gradients of slope component 1-4 has resulted in erosion in the past, ultimately degrading the cover material. The exposed material would have been vulnerable to droplet impact and further degradation, which ultimately could have induced sealed conditions. This phenomenon is backed by evidence that simulations indicate a lower infiltration rate during high-intensity rainfall events, which would induce droplet impact and ultimately a sealed off cover material. These sealed conditions would have resulted in implications for the double ring infiltrometer due to periodical crusting.

As per personal conversation with professor Simon Lorentz in October 2018, limitations existed for *in-situ* measurements due to large concentrations of rock. This phenomenon, according to Casablanca (1998) can result in higher than normal *Ks* measurements. Even though this might be the case, due to inverse modelling and constant VWC measurements, simulations could be carried out with a high amount of success.

As for seepage flow paths, the dominance of vertical seepage is evident in all five slope components via auxiliary objects, velocity vectors and zero fluxes through the seepage face boundary. The cover material is the driest part of the profile before rainfall events with the deeper depths characterised by higher VWC, which ultimately indicates vertical seepage through the free drainage boundary. Therefore, two dominant flow paths exist for slope components 1-4, namely overland flow and vertical seepage with the volumes of these flow paths directly correlating with the volume of infiltration an overland flow for each slope component. No lateral movement was identified in any of the slope components which indicates a lack of seepage face fluxes. As for slope component 5, only one flow path was identified, namely vertical seepage. Vertical seepage tends to be dominant during lower intensity rainfall events with overland flow dominating during high-intensity rainfall events.

Chapter 7: Recommendations

Given evidence of vertical seepage through the free drainage boundary associated with the volume of precipitation infiltrated into the profile and the evidence of dominant overland flow during high-intensity rainfall events, recommendations have been made to rectify the issue at a basic level.

Sealed off conditions occur (in this case) due to a combination of droplet impact and rapid saturation by the vermiculite material during high-intensity rainfall events, which results in a decrease of infiltration and an increase in overland flow. It is the researcher's opinion that a sealed cut-off trench should be installed around the TSF to contain overland flow from the TSF and divert it back into the pollution control dam. The overland flow however is not the main concern and can easily be remedied by surrounding cut-off trenches. The infiltration rate and the dominance of vertical percolation is of main concern given the mobilisation of ions trapped in the copper tailings material which will be precipitated or deposited within or close to the groundwater aquifer, ultimately resulting in the contamination thereof. Therefore, emphasise should be placed in reducing the volume of infiltration and the direction of percolation.

Simulations via the *HYDRUS-2D* tool has proven that lateral movement of water is more likely in cover materials with a low *Ks*. By increasing lateral flows and decreasing vertical percolation, cut-off trenches will ensure that shallow lateral flows be captured and rediverted into the pollution control dam, ultimately decreasing vertical percolation and the contamination of the groundwater aquifer. A decrease in the cover material's *Ks* will result in an increase in water holding capacity. Simulations via the *HYDRUS-2D* tool has proven that evaporation and transpiration is high in this region given climatic conditions. Therefore, by decreasing the percolation deeper than the cover material, evapotranspiration will remove more water, which will ultimately result in even less vertical percolation. As for overland flow, a lower *Ks* will result in high volumes of overland flow, which together with the lateral sub-surface flows will be captured by the cut-off trenches.

It is the opinion of the researcher that the cover material is an ineffective cover material due to the variations in *Ks*, which indicates the vulnerability of this material to droplet impact and sealed conditions as well as rapid saturation during high-intensity rainfall events. This material is fibrous and flaky of nature which increases *Ks* (if not saturated or sealed off) during low-intensity rainfall events.

To summarise, generic remedial actions should include the installation of cut-off trenches around the TSF and the application of a cover material characterised by a low *Ks* and a high water holding capacity. Cut-off trenches should be lined to decrease further infiltration and percolation and should regularly be pumped out into the pollution control dam. Lastly, basal cover should be increased on all slope components to decrease the effect of droplet impact. Due to the dominance of vertical seepage in all five of the slope components discussed and the absence of lateral seepage, the latter mentioned mitigation techniques is relevant to all five of the slope components regardless of their unique conditions pertaining to infiltration, sub-surface water movement or overland flow.

References

Allen, R.G., Pereira, L.S., Raes, D. and Smith, M. 2006. FAO Irrigation and Drainage Paper, no. 56. Crop evapotranspiration (guidelines for computing crop water requirements).

Arriaga, F.J., Kornecki, T.S., Balkcom, K.S. & Raper, R.L. 2010. A method for automating data collection from a double-ring infiltrometer under falling head conditions. USDA-Agricultural Research Service, National Soil Dynamics Laboratory.

Ashmole, I., Motloung, M. 2008. Reclamation and environmental management in dimension stone mining; *The Southern African Institute of Mining and Metalurgy*- Surface mining. *p. 155*.

Bevan, K. & German, P. Macropores and water flow in soils. Water resource research. *Department of Environmental Sciences, University of Verginia, Charlettesville. 18(5):1312*.

Bhanbhro, R. 2014. Mechanical Properties of Tailings; Basic Description of a Tailings Material from Sweden- Luleå University of Technology.

Brockwell, J., Searle, S.D., Jeavons, A.C., Waayers, M. 2005. Nitrogen Fixation in Acacias: an Untapped Resource for Sustainable Plantations, Farm Forestry and Land Reclamation-Australian Centre for International Agricultural Research. *p. 5-23*.

Bruce, D.A., Dreese, T.L. and Heenan, D.M. 2008. Concrete walls and grout curtains in the twenty-first century: The concept of composite cut-offs for seepage control.

Bruggeman, A.C. 1997. Preferential movement of solutes through soils. Doctor of Philosophy in biological systems engineering, Virginia Polytechnic Institute and State University. *P.1-7*.

Burger, E.P. 2013. An investigation of the carbonatites of the Kaapvaal Craton and their tectonic context, *p. 21-28*, MSc in Geology, faculty of Natural and Agricultural Sciences, University of Pretoria.

Campaner, V.P., Luiz-Silva, W. & Machado, W. 2013. Geochemistry of acid mine drainage from a coal mining area and processes controlling metal attenuation in stream waters, southern Brazil.

Campbell, C. S. 2010. Water content measurement methods and field applications. *Decagon Devices*.

Casanova, M.P. 1998. Influence of slope gradient and aspect on soil hydraulic conductivity measurements with tension infiltrometer. Field study in the Central Zone of Chile.

Collins, S. 2000. Hand dug shallow wells- Skat Consulting. *Series of manuals on drinking water supply*. (5): 30.

de Almeida, K.S.S.A., Souza, L.S., Paz, V.P.S., Filho, M.A.C. and Hoces, E.H. 2017. Models for moisture estimation in different horizons of yellow agrisol using TDR.

Department of Environmental Affairs and Tourism & Department of Water Affairs and Forestry. 1997. Discussion document towards a white paper on integrated pollution control and waste management. *p.1-14*.

Department of Water Affairs and Forestry. 1996. South African water quality guidelines (Second Edition). Volume 1: Domestic use

Department of Water Affairs and Forestry. 2007. Series A: Activity Guidelines. Pollution control dams- Best practise guidelines for water resource protection in the South African Mine Industry.

De Villiers, S. & Mkwelo, S.T. 2009. Has monitoring failed the Olifants River, Mpumalanga? 35(5):6 *Water SA*.

Dippenaar, M.A. 2014. Assessment of vadose zone hydrology: concepts, methods, applications and guidelines. Doctor of Pilosophy in Engineering- and Environmental Geology (option: Hydrogeology). *Department of Geology, School of Physical Sciences, Faculty of Natural and Agricultural Sciences, University of Pretoria*.

Edraki, M., Baumgartl, T., Manlapig, E., Bradshaw, D., Franks, D.M. Moran. C.J. 2014. Designing mine tailings for better environmental, social and economic outcomes: a review of alternative approaches:412.

Eijelkamp Agrisearch Equipment. 2012. *In-Situ* Hydraulic Conductivity Tests. *Eijelkamp Soil and Water*.

Engemoen, W.O. 2012. Design standard no. 13, Embankment Dams. *Reclamation, managing water to the West.*

Fatehnia, M., Abichou, T. & Tawfiq, K. 2014. Comparison of the methods of hydraulic conductivity estimation from mini disk infiltrometer. *Electronic Journal of Geotechnical Engineering.*

Glaesner, N. & Gerke, H.H. 2013. Single and Double Porosity Modeling of Solute Transport in Intact Soil Columns – Effects of Texture, Slurry Placement, and Intermittent Irrigation.

Hitsinani, H.M. 1999. The effects of transport infrastructure towards planning for tourism in South Africa. Master of Science degree in Development Planning, Department of town and regional planning, Faculty of Architecture, University of Witwatersrnd, Johannesburg, South Africa. *p. 54.*

Haude, W. 1952. Verdunstungsmenge und evaporationskraft eines klimas. Ber, Deutschen, Wetterd.

Hunt, A.G., Holtzman, R. & Ghanbarian, B. 2017. A percolation-based approach to scaling infiltration and evapotranspiration. 9:103.

International Atomic Energy Agency. 2008. Field estimation of soil water content. A practical guide to methods, instrumentation and technology. Soil and water management & crop nutrition section.

Jackson, J. 2004. Impacts and management of *Cenchrus ciliaris* (Buffel grass) as an invasive species in northern Queensland. Degree of Doctor of Philosophy, Tropical plant species, School of tropical biology, James Cook University. *p. 31*.

John, J., Garland, R., Genthe, B., Govender, D., Le Roux, W., Macandza, V., Manhique, J., Nortje, K., Oosthuizen, M.A., Pauw, C., Steyn, M., Swemmer, L. & Wright, C. 2012. Lower Olifants community health: risks and opportunities report. *p. 9-20.*

Klohn, E.J. 1979. Seepage control for tailings dams, Tailings and Waste Disposal-Seepage, Contamination, Regulations, and Control. *p. 671*.

Kim, J. & Mohanty, B.P. 2016. Influence of lateral subsurface flow and connectivity on soil water storage in land surface modelling. Journal of Geophysical Research: Atmospheres. *p.1-2*. AGU Publications.

Kohne, J.M., Junior, J.A., Kohne, S., Tiemeyer, B., Lennartz, B. & Kruse, J. 2011. Double ring and tension infiltrometer measurements of hydraulic conductivity and mobile soil regions.

Letts, S.A. 2007. The paleomagnetic significance of the bushveld complex and related 2 Ga magmatic rocks in ancient continental entities, *p. 6-148*, Ph. D, faculty of science, University of The Witwatersrand, Johannesburg.

Liu, Q. Q., Chen, L., Li, J.C. and Sing, V.P. 2004. Two-dimensional kinematic wave model of overland-flow. *Journal of Hydrology*.

Makkink, G.F. 1955. Toetsing van de berekening van de evapotranspiratie volgens Penman. Landbouwk Tijdskrift.

Mazaheri, M.R. & Mahmoodabadi, M. 2012. Study on infiltration rate based on primary particle size distribution data in arid and semiarid region soils. *Arabian journal of geoscience*.

McCarthy, T.S. 2011. The impact of acid mine drainage in South Africa. School of Geosciences, University of the Witwatersrand, Johannesburg, South Africa. *p.1-7*.

Morgenthal, T. L. 2003. The assessment of topsoil degradation on rehabilitated coal discard dumps. *School for Environmental Science and Development at the Potchefstroomse Universiteit vir Christelike Hoër Onderwys (North-West University)*

Moukodi, G.P., Usher, B.H. & Surmon, M. 2009. Hydrogeochemical characterization of waste deposits from a copper mine. Groundwater studies, University of the Free State, Bloemfontein. *p.766.*

Mucina, L. and Rutherford, M.C. (Eds.) 2006. The vegetation of South Africa, Lesotho and Swaziland. Strelizia 19. South African National Biodiversity Institute, Pretoria South African.

Munnik, M.C., Verster, E. & van Rooyen, T.H. 1996. Spatial pattern and variability of soil and hillslope properties in a granitic landscape. 3. Phalaborwa area, South African Journal of Plant and Soil. 13(1):9-16.

Mweso, E. 2003. Evaluating the importance of soil moisture availability (as a land quality) on selected rainfed crops in Serowe area, Botswana. *International Institute for Geo-information Science and Earth Observations*.

Nakhaei, M. & Simunek, J. 2013. Estimating the soil hydraulic and thermal properties of unsaturated porous media using HYDRUS-2D. *Department of Geology, Kharazmi University, Tehran, Iran* and *Department of Environmental Science, University of California, Riverside, USA*.

Nel, L., Kellner, K., van Deventer, P. & Truter, W. 2015. The Value of Coated Rhodes Grass Seed in Rehabilitation. *p.3*.

Neuman, D. & Ford, K.L. 2006. Phytostabilization as a Remediation Alternative at Mining Sites- Bureau of Land Management National Science and Technology Center Branch of Publishing Services. *P. 1*.

O'Connor, T.G. & Granger, J.E. 2014. Establishing Cynodon dactylon on mining tailings and mining-impacted soil of a copper–cobalt mine in the Democratic Republic of the Congo - *African journal of Range & Forage science*: 178-181.

Omofunmi, O.E., Kolo, J.G., Oladipo, A.S., Diabana, P.D. & Ojo, A.S. 2017. A review on effects and control of seepage through earth-fill dam. *Department of Mechanical Engineering and Department of Agricultre and Bio-Environmental Engineering, Yeba College of Technology, Yaba-Lagos State, Nigeria.*

Panuska, J., Sanford, S. & Newenhouse, A. 2015. Methods to monitor soil moisture. Department of Biological Systems Engineering, College of Agricultural and Life Sciences, University of Wisconsin-Madison and University of Wisconsin–Extension, Cooperative Extension. *p.3-4*.

Podmore, C. 2009. Urban salinity – causes and impacts. Primefacts. *NSW Industry and Investment*.

Potter, M.J. 2002. Vermiculite. *U.S. Geological Survey Minerals Yearbook*.

Puhalovich, A., Mundle, K., Pol, R., & Toll, N. 2012. One- and three- dimensional modelling of sub-surface solute transport processes in the region of Ranger uranium mine's tailings storage facility, Northern Teritory, Australia. *p. 107-110*.

Reichert, J.M., Albuquerque, J.A., Kaiser, D.A., Reinert, D.J., Urach, F.L. & Carlesso, R. 2009. Estimation of water retention and availability in soils of Rio Grande Do Sul. 33:1550.

Reynolds, W.D. & Zebchuk, W.D. 1993. Performance assessment of tension infiltrometers. Soilmoisture Equipment Corp., Santa Barbara, California.

Reza, S. 2016. 3 Grasses that are effective in rehabilitation of the ecosystem of mine tailings. *Permaculture Research Institute.*

Rezagholilou, A. 2006. Seepage design criteria in embankment dams on alluvium foundations. *Ineternational conference of hydropower, Kumming, China*.

Rösner, T. 1999. The environmental impact of seepage from gold mine tailings dams near Johannesburg, South Africa, *p.27-28,* Ph.D, faculty of Natural and Agricultural Sciences, University of Pretoria.

Rijtema, P.E. 1965. Calculation methods of potential evapotranspiration. Instituut voor Cultuurtechniek en Waterhoushouding, Wageningen, Nederland.

Rumynin, V.G. 2015. Surface Runoff Generation, Vertical Infiltration and Subsurface Lateral Flow. Overland flow dynamics and solute transport. *p.1*.

Schoeman, J.J. 1989. Mica and vermiculite in South Africa. *J.S. Afr. Institute for Minerals and Metalloids. 89(1):1-12*

Skipton, S.O., Dvorak, B.I. & Woldt, W. 2010. Drinking water: Sulfur (sulphate and hydrogen sulfide)-University of Nebraska, Institute of Agriculture and Natural Resources. *p. 2*.

Smiley, E.T. & Martin, T.R. 2016. Soil drainage analysis and treatment considerations. *p.2*.

Soilmoisture Equipment Corp. 2010. Operating instructions- 2826D08 Tension Infiltrometer.

Simunek, J., van Genuchten, M. Th. & Sejna, M. 2008. Development and applications of the HYDRUS and STANMOD software packages and related codes. *Vadose zone journal*. *p. 587-597*.

Sing, V.P., Xu, C., Chen, Y.D. & Chen, D. Evaporation and Evapotranspiration. Hydrology and Hydraulics. 1(6): *229-276*.

Surmon, M. 2010. Rehabilitation programme- Fact sheet. *P. 1-2*.

Thompson, R.B., Gallardo, M., Agüera, T., Valdez, L.C. & Fernándes. 2005. Evaluation of the Watermark sensor for use with drip irrigated vegetable crops. *p.2*.

Truter, W., Dannhauser, C., Smith, H. & Trytsman, G. 2014. Conservation agriculture on farm level- SA Grain. *p.45-47*.

Turc, L. 1954. Le bilan d'eau des sols. C.R. des troisiemes jurnees de l'hydraulique. Soc. Hydraulic technique de France.

Vale, N.D., Potthast, K., Meyer, S., Michalzik, B., Hildebrandt, A. & Wutzler, T. 2017. Modeling macropore seepage fluxes from soil water content time series by inversion of a dual permeability model. *p.1-2*.

Vrugt, J.A., Stauffer, P.H., Wöhling, Th., Robinson, B.A. & Vesselinov, V.V. 2008. Inverse modeling of subsurface flow and transport properties: A review with new developments. 7(2):843.

Weiler, M. 2017. Macropores and preferential flow- a love-hate relationship. Hydrological processes. 31(1):15-19.

Westcot, M. 2011. An evaluation of the germination and establishment of three selected coated grass species in different soil types for rehabilitation, Magister Scientiae in Environmental Sciences, Potchefstroom Campus of the North-West University, South Africa. *p.10.*

Woodborne, S., Huchzermeyer, K.D.A., Govender, D., Pienaar, D.J., Hall, G., Myburgh, J.G., Deacon, A.R., Venter, J. & Lübcker,N. 2012. Ecosystem change and the Olifants River crocodile mass mortality events.

Zotarelli, L., Dukes, M.D., Romero, C.C., Migliaccio, K.W. & Morgan, K.T. 2010. Step by step calculation of the Penmain-Monteith evapotranspiration (FAO-56 Method). University of Florida, IFAS Extension.